



## Durham E-Theses

---

### *A study of extended red emission in reflection nebulae*

Watkin, Susan

#### How to cite:

---

Watkin, Susan (1994) *A study of extended red emission in reflection nebulae*, Durham theses, Durham University. Available at Durham E-Theses Online: <http://etheses.dur.ac.uk/5158/>

#### Use policy

---

The full-text may be used and/or reproduced, and given to third parties in any format or medium, without prior permission or charge, for personal research or study, educational, or not-for-profit purposes provided that:

- a full bibliographic reference is made to the original source
- a [link](#) is made to the metadata record in Durham E-Theses
- the full-text is not changed in any way

The full-text must not be sold in any format or medium without the formal permission of the copyright holders.

Please consult the [full Durham E-Theses policy](#) for further details.

# A STUDY OF EXTENDED RED EMISSION IN REFLECTION NEBULAE.

Susan Watkin B.Sc.

A thesis submitted to the University of Durham  
for the degree of Doctor of Philosophy.

The copyright of this thesis rests with the author.  
No quotation from it should be published without  
her prior written consent and information derived  
from it should be acknowledged.

Department of Physics  
March 1994.

The copyright of this thesis rests with the author.  
No quotation from it should be published without  
his prior written consent and information derived  
from it should be acknowledged.



10 MAR 1995

## Abstract

In the first part of this thesis spectroscopic observations of the Red Rectangle nebula are presented. A link is made between the most prominent unique emission line features, which are superimposed on the broad emission spectrum of the Red Rectangle, with the absorption features of the diffuse interstellar bands (DIBs). The shape of the emission lines are shown to be temperature dependent with the bandwidth decreasing by  $4\text{\AA}$  and the peak wavelength altering by  $5\text{\AA}$  in the cooler outer parts of the nebula when compared with the hotter inner regions. Both peak wavelength and bandwidth can be extrapolated to the values of the associated DIBs. A possible common carrier is discussed for the absorption/emission line pairs.

In the second part polarimetric observations of two reflection nebulae, NGC 7023 and NGC 2023, are presented in the  $B$ ,  $V$ ,  $R$ ,  $I$ , and  $V$ ,  $R$ ,  $I$  wavebands respectively. Through the use of colour and polarization colour diagrams a search was made for intrinsic emission, also known as extended red emission (ERE). Two such regions were found in NGC 7023, one  $64''\text{S}$  and the other  $53''\text{N}$  of HD 200775, in which there was a reduction in the  $R$  and  $I$  polarizations when compared with the values expected from scattering alone together with an increase in reddening. Calculations show that the ERE contributes as much as 22% of the light in the  $R$  waveband and approximately 16% in the  $I$  waveband. For NGC 2023 two suspected regions were investigated, the first  $62''\text{ENE}$  and the second  $84''\text{ENE}$  of HD 37903. It was found that the region nearest to the central star was unlikely to be a region of ERE however the second region exhibited a decrease in the  $R$  polarization together with an increase in  $R$  intensity but this was not shown to be the case in the  $I$  waveband. Several explanations are provided to explain this behaviour. The ERE is thus shown to be localised and varying in quantity between different positions in a nebula. None of the emission line features prominent in the Red Rectangle were found in the spectrum of the filament  $84''\text{ENE}$  of HD 37903 and the implications of this are discussed.

# Contents

Abstract . . . . .	i
List of figures . . . . .	iv
Preface . . . . .	viii
<b>1 Introduction</b>	<b>1</b>
1.1 Reflection nebulae . . . . .	1
1.2 Extended Red Emission (ERE) . . . . .	4
1.2.1 General properties . . . . .	4
1.2.2 The effect of ERE on the polarization . . . . .	6
1.3 Interstellar Grains . . . . .	7
1.3.1 Hydrogenated amorphous carbon . . . . .	7
1.3.2 Quenched carbonaceous composite . . . . .	14
1.3.3 Polycyclic aromatic hydrocarbon . . . . .	16
1.4 Diffuse interstellar absorption bands . . . . .	25
1.4.1 General background . . . . .	25
1.4.2 Families of diffuse interstellar bands . . . . .	28
1.4.3 Possible carriers of the bands . . . . .	32
1.5 Summary . . . . .	37
1.5.1 ERE and the interstellar grains . . . . .	37
1.5.2 DIBs . . . . .	38
1.5.3 Relevance to ERE of observations on the Red Rectangle and on NGC 7023 and NGC 2023 . . . . .	39

<b>2</b>	<b>The Red Rectangle</b>	<b>40</b>
2.1	Physical conditions . . . . .	40
2.2	Polarization . . . . .	50
2.3	The Nebula Spectrum . . . . .	51
2.3.1	The Optical Features . . . . .	51
2.3.2	The Emission Source . . . . .	54
2.3.3	The Emission Mechanism . . . . .	59
2.3.4	The Association with the Diffuse Interstellar Absorption Bands	61
2.3.5	Summary . . . . .	62
2.4	New Results . . . . .	64
2.4.1	Observation and Reduction Details . . . . .	64
2.4.2	Analysis of the spectra . . . . .	64
2.5	Discussion . . . . .	73
2.5.1	The link with the DIBs . . . . .	73
2.5.2	The emission mechanism . . . . .	73
2.5.3	A possible carrier . . . . .	74
<b>3</b>	<b>Review of NGC 7023 and NGC 2023</b>	<b>77</b>
3.1	Introduction . . . . .	77
3.1.1	Physical Conditions in NGC 7023 . . . . .	77
3.1.2	Physical Conditions in NGC 2023 . . . . .	86
3.2	Polarization Observations . . . . .	94
3.2.1	NGC 7023: Visible and Infrared Wavelengths . . . . .	94
3.2.2	NGC 2023: Visible and Infrared Wavelengths . . . . .	97
3.2.3	Star C in NGC 2023 . . . . .	100
3.3	Extended Emission . . . . .	102
3.3.1	Infrared Excess . . . . .	102
3.3.2	Molecular Hydrogen . . . . .	106
3.3.3	Visible and Near-infrared Excess . . . . .	108
3.3.4	Diffuse Interstellar Bands . . . . .	115

3.3.5	Summary . . . . .	115
<b>4</b>	<b>New Observations of NGC 7023 and NGC 2023</b>	<b>117</b>
4.1	The Observation and Reduction Details of NGC 7023 . . . . .	117
4.2	Polarimetry Results of NGC 7023 . . . . .	118
4.3	The Observation and Reduction Details of NGC 2023 . . . . .	135
4.4	Polarimetry Results of NGC 2023 . . . . .	140
4.5	Spectroscopic Results of NGC 2023 . . . . .	148
4.6	Discussion . . . . .	148
<b>5</b>	<b>Summary and Conclusion</b>	<b>156</b>
5.1	The Red Rectangle . . . . .	156
5.2	NGC 7023 and NGC 2023 . . . . .	157
	References . . . . .	160
	Acknowledgements . . . . .	172

# List of Figures

1.1	Reproduction by Witt and Schild (1988) of the photoluminescence spectra of laboratory HAC films observed after excitation with 5145 Å radiation by Watanabe <i>et al.</i> (1982). . . . .	9
1.2	Schematic energy level diagram for a solid with bandgap energy $E_g$ (Duley 1992). . . . .	14
1.3	Some polycyclic aromatic hydrocarbon molecules. . . . .	17
1.4	Fluorescence spectra of laboratory naphthalene excited at progressively higher energies (Beck <i>et al.</i> 1980; 1981). . . . .	20
1.5	A schematic diagram of the lower energy levels of an organic molecule (d'Hendecourt <i>et al.</i> 1986). . . . .	24
2.1	The model of the inner parts of the Red Rectangle, proposed by Leinert and Haas (1989), in which the central source is within the extended infrared structures. They have chosen the tilt (unknown) of the system to bring out HD 44179 into the equatorial plane. . . . .	44
2.2	The three positions of the slit with respect to the Red Rectangle. . . . .	65
2.3	The summed spectra of the Red Rectangle with the slit at a position angle of 162°. The integrated data represents the inner $\pm 3''$ , excluding those that contain the central star. . . . .	67

2.4	The summed spectra of the Red Rectangle with the slit at a position angle of $162^\circ$ . The integrated data represents the inner $\pm 3''$ , excluding those that contain the central star. A polynomial fit was made to the background representing the ERE which was subtracted in order to highlight the small scale emission features. . . . .	68
2.5	Spectra for the region $5700\text{--}5920\text{\AA}$ with the slit at a position angle of $162^\circ$ for increasing offsets from the central star. . . . .	70
2.6	The spectra of the $5800\text{\AA}$ feature at increasing offsets from the central star for the slit at a position angle of $162^\circ$ . . . . .	71
2.7	Spectra for the region $5700\text{--}5920\text{\AA}$ with the slit at a position angle of $120^\circ$ for increasing positions along the slit. . . . .	72
2.8	The smooth curve represents the profiles generated from the $C_{60}$ entity contour calculations with a 3% reduction in rotational constant on electronic excitation. These are superimposed on the observational data for the DIB and Red Rectangle band at $5797\text{\AA}$ . . . . .	76
3.1	NGC 7023 in blue light (Moore 1982). . . . .	78
3.2	NGC 2023 in red light (Witt and Malin 1989). . . . .	87
4.1	Intensity image of NGC 7023 in the $R$ waveband. . . . .	120
4.2	Intensity image of NGC 7023 in the $B$ waveband. . . . .	121
4.3	Intensity image of NGC 7023 in the $R$ waveband. . . . .	122
4.4	Polarization and intensity contour map of NGC 7023 in the $B$ . . . . .	123
4.5	Polarization and intensity contour map of NGC 7023 in the $V$ . . . . .	124
4.6	Polarization and intensity contour map of NGC 7023 in the $R$ . . . . .	125
4.7	Polarization and intensity contour map of NGC 7023 in the $I$ . . . . .	126
4.8	The wavelength dependence in five different regions of NGC 7023 including data from Sellgren, Werner and Dinerstein (1992) and Elvius and Hall (1967). . . . .	127
4.9	Colour difference image $I_{V-R}$ of NGC 7023. . . . .	130

4.10	Polarization colour difference image $P_{V-R}$ of NGC 7023. . . . .	131
4.11	Traces of percentage polarization across the filament 65" S of the central star . . . . .	132
4.12	Traces of polarized intensity across the filament 65" S of HD 200775. . . . .	133
4.13	Traces of colour difference and polarization colour difference across the filament 65" S of HD 200775. . . . .	134
4.14	Traces of percentage polarization across the filament 53" N of the central star . . . . .	136
4.15	Traces of polarized intensity across the filament 53" N of HD 200775. . . . .	137
4.16	Traces of colour difference and polarization colour difference across the filament 53" N of HD 200775. . . . .	138
4.17	Intensity image of NGC 2023 in the $R$ waveband. . . . .	141
4.18	Polarization and contour image of NGC 2023 in the $V$ waveband. . . . .	142
4.19	Polarization and contour image of NGC 2023 in the $R$ waveband. . . . .	143
4.20	Polarization and contour image of NGC 2023 in the $I$ waveband. . . . .	144
4.21	Colour difference image $I_{V-R}$ of NGC 2023. . . . .	147
4.22	Traces of the polarized intensity across the filaments 84" ENE and 62" ENE of HD 37903. . . . .	149
4.23	Traces of colour difference and polarization colour difference across the filaments 84" ENE and 62" ENE of HD 37903. . . . .	150
4.24	Spectrum of HD 37903. . . . .	151
4.25	The nebula spectrum of NGC 2023 with the continuum subtracted. The slit was positioned across the filament 84" ENE of HD 37903. . . . .	152

## Preface

The work described in this thesis was carried out by the author between October 1990 and March 1994, while a research student of the Department of Physics at the University of Durham under the supervision of Dr. S.M. Scarrott.

The work presented here is wholly that of the author. Some of the results of chapter 2 and 4 have already been published but in all cases the data was re-analysed by the author for this thesis.

None of the material contained within this thesis has been previously submitted by the author for a degree in this or any other university.

# Chapter 1

## Introduction

### 1.1 Reflection nebulae

Nebulae are clouds of interstellar gas and dust of which there are various different types. Reflection nebulae fall into the category of the more general group of diffuse galactic nebulae which also consists of HII regions and dark nebulae. Diffuse galactic nebulae are divided into subgroups according to the nature of the illumination and excitation. The nebulae are visible only if

- the gas is intrinsically luminous as a consequence of ionization by hot nearby stars. To produce photo-ionization luminosity of the local gas a star must be of at least spectral type B0 (Kaplan and Pikelner 1970). In this case nebulae become emissive or gaseous nebulae.
- the dust scatters light from associated stars in the immediate neighbourhood, or from more distant sources e.g. galactic nucleus. If the illuminating star is a B2 or cooler then the resulting structure will be a reflection nebula.

Stars of spectral type B0 or B1 can produce nebulae which are a combination of both emission and reflection. In fact the majority of bright nebulae are intermediary forms. The emission nebulae although primarily seen due to an intrinsic component still possesses a scattered light component.



We know that visual reflection nebulae are seen primarily due to scattered starlight because of

1. the similarity of the spectra of the central star and the reflection nebula (Slipher 1918, 1919). The expected spectrum is a continuous spectrum overlaid by a series of absorption or emission features. Ionised gas would produce a line spectrum characteristic of the material composition of the nebula thus indicating the chemical makeup of the gas.
2. the good agreement between observations and scattering calculations for reflection nebular models (Witt and Cottrell 1980*a*; Witt *et al.* 1982).
3. the high linear polarization, which shows the centrosymmetric pattern characteristic of the scattering light from a central source (Elvius and Hall 1967; Watkin, Gledhill and Scarrott 1991).

Visible reflection nebulae most commonly result from the close spatial association of relatively dense interstellar clouds,  $n_H = 10^2 - 10^3 \text{ cm}^{-3}$ , with luminous stars of spectral type B1 or later. They are not a uniform category of objects, neither are they uniformly distributed throughout the galaxy. In general they are characteristically bluer than their illuminating star. The difference in colour can be attributed to: differences in reddening of the stellar and nebular light; the degree of multiple scattering; differences in the wavelength dependence of dust albedo; phase function effects; and most often to an increase in scattering optical depth with a decrease in wavelength. The latter effect is what renders the nebular colour bluer than that of the star unless modified by one of the other effects. Extreme cases of nebular colour bluer than that of the star tend to be instances where stars are very deeply embedded in the nebulae and substantial multiple scattering occurs e.g. NGC 2068, NGC 1999. Cases of extremely red nebulae occur when nebulae are illuminated under large scattering angles by externally located stars so that the variation of phase function asymmetry with wavelength becomes the determining factor e.g. IC 426, IC 59, IC 63.

There are three types of reflection nebulae:-

- Interstellar type in which the illuminating star and the interstellar medium are not closely related. The dusty matter is almost always part of an extensive molecular cloud. The surface brightness in the visible falls between 20 and 23 mag (arcsec)<sup>-2</sup>. They are described as being intensity bounded rather than density limited objects and their size is given by the Hubble relationship. Visually these nebulae are frequently characterised by wispy filaments e.g. Pleiades association.
- Compact reflection nebulae in which the associated dust and gas may be intimately connected with the illuminating star. The illuminating star is frequently heavily obscured and the evolutionary status of these objects is somewhat unclear. Some are proposed as early main sequence stars that are illuminating the clouds of dust and gas from which they formed and are therefore the sites of recent or continuing star formation e.g. NGC 2261 while others are in the last stages of evolution e.g.  $\eta$  Carinae. These nebulae are found to be density bounded and most tend to be amorphous in appearance but there are some which are biconical, called bipolar, and others which consist of a single star at the apex of a single core, known as cometary.
- High galactic latitude nebulosity i.e. due to clouds of gas and dust at a distance of 100 pc above the galactic plane with no apparent illuminating star. These are visible as a result of scattering of the integrated light of the galactic nucleus. This was determined from the spatial distribution of the clouds at intermediate and high galactic plane since the vast majority are located south of the galactic plane with a strong concentration towards the galactic center.

Hubble (1922) realized that reflection nebulae could be treated as natural laboratories in which the interaction of interstellar grains with photons could be studied. He derived a simple relationship between the angular sizes of reflection nebulae and

the apparent magnitude of the respective illuminating stars. This is given by

$$m + 4.9 \log a = 11.02 \pm 0.1$$

where  $m$  is the magnitude of the illuminating star and  $a$  is the radius of the nebula (in arcminutes). This well known statistical study led to a first determination of the dust albedo. Several detailed analyses of individual reflection nebulae have confirmed the high value of the albedo in the visible of  $a \geq 0.6$  and have also demonstrated the strongly forward scattering phase function expected from wavelength sized scattering particles. In addition to scattering the conversion of stellar UV and visible photons into longer wavelength radiation by nebular grains has also been studied successfully in reflection nebulae.

In reflection nebulae the star–nebula geometry is unknown in three dimensions. However for bright reflection nebulae their geometry must approach the optimal geometry for maximising surface brightness. The range of such geometries is extremely narrow and always requires that the illuminating star be inside or behind a moderately dense interstellar cloud with an optical depth in front of the star of the order of unity. For nebulae located in regions of apparently active star formation, the illuminating star is simply the most massive and luminous member of a low mass star cluster residing in the environment of its formation.

## 1.2 Extended Red Emission (ERE)

### 1.2.1 General properties

Widespread evidence has been found amongst reflection nebulae illuminated by B- and early A-type stars for excess emission beyond that expected from scattering alone, called extended red emission (ERE). It appears in the  $R$  ( $0.67 \mu\text{m}$ ) band with many objects also displaying strong emission in the  $I$  ( $0.88 \mu\text{m}$ ) band (Witt, Schild, and Kraiman 1984; Witt and Schild 1985, 1986). This excess over scattered starlight appears to be a mixture of continuous emission and a broad emission feature whose central wavelength ranges from  $0.65$  to  $0.7 \mu\text{m}$  and whose width varies from  $0.06$  to

$0.10\ \mu\text{m}$  (Witt and Schild 1988; Witt and Boroson 1990). In fact the ERE appears to be the short wavelength wing of an intense near-infrared continuum observed both in nebulae displaying ERE and other objects. ERE was first detected in the Red Rectangle nebula (Cohen *et al.* 1975) but has since been observed in 14 other reflection nebulae (Witt and Schild 1986) and is therefore quite a common phenomena amongst reflection nebulae illuminated by B and early A stars. The excess radiation can amount to between 20–50% of the underlying scattering continuum. In the *R* band the ERE contributes typically 15–25% of the surface brightness and 30–50% in the *I* band. Furthermore individual nebulae exhibit a very wide range of (*V*–*I*) colour differences consistent with the contribution of the emission in the *I* waveband showing a local variation. This led to the conclusion that ERE is a luminescence process most likely excited by mid-UV radiation from the illuminating stars embedded in the respective nebulae. Although the maximum ERE intensity shows little variation from source to source, except for the Red Rectangle, the scattered light varies strongly. The peak wavelength was also found to vary between objects. Witt and Boroson (1990) deduce that the ERE band arises in grains that are being rehydrogenated in  $\text{H}_2$  photodissociation zones around the exciting star of each nebula.

Witt and Boroson (1990) made an extensive spectroscopic survey of a number of relatively bright reflection nebulae in order to explore the conditions under which the red luminescence band is present. Early results showed that it occurs in nebulae such as NGC 1333, 2327, 2247, 1999, 2068, 2023 and 7023. The band is conspicuously absent in objects such as the Merope nebula and IC 435. Since IC 435 is located in the molecular cloud which contains NGC 2023 the presence/absence of the red luminescence band provides information on the local processing of grains i.e. the degree of hydrogenation of amorphous carbon, for example, which may depend on the availability of atomic hydrogen in the nebular environment. There is some evidence that ERE may also have been observed in the spectrum of diffuse light from the dark cloud L1780 (Chlewicki and Laureijs 1987) where it would have been

excited by the interstellar radiation field. This raises the possibility that the general diffuse galactic light might contain a component due to the red luminescence. In fact van Breda and Whittet (1981) claim to have detected a diffuse ERE component in the general interstellar medium although at  $\sim 0.55\mu\text{m}$  rather than at  $0.65\mu\text{m}$ .

Sellgren *et al.* (1985) raise the possibility that ERE is related to the infrared emission bands at 3.3, 6.2, 7.7, 8.6, and  $11.3\mu\text{m}$ . Such infrared emission features are seen in reflection nebulae as well as in other objects and are generally attributed to some type of carbonaceous material under strong ultraviolet irradiation (Sellgren 1990). It is therefore important to clarify the nature of the emitting material giving rise to the ERE, the emission mechanism and the possible connection between the ERE and the infrared emission features associated with reflection nebulae.

### 1.2.2 The effect of ERE on the polarization

If the nebular emission were purely due to the reflected light at all wavelengths observed, then one would expect to see the percentage polarization monotonically increase with wavelength, owing to the following two effects. First, the optical depth of the nebula decreases at longer wavelengths, because of the wavelength dependence of extinction by dust. Multiple scattering is less important at lower optical depths and since the multiple scattering tends to depolarize reflected light, the polarization is higher when the optical depth is lower (Warren-Smith 1983). Second, in the infrared band the wavelengths of photons become larger than the typical interstellar grain size, for standard models of interstellar dust (Mathis, Rumpl and Nordsieck 1977). As the ratio of wavelength to particle size increases, the predicted polarization increases, approaching the limit of Rayleigh scattering where light becomes 100% polarized if scattered through an angle of  $90^\circ$ . At visual wavelengths, where the grain size is comparable to the wavelength of the photons, Mie scattering models show that the scattered light is less than 100% polarized even when scattered through an angle of  $90^\circ$  (White 1979).

The effect of an intrinsic component to the emission will be to reduce the po-

larization since the intrinsic component is unpolarized and will therefore dilute the polarized component arising from scattered light. If the ERE does exist in NGC 2023 and NGC 7023 then one will be expected to detect a fall in the percentage polarization in the  $R$  and to some extent the  $I$  wavebands when compared to the  $V$  and  $B$  wavebands provided that the polarization in the latter two bands is purely due to scattered light.

## 1.3 Interstellar Grains

Carbon has long since been considered as a major constituent of interstellar grain material but the precise form remains uncertain. Graphite, amorphous carbon, and polycyclic aromatic hydrocarbon particles are now viewed as the most probable hosts for the bulk of the nongaseous carbon in interstellar space. All of these have been proposed as the source of the ERE whose origin is a matter of considerable debate and still remains unresolved. Many other molecules have been suggested in order to explain the ERE e.g. Wdowiak *et al.* (1989) synthesized depositions from a plasma composed of CO, CH<sub>4</sub>, N<sub>2</sub>, H<sub>2</sub>O, and Ar at 20K and measured the fluorescence spectra. The depositions showed fluorescence but the peak emission was located at a shorter wavelength than that of ERE. The following section will concentrate mainly on the carbon based molecules.

### 1.3.1 Hydrogenated amorphous carbon

Hydrogenated amorphous carbon (HAC) is known to exhibit a broad luminescence band in the 0.5–1.0  $\mu\text{m}$  spectral region (Watanabe, Hasegawa and Kurata 1982; Lin and Feldman 1982), where the ERE has been detected, with high efficiency when exposed to short wavelength light. The luminescence is due to edge emission i.e. to the radiative recombination of electron-hole pairs. Duley and Williams (1983) state that HAC contains  $\sim 1-10\%$  of the hydrogen bonded as CH<sub>*n*</sub> groups in an amorphous carbon matrix and has very similar properties to pure amorphous carbon (Duley 1984) but is relatively transparent in the visible and near infrared.

Watanabe *et al.* (1982) prepared HAC films by the glow discharge decomposition of ethylene gas with an rf power of 5–20 W. In such experiments the molecules introduced into a plasma chamber are not fully decomposed but partially modified to an active state. The active species and neutral source molecules react with each other to form a carbon film in the plasma chamber. The film is highly polymerized material and insoluble in a variety of solvents. They observed three photoluminescence spectra in HAC samples produced at gas temperatures of (1) 200° C (2) 250° C (3) 300° C resulting in materials with inferred hydrogen concentrations of (1)  $9.1 \times 10^{22} \text{ cm}^{-3}$  (2)  $6.4 \times 10^{22} \text{ cm}^{-3}$  (3)  $5.3 \times 10^{22} \text{ cm}^{-3}$  corresponding optical bandgaps of 2.6, 2.48 and 2.0 eV. As the hydrogen concentration decreases the bandgap decreases because of the increased density of defects. The peak luminescence in laboratory samples has been observed to occur between 6400 Å and 7600 Å depending on conditions, with the maximum luminescence yield occurring when  $\lambda_{\text{max}} \approx 6700 \text{ Å}$  (sample 2), shown in fig. 1.1. Hence the peak wavelength, determined by the bandgap energy ( $E_g$ ), increases with a decrease in the hydrogen concentration.

By comparison with other semiconductors such as amorphous Si:H, emission at longer wavelengths involves defect luminescence (Street 1980) from levels within the bandgap. Such luminescence is observed at  $\sim 1.45 \mu\text{m}$  in Si:H which suggests that the near-infrared continuum detected in the 1–2  $\mu\text{m}$  region in interstellar sources arises from analogous defects in HAC. The bandgap energy ( $E_g$ ) is sensitive to temperature, as seen in the experiment by Watanabe *et al.* (1982) and environment effects. On heating to 950 K Smith (1984) has shown that  $E_g$  decreases from 2.2 eV to zero. HAC films also become more absorbing in the visible on exposure to near-ultraviolet light i.e. the film darkens (Iida *et al.* 1984). This photodarkening accompanies a decrease in  $E_g$  as a result of a release in hydrogen atoms.

HAC would appear to form continuously in the diffuse ISM via accretion of C and C<sup>+</sup> by silicate dust. The timescale for the accretion is  $t_c \sim 4 \times 10^8 n^{-1} \text{ yr}$ , where  $n$  is the total H density. The photodarkening of HAC occurs for a total photon flux  $F = 1.6 \times 10^{20} \text{ cm}^{-2}$  as shown by Iida *et al.* (1984). This implies that the time

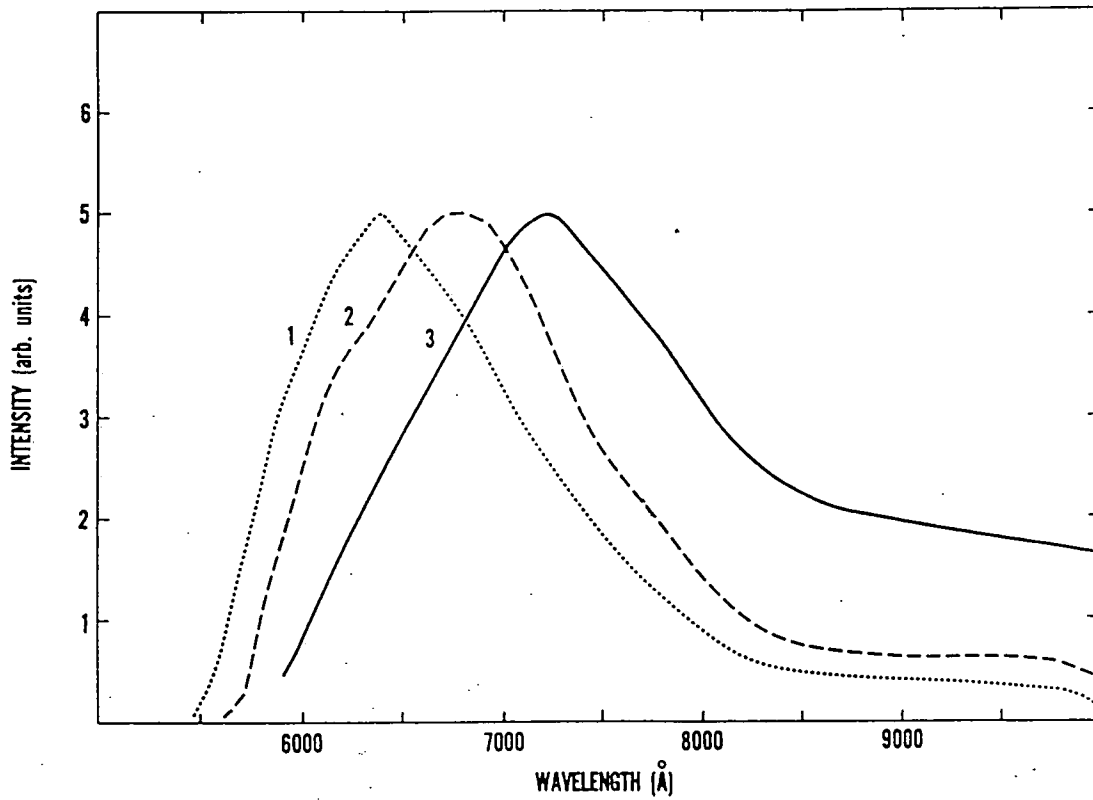


Figure 1.1: Reproduction by Witt and Schild (1988) of the photoluminescence spectra of laboratory HAC films observed after excitation with  $5145 \text{ \AA}$  radiation by Watanabe *et al.* (1982). Curves 1, 2, and 3 correspond to samples at increasing temperatures.

scale for photodarkening  $t_{\text{pd}} \sim 1.7 \times 10^6 \text{yr} \sim t_c$  since the interstellar radiation field corresponds to  $\sim 3 \times 10^6 \text{photon cm}^{-2} \text{s}^{-1}$  at ultraviolet wavelengths in a cloud with  $A_V = 0.5$  (Duley and Williams 1984). Recently accreted HAC will have  $E_g \sim 2 \text{eV}$  and a large diamond like component (carbon electronic structure  $sp^3$ ) (Duley and Williams 1988). Robertson and O'Reilly (1987) have shown that under these conditions 30–40% of the carbon atoms have graphite like bonding (carbon electronic structure  $sp^2$ ). The  $sp^2$  component increases to  $\sim 50\%$  as  $E_g$  decreases and HAC becomes more like amorphous carbon. Jones *et al.* (1987) conclude that for normal diffuse clouds the ratio of  $sp^2:sp^3$  is  $\sim 1$ , with the  $sp^2$  component having  $E_g = 0.3 \text{eV}$  and the  $sp^3$  component having  $E_g = 2.5 \text{eV}$  (Duley 1987). This implies that significant photoprocessing has occurred after the deposition of HAC on dust in these objects.

In the Red Rectangle, NGC 2023 and NGC 7023 where the ERE is observed to be extensive the carbon dust is assumed to be recently created. This dust can either be produced by the condensation from the gas in these objects resulting in HAC with  $E_g \sim 2 \text{eV}$ , or by the re-hydrogenated of pre-existing hydrogen poor amorphous carbon through the reaction with energetic H atoms in a localized shock area when a high bandgap material is recovered. It is well known that further exposure to energetic H-atoms (and/or ions) ultimately attacks the carbon with the release of organic molecules. HAC grains therefore respond to changes in their environment. In both cases the newly formed HAC dust will be rich in diamond like carbon and will emit strongly in the *R*-band. The HAC will lose hydrogen, become more graphitic over a period of  $\sim 10^6 \text{yr}$  via heating and ultraviolet irradiation and as the  $sp^2/sp^3$  ratio increases the emission then shifts to the *I*-band and then into the near-infrared. Still older dust will emit at longer wavelengths as  $E_g$  decreases further. This is in agreement with the observations that the peak wavelength shifts to longer wavelengths in areas where the carbon dust appears to be older. Objects that show extended ERE are therefore sources where the conditions favour the formation of diamond like dust which may have an origin in interstellar, circumstellar

or interplanetary dust. Calculations (Jones *et al.* 1987) indicate that this diamond like carbon is in the form of coatings of  $< 100 \text{ \AA}$  thickness on silicate cores. A mechanism for the conversion of this material to diamond particles could involve the collision and shattering of grains in interstellar shocks.

Structural studies of HAC and amorphous carbon (aC) (Robertson and O'Reilly 1987) show that these solids can be considered to be a collection of clusters of aromatic rings aggregated to form an extended solid. The size of these molecular clusters depends on the hydrogen content and is typically one to eight rings in HAC and 20–40 rings in aC. These clusters give HAC the properties of a collection of polycyclic aromatic hydrocarbons (PAH) molecules and are responsible for the emission properties of the material (Duley 1988). Under interstellar conditions in diffuse clouds, the surface of an HAC/aC solid will be bombarded with energetic photons as well as with reactive species, such as atomic oxygen. The growth of carbon atom clusters on the surface of HAC/aC will occur by accretion of carbon atoms, while destruction will occur by photolytic and photo-oxidation reactions (Duley and Williams 1986). Clusters with fewer than five to seven rings are shown to be unstable on the surface of the HAC under diffuse cloud conditions (Duley 1988). Robertson and O'Reilly (1987) show that laboratory HAC contains a range of cluster size with approximately equal concentrations of clusters containing one to eight rings. In diffuse clouds however there will be a bias towards clusters with more than five rings. The smaller clusters will therefore be removed by photolytic oxidation reactions from the surface of the HAC leaving clusters of five to eight rings, with these rings being poorly connected to each other. This material will therefore have a lower density than that of the laboratory HAC, with the volume of the interstellar clusters in the range  $10^{-21} - 10^{-22} \text{ cm}^3$  (Duley 1986).

Robertson and O'Reilly (1987) form a relationship between optical bandgap in HAC and probable compact cluster size:-

$$E_g = \frac{5.6}{(M)^{1/2}} \text{eV}$$

where  $M$  is the number of rings in each cluster. It should be noted that when

$E_g = 2 - 2.5$  eV then  $M = 5 - 7$ , the range of stable cluster size as noted earlier. Barker *et al.* (1987) also deduced the same size range from fits to the ratio of the intensity of 3.3 and 3.4  $\mu\text{m}$  features which suggests that these features are related to the ERE and in fact consists of five to seven ring PAH like clusters in HAC. For aC the equation shows that  $E_g = 0.89 - 1.25$  eV, which suggests that the near infrared emission may arise via the luminescence of more graphite aC-type interstellar dust. Such emission would be expected in a broadband at energies  $E \leq E_g$ . These clusters will also emit thermally with  $\Delta T = 400 - 500$  K which will be seen as emission at 12 and 25  $\mu\text{m}$ . This implies that a diffuse near infrared continuum should be seen in the interstellar medium which will be correlated spatially with the 12 and 25  $\mu\text{m}$  excesses. The near infrared continuum will be due to electronic as opposed to vibrational transitions. The equilibrium cluster size on HAC will also depend on the ambient radiation conditions.

Duley and Williams (1990) show that the mechanism of rehydrogenation of HAC grains and a gain in luminescence efficiency can occur in narrow  $\text{H}_2$  photodissociation zones near bright stars, and the process is available for times in excess of  $10^5$  yr after onset. The conditions in the dissociation zone are those of elevated temperatures, high H-atom abundances, and high UV flux. These conditions are identical to those in the laboratory in which rehydrogenation is known to occur (Rye 1977) and also ensure that any icy mantles will be rapidly destroyed. The outer layer of the HAC mantle, which is soft polymeric ( $sp^3$ ) consisting of a loose assembly of hydrocarbon chains, will also be removed. Rehydrogenation involves the graphite  $sp^2$  HAC which is physically hard. Duley and Williams (1988) have shown that the absorption of a single photon in HAC causes a localized transient hotspot with temperature  $\sim 1000$  K, with the cooling time for each hotspot about  $\sim 1$  s. The high excitation rate  $\sim 10^2 \text{ s}^{-1}$  ensures that perhaps 10–100 hotspots exist in any grain at any time. The arrival rate of H-atoms at the grain (typically  $\sim 1 \text{ s}^{-1}$ ) is sufficiently low that each H-atom has a high probability of locating a hotspot in the bulk of the HAC material, since H-atoms have high mobility. Rehydrogenation therefore requires

both a high abundance of hot H-atoms and a high ultraviolet flux, ensuring high temperature zones within each HAC grain. What happens next depends on the size of the dissociation zone and its speed. If rehydrogenation continues indefinitely it will ultimately destroy HAC, giving  $\text{CH}_4$  and  $\text{C}_2\text{H}_6$  as the major products. These products will in turn be destroyed by the radiation field giving rise to transient populations of  $\text{CH}$  and  $\text{CH}^+$  in approximately equal abundance.

### The luminescence process in HAC

Luminescence due to electron-hole recombination can occur from solids whenever a bandgap,  $E_g$ , exists (Madan and Shaw 1988) and typically occupies a range of energies  $\Delta E \sim (0.1 - 0.3)E_g$ . The efficiency,  $\eta$ , with which luminescence occurs depends on such factors as impurity content, temperature and structural disorder and can approach unity under certain conditions, although values of  $\eta \ll 1$  are more common. Infrared luminescence from narrow bandgap semiconductors ( $E_g \leq 0.4 \text{ eV}$ ) is a well known phenomenon. Fig. 1.2 shows the relation between absorption energy and luminescence in a typical solid. Photons with energy  $h\nu$  excite electrons from valence band states to the conduction band. Non-radiative relaxation lowers the energy of the charge carriers involved until they occupy states near the top of the valence band (holes) and bottom of the conduction band (electrons). The excess energy,  $h\nu - E_g = H$ , is converted to heat in the material and will be radiated away as infrared radiation for isolated interstellar grains. Since there might be defect and impurity states within the bandgap the photogenerated electron-hole pair may decay non-radiatively which would also generate heat within the solid. There will however be a probability  $\eta$  that direct electron-hole recombination with the emission of a photon with  $h\nu_L \leq E_g$  can occur.  $\eta (< 1)$  is then the ratio of the number of luminescent photons to absorbed photons.

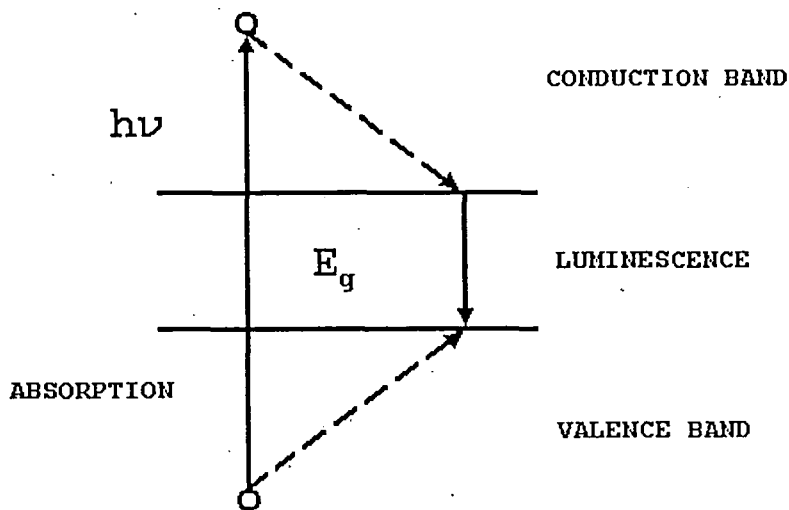


Figure 1.2: Schematic energy level diagram for a solid with bandgap energy  $E_g$  (Duley 1992).

### 1.3.2 Quenched carbonaceous composite

Sakata *et al.* (1992) proposes that a type of amorphous carbonaceous material called quenched carbonaceous composite (QCC) has a photoluminescence spectrum that can match the ERE. They have previously shown that components of QCC have features similar to the 2200 Å extinction hump (Sakata *et al.* 1983) and to the infrared emission features (Sakata *et al.* 1984; 1987; 1990). The thermally altered filmy QCC showed 3.3 and 11.3 μm features (Sakata *et al.* 1984; 1990) and the oxidized filmy QCC showed 6.2, 7.7, and 8.6 μm features (Sakata *et al.* 1987).

They made a film of laboratory synthesized QCC from a hydrocarbon plasma using a microwave discharge with an rf power of 300 W. In the microwave plasma methane gas introduced into a plasma chamber decomposes immediately into active species such as H, CH and C<sub>2</sub>. They are ejected into a vacuum chamber, cooled rapidly and deposited on a quartz substrate set on a vacuum chamber wall to form the filmy QCC. The decay of the fluorescence of filmy QCC exposed to air un-

der ultraviolet irradiation indicates that it contains highly reactive species, such as radicals and highly unsaturated molecules like polyynes, which might cause the fluorescence. When exposed to air, the colour becomes darker and the active species presumably reacted with oxygen to polymerize QCC. The solubility in liquid Freon implies that the filmy QCC, obtained on the substrate at low temperatures is an aggregate of nonpolar molecules and active species of low molecular weight. The blue-green fluorescence of the dissolved QCC is observed even after a few years of storage which suggests that this fluorescence is not caused by active species but by a stable component, such as an aromatic hydrocarbon component in the QCC. There is a major difference between filmy QCC and HACs: filmy QCC would appear to be an aggregate of low-molecular weight chemical species that contains active species, whereas HAC is a polymerized film and is stable in air.

QCC is shown to produce a single broad emission feature with peak wavelength that varies from 6700 Å to 7250 Å and coincides with that of the ERE observed in reflection nebulae. The peak wavelength depends on the substrate temperature during deposition. The onset of the fluorescence of the QCC is in the range 5400–5800 Å, compared to 5400 Å of the ERE in nebular spectra; with the FWHM being only slightly larger than that observed by Witt and Boroson (1990). The direct relation between the substrate temperature in the experiment and the astrophysical environment is not certain at the present. However it is clear the variations in peak wavelength and FWHM of the QCC emission feature more or less overlaps with that associated with the nebular variations within a given nebula and between different nebulae. The fine structure, narrow emission and additional features detected in the Red Rectangle are not found in the fluorescence profile of QCC at the spectral resolution used in the experiment. They believe that the fine structure has a different origin from the broad luminescence emission since it has not been discovered in other objects. The peak wavelengths of the fluorescence of the dissolved QCC in liquid Freon is 4400 Å. The large difference between the QCC film as deposited from the plasma and the dissolved QCC indicates that an additional fluorescence mecha-

nism to the aromatic molecule fluorescence is necessary to explain the fluorescence of the filmy QCC. An electronic interaction between active species and aromatic components in the filmy QCC may be present.

The observed infrared emission features indicate the presence of hydrogen attached to an aromatic ring (Sakata *et al.* 1984; Léger and d'Hendecourt 1987). If the QCC particles are exposed to a hydrogen plasma, the active species will be formed on its surface. The aromatic components of the dust and the active species formed there may interact electronically and cause orange-red fluorescence upon ultraviolet irradiation. The rapid decay of the fluorescence activity of QCC may explain the fact that the ERE is observed to be very localised i.e. an area in which the active species is forming on the grain surface.

### 1.3.3 Polycyclic aromatic hydrocarbon

The suggestion that polycyclic aromatic hydrocarbons (PAHs) could be present in the interstellar medium was first made by Platt(1956) and Donn (1968). The molecules were proposed to account for parts of the extinction but the absence of clear spectroscopical identification prevented further development of this hypothesis for many years. The main difference between PAHs and HACs is not the nature of the species, they are both aromatic but their size. In the HAC or QCC model, the grains have the classical size (200–2000 Å). A selection of PAH molecules are shown in fig. 1.3.

Recently PAH molecules with about 50 carbon atoms have been proposed for the origin of the unidentified infrared emission features (Léger and Puget 1984; Allamandola *et al.* 1985; Blanco *et al.* 1988) and the association is gaining increasing acceptance. Since the binding energy between carbon atoms in graphite is very anisotropic, a 50-atom cluster is more likely planar than spherical. Léger and Puget (1984) calculated the expected emission using the largest measured PAH at the time; coronene (C<sub>24</sub>H<sub>12</sub>). They found a spectrum with strong bands that impressively resembled the infrared features. The explanation based on the ability of

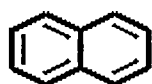
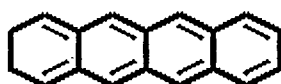
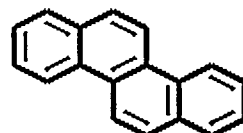
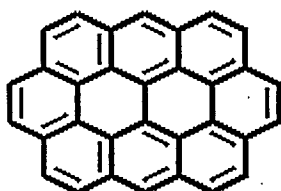
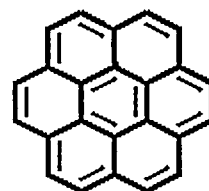
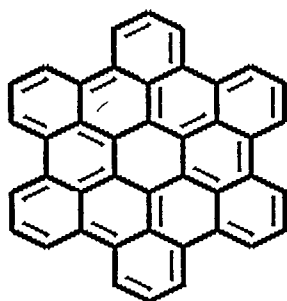
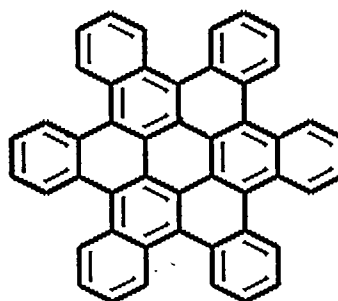
NAPHTHALENE  $C_{10}H_8$ TETRACENE  $C_{18}H_{12}$ CHRYSENE  $C_{18}H_{12}$ PYRENE  $C_{16}H_{10}$ OVALENE  $C_{32}H_{14}$ CORONENE  $C_{24}H_{12}$ HEXABENZOCORONENE A  
 $C_{42}H_{18}$ HEXABENZOCORONENE B  
 $C_{48}H_{24}$ 

Figure 1.3: Some polycyclic aromatic hydrocarbon molecules.

such molecules to survive heat impulses to high temperatures ( $\sim 10^3$  K) leads to an unambiguous spectroscopic identification of the observed bands and simultaneously accounts for their excitation mechanism. Léger and Puget concluded that only a few percent of the cosmic abundance of carbon in the PAHs would be required to explain the intensities of the observed infrared bands. It would raise those species to third place in abundance for detected molecules after  $H_2$  and CO. This theory therefore predicts that the infrared emission features will be found in carbon and not in oxygen rich environments. As reviewed by Barlow (1983) this is exactly the case in planetary nebulae in which he explains the result in terms of the features originating from carbon grains. The PAH proposed molecules are in fact very small hydrogenated carbon grains. To account for the observed intensities requires that the carriers of the bands must be small enough ( $< 10 \text{ \AA}$ ) (Allamandola *et al.* 1989; Puget and Léger 1989) and must absorb over a wide energy range from ultraviolet, through visible to near infrared (Sellgren 1984; Sellgren, Luan and Werner 1990). Léger and Puget (1984) concluded that a mixture of free PAH molecules is a major and ubiquitous component of the interstellar matter. Allamandola *et al.* (1985) reached the same conclusions by considering the spectra of other PAHs and pointed out that these molecules should be ionized in strongly irradiated regions e.g. reflection nebulae.

D'Hendecourt *et al.* (1986) suggest that red excess emission found in the Red Rectangle and other nebulae results from red phosphorescence of polycyclic aromatic hydrocarbons (PAH) molecules. However the suggested luminescence is observed in neutral PAH but is not expected for ions (Allamandola *et al.* 1986). Under conditions prevailing in reflection nebulae any PAH molecule would be expected to be completely ionised (Omont 1986). Furthermore, d'Hendecourt *et al.* (1986) point out the lack of appropriate laboratory data on PAH luminescence which prevents them from providing even an approximate match for the observed nebula spectra.

Luminescence is a typical property of PAHs. The fluorescence spectra of aromatic molecules dissolved in organic solvents has been summarized by Berlman (1971).

There is as yet no spectrum in this collection which shows a single broad feature as seen in reflection nebulae. Chrysene and coronene films have a few peaks near 4500 Å and 5000 Å respectively, while larger PAH molecules show fluorescence peaks at longer wavelengths. There have been various laboratory experiments done involving PAHs, including molecules like anthracene, naphthalene and naphthalene (Parmenter 1982; Beck *et al.* 1980; 1981). Fig. 1.4 shows the fluorescence spectra of jet cooled naphthalene molecules which are selectively excited by a tunable laser to successively higher vibrational energies above the  $S_1 - S_0$  transition (Beck *et al.* 1981). At low excitation energies the fluorescence spectra display sharp peaks which show optical transitions to various excited vibrational levels of the ground state. When the excitation energy is increased the nature of the emission changes from sharp well separated peaks, to a broad and diffuse emission. This can be explained in terms of fast intramolecular redistribution of the excess vibrational energy imparted selectively to one particular mode, to many of the available vibrational modes of the molecule, including the optically inactive modes as well, provided the total energy is conserved. This intramolecular vibrational energy randomization (IVR) process is extremely fast ( $10^{-12}$ ) and occurs because the large size of the molecule considered provides a very high density of states at that energy. The interaction between the vibrational modes of the molecule gives rise to the population of many different vibronic states whose radiative transitions to the ground electronic state are at somewhat different energies. As a result the emission appears as a broad and featureless spectrum. Coveleskie *et al.* (1980) have demonstrated that the introduction of collisions in the system, by the introduction of a buffer gas in the vacuum chamber, results in collisional sharpening of the emitted spectrum because the collisions bring the molecules to the ground vibrational state of  $S_1$  and the subsequent fluorescence is similar to that of the first spectrum of fig. 1.4.

In small molecules like naphthalene for example the half width of the emission  $\sim 300\text{Å}$ . If this result is applied to the hexabenzocoronene molecule its phosphorescence spectrum will display a broad and featureless emission of position and width

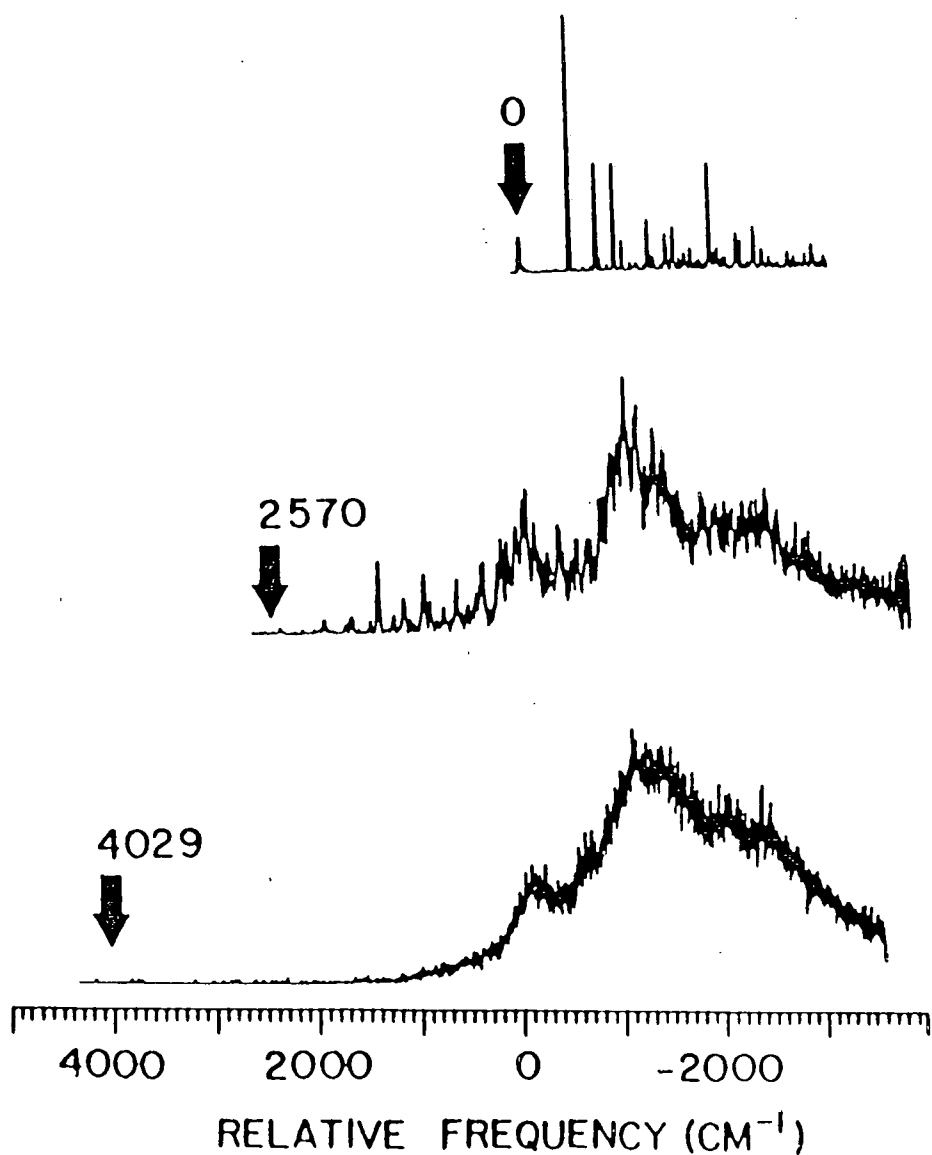


Figure 1.4: Fluorescence spectra of laboratory naphthalene (Beck *et al.* 1980; 1981). The number at the beginning of the spectra indicates the energy which is provided by a tunable laser in excess to the  $S_1 - S_0$  transition. The molecule is excited at progressively higher energies.

similar to the one observed in the Red Rectangle. In the case of hexabenzocoronene, phosphorescence is more applicable to reproduce the observed spectrum. In an isolated molecule McGlynn *et al.* (1969) have postulated that the rate of internal transitions from the singlet to the triplet state is favoured because at high vibrational excitation energy the density of states in the triplet state is higher than it is in the singlet one. Very few experiments have been conducted to test this theory. Van der Meer *et al.* (1982) have shown that this transition rate is indeed favoured in isolated pyrazine and they conclude that IVR proceeds to completion in the triplet manifold on an extremely short timescale. In this molecule phosphorescence will dominate over fluorescence and the observed IVR in the triplet state will display a very broad phosphorescence spectrum.

Puget and Léger (1989) conclude that there is convincing evidence mainly from near and mid infrared emission but also from the ultraviolet extinction curve that very small particles are destroyed by strong UV radiation and that this destruction affects primarily the smallest particles i.e. PAHs. The main method of destruction for standard interstellar grains (reviewed by Seab 1987) is erosion by the collision with the gas in shocks. The efficiency of the mechanism is reduced by the presence of interstellar magnetic fields which soften the interstellar shock. The largest PAHs will be destroyed by shocks on a time scale of  $1 - 2 \times 10^8$  yr (Omont 1986). The method of photo-oxidation which competes with the growth of PAHs by  $C^+$  accretion, proposed by Duley and Williams for the HACs, might also apply to PAHs.

Puget *et al.* (1985) and Omont (1986) consider the destruction by photothermodissociation which leads to a minimum PAH dependent on the UV radiation field and on the hydrogen density. A good estimate as to the importance of this process is difficult since there are no reliable values for the minimum sizes allowed. Leach (1986) suggests a mechanism whereby he shows that the double ionization of a PAH leads with a high probability to a coulomb explosion where the doubly ionized PAH splits into two singly ionized fragments. Double ionization in two steps can be achieved even with photons of energy less than 13.6 eV for most PAHs containing

more than 20 carbon atoms. A combination of photothermodissociation for smaller PAHs and double ionization for the larger ones could account for the destruction of PAHs by UV radiation.

The formation of PAH molecules in the atmosphere of carbon-rich cool stars has been studied in detail by Keller (1987) which show that cyclic molecules can be formed via acetylene polymerization. Frenklach and Feigelson (1989) have constructed a chemical reaction mechanism for PAH formation. Their results differ from those of Keller, who concludes that PAH growth in circumstellar envelopes proceeds rapidly until extremely large molecules are formed. Frenklach and Feigelson find a mean size of about 40 carbon atoms per molecule and they conclude that carbon rich circumstellar envelopes could be the source of the interstellar PAHs, if their acetylene to hydrogen ratio and residence time in the 900–1000 K window are sufficiently high. However the method of condensation in carbon rich envelopes would mean that the matter is not cycled often enough to replenish the interstellar medium since the evidence for the destruction of PAHs by UV radiation implies that an efficient mechanism of formation exists.

PAH formation could take place in molecular clouds either in the gas phase or in grain mantles. However there is no useful upper limit on the amount of aromatic carbons in the organic mantles formed on grains in molecular clouds. If a significant amount of aromatic carbon is formed, together with the aliphatic carbon that is observed, then it is expected that the recycling of interstellar matter from regions shielded from the UV to more diffuse regions, where only the most refractory elements survive, including PAHs, could build up the typical abundances of PAHs seen in the interstellar medium. In diffuse regions the reconstruction of PAHs by  $C^+$  ions probably plays an important role.

### **Luminescence emission mechanisms in PAHs**

It is well known that PAHs in condensed phases exhibit a very high quantum efficiency for optical luminescence. The following is a brief description of the main

processes following the absorption of UV-visible light by a PAH molecule. The molecule, initially in the ground singlet state ( $S_0$ ), undergoes a transition into the singlet manifold of states ( $S_1$  to  $S_n$ ) upon the absorption of an UV photon. From the excited state there are many competing relaxation channels which can be separated into radiative de-excitation (fluorescence or phosphorescence) and non-radiative decay (internal conversion) (Avouris *et al.* 1977), these are shown in fig. 1.5. The relative rates for these channels are dependent on the nature and critically on the environment of the molecule. Internal conversion is usually the more probable pathway and corresponds to a transfer of energy from the excited electronic state to vibrational excitations in a short time ( $\sim 10^{-8}$  s).

In the classical studies of fluorescence (Birks 1970), the molecules studied are usually diluted in a matrix, often a liquid solution of an organic solvent, and the interaction between the excited molecule and the molecules of the solvent is strong. Consequently the excess vibrational energy can be quickly transferred to the environment. Because of the high density of states provided by the matrix molecules, internal conversion to the ground vibrational state of the electronically excited state  $S_1$  is fast, finally emission of a visible photon takes place in the  $S_1 \rightarrow S_0$  transition. This transition is called fluorescence and in condensed phases is practically always observed from the  $S_1$  ground vibrational state to  $S_0$ , at various vibrational energies (McGlynn *et al.* 1969). The emission appears then as a vibrational progression and the intensity of each line is governed by the Franck-Condon factor of each transition. Alternatively another phenomenon can occur, the radiationless transition which connects, at the same energy, the singlet to the triplet state. In condensed phases relaxation to the ground triplet state  $T_1$  is achieved quickly by releasing energy to the surroundings. From  $T_1$  relaxation to  $S_0$  is done either via a radiationless process or by emitting a photon in the spin forbidden transition  $T_1 \rightarrow S_0$ . The latter process is known as phosphorescence, it has a long lifetime and occurs at longer wavelength than fluorescence.

The situation which occurs in the astrophysical case is however extremely dif-

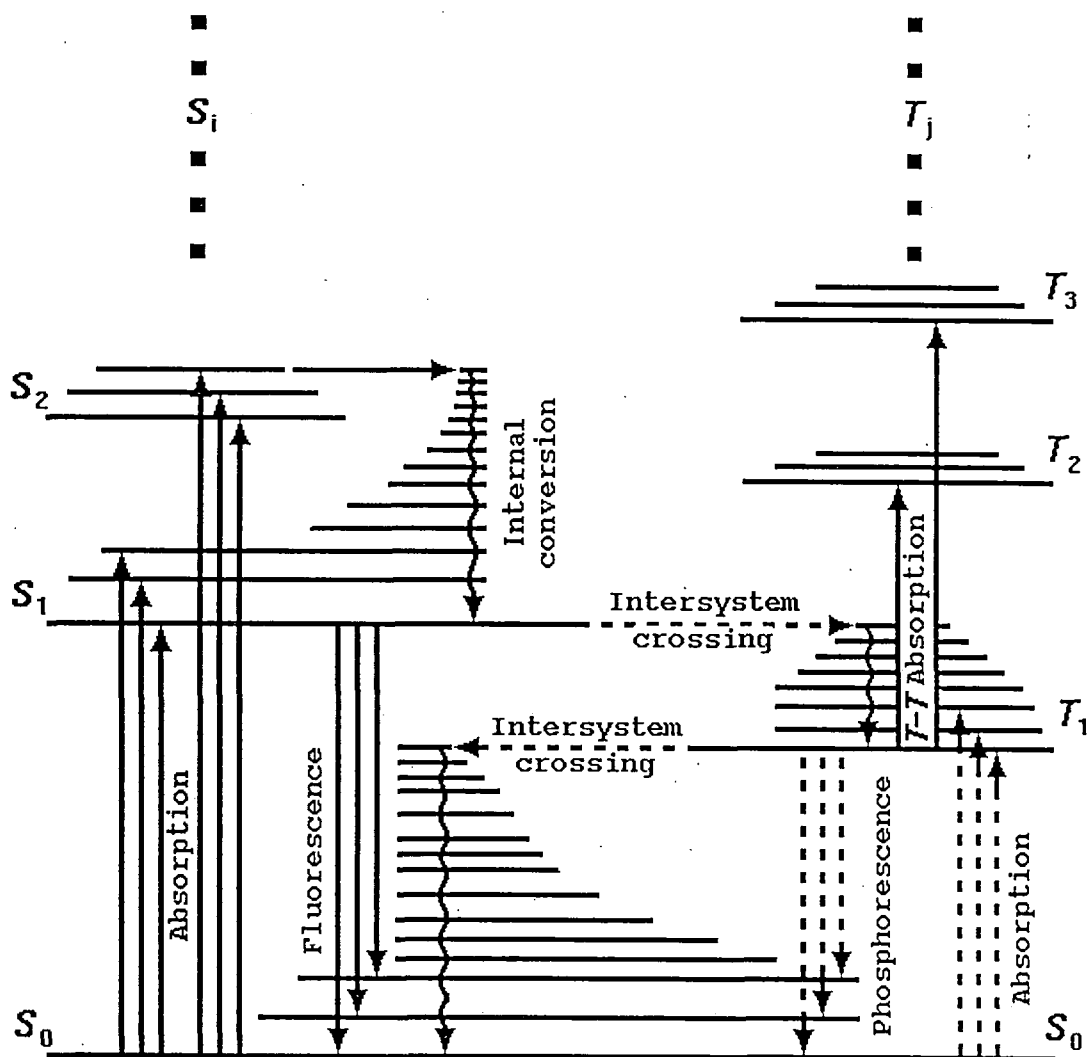


Figure 1.5: A schematic diagram of the lower energy levels of an organic molecule (d'Hendecourt *et al.* 1986).

ferent as well as difficult to reproduce in the laboratory. In a medium where the molecules are completely isolated and thus collision free, the fate of the energy imparted to the molecule is very different. Note that isolation is the required criterion to satisfy the emission mechanism to explain the aromatic infrared bands because the molecule cannot relax its excess energy via other radiationless transitions. Transitions within the molecule, at a constant total energy, will play an important role e.g. IVR is expected to occur (Parmenter 1982; Smalley 1983). Spectroscopic studies of isolated molecules have been made possible only very recently with experiments involving isolated ultracold molecules which are produced in supersonic expanding jets so that the study of the relaxation of collision free molecules can be undertaken.

## 1.4 Diffuse interstellar absorption bands

### 1.4.1 General background

There are now about 105 diffuse interstellar bands (DIBs) which are observed in the line of sight of a variety of galactic and extragalactic objects as absorption features (Herbig 1975; Herbig 1988). The DIBs were discovered by Merrill (1934) nearly six decades ago and have been the subject of much observational and theoretical research. However their origin still remains a mystery. The strongest of these features near  $4430 \text{ \AA}$  was observed and originally misidentified as  $H\gamma$  by Cannon, some time between 1911 and 1919, in the spectrum of a heavily reddened B supergiant (Code 1958). The bands at  $5780$  and  $5797 \text{ \AA}$  were noted and considered as possible stationary by Heger (1922) in her study of early type spectroscopic binaries, though their significance was not realised at the time. It was not until Merrill (1934) that the interstellar nature of four of the narrow features in the yellow-red was established. That these features arise in the cold intervening interstellar medium and seem to be associated with at least one component of the dust, which gives rise to the interstellar extinction, has now been established, by many authors, from the good agreement between their intensities and the degree of interstellar reddening.

However the correlation is not good enough to isolate any particular grain population as the carrier. In some cases the intensities of the various bands correlate better with each other than with colour excess, indicating a common source (Deeming and Walker 1967). When the band strengths are compared with IR, visible and UV extinction measurements the correlations are weak, except for the 4430 Å band which correlates strongly with the 2175 Å extinction bump (Wu *et al.* 1981). No correlations remain between the UV extinction and band strengths when the basic dependence on  $E(B-V)$  is removed, except for a marginally positive correlation between  $4430 \text{ Å}/E(B-V)$  and the 2175 Å bump strength (Seab and Snow 1984). As the correlation evidence began to favour the dust hypotheses in 1939 the arguments between gas and dust were triggered.

Both the equivalent width ( $W_\lambda$ ) and the reddening  $E(B-V)$  are measures of the total column density of interstellar matter. A strong and simple relationship is expected between them, but the relationship is observed to be neither. The lack of strength is seen by the fact that a variety of indicators of the extinction have been found to correlate better with each other than they do with the bands (Wu *et al.* 1981), and the lack of simplicity is seen in the way in which the regression lines of ( $W_\lambda$ ) on  $E(B-V)$  usually make positive intercepts on the ( $W_\lambda$ ) axis instead of passing through the origin (Herbig 1975). The value of the slope of the regression is poorly defined and can vary between investigations by more than the errors of measurement e.g. the slope for 5780 Å found by Snell and Vanden Bout (1981) is a factor of 2 greater than that found by Herbig (1975). Also the ratio of the equivalent widths of pairs of bands from star to star varies considerably (Chlewicki *et al.* 1986; Josafatsson and Snow 1987; Krelowski and Walker 1987). There is therefore more influences on ( $W_\lambda$ ) than can be described by a simple measure of the column density such as  $E(B-V)$ .

Herbig conducted a major survey in 1975 and produced a list containing 39 diffuse features between 4400 Å and 6850 Å that were regarded as interstellar. He measured their equivalent widths and central intensities in the photographic spectra

of 57 early type stars. Since then Sanner *et al.* (1978) and Herbig and Soderblom (1982) have added bands between 6850 and 8700 Å together with a group of 29 weak lines between 6767–6862 Å by Herbig (1988). Regions which contain a number of prominent DIBs have received special attention especially in the region 5700–6400 Å (Josafatsson and Snow 1987; Westerlund and Krelowski 1988*a*; 1988*b*; Benvenuti and Porceddu 1989). Herbig and Leka (1991) have recently found 22 new DIBs on high signal to noise scans of reddened O- and B-type stars, in the region 5840–8650 Å. Most of the new DIBs occur in the region masked by atmospheric O<sub>2</sub> and H<sub>2</sub>O. Joblin *et al.* (1990) have recently detected new DIBs in the near infrared at 1.18 and 1.32 μm.

The DIBs have remained unidentified partly due to the lack of precisely determined observational profiles thus making it impossible to compare with profiles derived theoretically by laboratory experiments. The lack of intrinsic profiles is essentially due to two reasons. Firstly in the cases where one would expect to find DIBs formed in single clouds i.e. nearby slightly reddened stars, the DIBs are very weak. When the DIBs are seen in nearby virtually unreddened stars they are often ill-defined due to insufficient signal to noise ratios and in some cases due to blends with weak stellar lines. Secondly DIBs as well as other interstellar absorption features are usually studied in the spectra of OB stars, many of which may still be embedded in the remnants of their parent clouds. As these stars are frequently rather distant the interstellar features are often built up of contributions from several clouds along the line of sight. These clouds may differ appreciably in their optical properties i.e. their ability to produce certain DIBs, as well as radial velocities producing composite DIBs, with profiles differing from intrinsic ones (Herbig and Soderblom 1982; Krelowski and Westerlund 1988). Herbig and Soderblom (1982) have demonstrated that the sharp DIB at 6196 Å and possibly that at 6614 Å showed several components in certain directions, where galactic rotation introduced differences in radial velocity between the intervening interstellar clouds. Westerlund and Krelowski (1988*a*, 1988*b*) have determined ‘intrinsic’ DIB profiles of the lines at

5780, 5797, 6196, 6284, and 6379 Å by the deconvolution of multicomponent data, as well as from observations on nearby stars which have relatively small colour excesses. Modern detectors have permitted the study of very weak DIBs provided that high resolution is also available. These type of observations are rather scarce though.

High resolution observations enable the determination as to whether the DIBs features are resolvable into fine structure and if not to determine their intrinsic profiles which could provide some indication as to the absorption mechanism. A detection of fine structure would indicate a gas phase molecular origin, however several observers (Danks and Lambert 1976; Snell and Vanden Bout 1981 etc) have found asymmetries or broadening but even with high signal to noise ratio and resolution as good as 0.1 Å there was in no case any breakdown into discrete structure. Unfortunately profile variations might also be expected if the bands originated in either small dust or in impurity absorptions. Also large asymmetric molecules will have a high density of fine structure lines producing less readily resolved variations in the bands.

Conflicting results have been reported when band strengths have been compared with the total column density of molecular hydrogen in the same line of sight. In some cases the bands are observed to correlate with  $N(\text{H}_2)$  (Kumar *et al.* 1982; Federman *et al.* 1984) but Meyer (1983) finds fairly strong 5780 Å and 5797 Å bands in the lines of sight where  $N(\text{H}_2)$  is quite low. Abundance considerations argue against a gas phase carrier indicating that the DIBs arise in molecular grain mantles but this does not rule out the presence of some exotic molecules that do not depend upon the supply of molecular hydrogen for their existence.

### 1.4.2 Families of diffuse interstellar bands

Krelowski and Walker (1987) in a recent extensive study noticed that 10 of the yellow/red and the 4430 Å DIBs in the spectrum of the lightly reddened star ζ Persei (HD 24398,  $E(B-V) = 0.29$ ) showed unusual relative intensities and together with the broad 2200 Å interstellar feature were compared with the stars ζ Ophiuchi

( $b = 23^\circ$ ),  $\theta$  Orionis ( $b = -18^\circ$ ), and HD 200775 ( $b = 14^\circ$ ), all of which lie at high galactic latitude. If the clouds were circumstellar the grains would be subject to the effects of the high ultraviolet flux from the star. However in the case of  $\zeta$  Persei it is likely that the effect is more typical of interstellar clouds at high galactic latitude.  $\zeta$  Persei ( $b = 16^\circ$ ) is a member of the OB2 association and lies more than 100 pc above the galactic plane. The DIBs in  $\zeta$  Persei appear to fall into 3 well defined groups.

1. 4430 Å and 6180 Å are both absent
2. 5780, 6196, 6203, 6269, and 6284 Å are about a third of the strength expected for the colour excess
3. 2200 Å feature and 5797, 5850, 6376, 6379, and 6614 Å are approximately normal strength for the colour excess

This suggests that the DIBs may be caused by at least three agents where the proportions vary from cloud to cloud. They also note that other stars with markedly anomalous DIB intensities also tend to lie at high galactic latitude ( $b > 15^\circ$ ). Krelowski (1989) gives one clue as to why the proportion of the different carriers is not fixed, if it were the existence of families would never have come to light. He notes that the density of the interstellar gas seems to be important in defining the preferred habitats of the carriers, with the carrier of family 1 preferring dense gas. In subsequent studies supporting evidence has been found for the importance of density and that the carrier of family 2 prefers denser gas than that of family 3 (McIntosh and Webster 1992). Less is known about family 1 and its relationship to the other two families. The bands in this family are so different from the others since it only contains broad bands whilst the other families contain only narrow bands. This could possibly reflect an important difference in the carriers which an understanding of the habitat might help to solve. McIntosh and Webster (1993) have found that the relative strengths of the bands at 4430, 5780 and 5797 Å correlate

with the modulus of the galactic latitude. Family 3 was found to prefer high latitudes and family 1 low latitudes, with the carrier of family 2 showing intermediate behaviour. It is supposed that this dependence reflects a more basic dependence on height above and below the Galactic plane, the carrier of 4430 Å evidently prefers conditions near the plane where the gas density is high and the carrier of the 5795 Å prefers the more tenuous gas further out.

Spectra of 59 stars were obtained by Josafatsson and Snow (1987) in order to measure the diffuse band strengths between 5690 Å and 5870 Å. In particular they measured the equivalent widths of the DIBs in the lines of sight towards stars in reflection nebulae and tested for correlations among the bands. Based on the degree of correlation between the band pairs, as well as with  $E(B-V)$  and the 2175 Å extinction bump, they divide the bands into three groups, each class being the result of either a specific carrier or physical process.

1. narrow bands at 5780, 5797, and 5849 Å which show good correlation with each other and  $E(B-V)$ . Note that Krelowski and Walker (1987) divided this group into two.
2. broad bands at 5778 Å and 5844 Å, these correlate very badly with  $E(B-V)$  and the very broad 5778 Å band is the only one that shows a very good correlation with the 2175 Å bump.
3. 5705 Å which correlates fairly well with all the other bands as well as with  $E(B-V)$ .

Krelowski (1989) suggests that the measurements of equivalent width and reddening can be divided into two regimes depending on whether the value of  $E(B-V)$  is greater than or less than 0.7 mag. In the first regime there is a strong correlation with  $E(B-V)$  whereas in the second any correlation is much weaker.

Porceddu *et al.* (1991) show high resolution data on the red DIBs at 6196, 6203 and 6205 Å and provide convincing evidence that each belongs to a different family. They note that the changes in intensity ratios are not accompanied by any changes of

the profile shapes. Chlewicki *et al.* (1987) had previously suggested that the whole system around 6200 Å had a common origin because the relative intensities of the bands in all the observed lines of sight seem to be constant within the observational error. However these observations of heavily reddened stars had a high probability of averaging the effects of several different clouds along the line of sight and so a constant ratio may only represent a galactic average. The spectra presented by Benvenuti and Porceddu (1989) may indicate a contrary result to that of Chlewicki *et al.* (1987).

Herbig and Leka (1991) mention the large number of DIBs that are now known. This is far more than would be expected in the spectrum of a single species at interstellar temperature which must mean that a substantial number of different carriers are responsible for the DIB spectrum. A single substance would only produce a small number of absorption lines under interstellar conditions unless absorptions from excited levels were possible. With one or two exceptions they found no convincing regularities in the positions or spacings of the known DIBs in their investigation which also argues against the spectrum being produced by one or a very few carriers. The spectrum must therefore be able to be divided up into different families according to the carriers responsible. It has therefore become increasingly evident during the past few years that the DIBs are caused by several different agents and therefore their classification into subsets or ‘families’ sharing an intrinsic common behaviour is of basic importance for a possible identification of their carrier.

One of the families of DIBs with bands at 5797, 5850, 6376/9, and 6614 Å has counterparts in the emission spectrum of the Red Rectangle at very similar wavelengths (Fossey 1991; Sarre 1991), see section 2.3.4. The shapes of the emission and absorption bands are similar for the cases where profiles of the DIBs are known (Herbig and Soderblom 1982; Westerlund and Krelowski 1988*a*).

### 1.4.3 Possible carriers of the bands

Since 1934 a wide variety of processes which might be operative under interstellar conditions and might be capable of producing this enigmatic spectrum have been proposed. These processes involve either small dust grains, impurities embedded in grains, or gas phase molecules. Smith *et al.* (1977) reviewed the problem and presented arguments both for and against the dust particle origin and the gas phase molecular origin of the bands. The strongest argument against a molecular origin of the bands has been the belief that gas phase molecules would be unable to survive the harsh environment of the ISM making it impossible for them to exist in quantities large enough to account for the observed band strengths. Recently a collection of ionized very stable complex gas phase molecules known as PAHs have been suggested as possible carriers of the DIBs (van der Zwet and Allamandola 1985; Léger and d'Hendecourt 1985; Crawford *et al.* 1985).

The PAHs have certain thermodynamic and spectroscopic properties that make them attractive candidates as the carriers of the DIBs. They are much more stable than other molecules with the same number of atoms due to delocalization of electrons in the molecular orbitals. For a given number of rings the most stable molecules will have the most condensed configuration possible (Stein 1978) e.g. pyrene is more stable than chrysene which is more stable than tetracene and hexabenzocoronene A is more stable than form B (see fig. 1.3). Van der Zwet and Allamandola (1985) believe that it is these condensed configurations that will be most favoured in the interstellar medium. Multiply charged PAHs are also quite stable. They have exceedingly low photodissociation rates for carbon skeleton break-up and can therefore exist in sufficient numbers to account for the DIBs, if they are formed at reasonably high rates. The first ionization potential lies in the range 6–8 eV, with the second ionization potential at about 20 eV. The long wavelength absorption band limit depends on the dimensions of the molecule with the longest linear dimension dominant e.g. pyrene, hexabenzocoronene A, and ovalene the limits are 3800, 4500, and 4700 Å respectively (Clar 1964). In nearly all cases the spectrum consists of sev-

eral broad, largely temperature independent overlapping bands with an increase in absorption strength towards shorter wavelength. In the diffuse interstellar medium many of these species will be partially hydrogenated and positively charged which leads to strong absorption bands in the visible (Crawford *et al.* 1985). The observed line-shapes and widths of the DIBs can be explained by rovibronic band contours and linebroadening due to internal conversion. PAH appear to be better candidates than the long carbon chains that have previously been proposed.

Léger and d'Hendecourt (1985) predict the absence of the DIBs in special astrophysical environments is such that all the carbon is locked up in CO. Further observations are required in order to confirm this. Likewise if the observed bands are due to ions then in the case of dense clouds, where the stars are deeply embedded, the degree of ionization of PAH should decrease and consequently the DIBs intensity. An example is HD 200775, the illuminating star of NGC 7023. Here the PAHs are submitted to a higher radiation flux as a consequence of the star proximity but it is still possible to estimate that the higher density of the medium may overcompensate that and lead to a lower ionization of these molecules. Snow (1973) has reported that neither the 4430 Å nor the 5780 Å bands are observed.

Rotational contours of electronic spectra of candidate molecules as possible carriers of the DIBs have been calculated and compared with the profiles of some of the DIBs (Danks and Lambert 1976; Cossart-Magos and Leach 1990). Cossart-Magos and Leach (1990) test the possibility that the carriers are large organic molecules such as PAH's and their ionized species. In particular they calculated the rotational contours of coronene at various temperatures ranging from 3–100K and different spectral resolution. These simulations showed multi peaked structures which did not correspond to the observations of the four narrow DIBs profiles obtained by Westerlund and Krelowski (1988*b*). They suggest various mechanisms by which the spectra could be smoothed into single peaks in the ISM. They suggest inadequacies in the technique used for determining the intrinsic profiles of the observed DIBs; line broadening due to intramolecular relaxation in neutral or ionic PAHs; and temper-

ature variations within a single molecular cloud. They conclude that their results cannot definitely rule out the PAH assignment. The problem with PAHs is that there are a large number of such molecules and as yet the few which have been studied in the laboratory do not have spectra that match those of the DIBs. Support for the PAH assignment is suggested by Cohen and Jones (1987) in the claim that the intensity of some of the DIBs is enhanced in regions where infrared emission ascribed to PAH/PAH ion species occur.

Absorption bands of the naphthalene cation,  $C_{10}H_8^+$ , in an argon matrix at 5 K, are claimed to match in wavelength some DIBs (Salama and Allamandola 1992). One of the strongest features in their spectrum coincides with a weak DIB at 6742 Å. They estimate that 0.3% of the carbon in the ISM would have to be in the form of  $C_{10}H_8^+$  if this species were responsible for the observed DIBs. A discrepancy though is that their laboratory spectra show the 6741 Å feature (FWHM 55 Å) to be much wider than the interstellar band 6742 Å (FWHM 3.5 Å). Since the laboratory data were obtained under conditions that do not match those of the diffuse interstellar medium, particularly in density, it is possible that environmental effects are responsible for the discrepancy and that the same transition is really much sharper in free gas phase  $C_{10}H_8^+$  at low density. They also predict the possible existence of diffuse bands at other wavelengths where  $C_{10}H_8^+$  showed strong transitions. Snow (1992) has sought evidence for a diffuse band at 6151 Å with negative results. They derive upper limits which seem to conflict with the  $C_{10}H_8^+$  hypothesis. However there are uncertainties in the expected width of the predicted DIB and since the observations did not include data on the 6742 Å feature it is not known if the  $C_{10}H_8^+$  feature is actually present in the observed cloud. There is also uncertainty about the possible wavelength shift between laboratory data and the interstellar spectra due to matrix effects in the laboratory spectra. More laboratory spectra are really required for a greater variety of PAHs. Attempts to find the DIBs at positions expected for a transition in the hypothetical spectrum of interstellar  $H^-$  and at wavelengths of lines in the laboratory spectrum of  $Cr^{3+}:MgO$  were inconclusive (Herbig and Leka

1991). The  $H^-$  transitions have been proposed as relevant to the DIB problem and  $Cr^{3+}:MgO$  has been suggested as a constituent of the interstellar grains. They made a systematic search in the wavenumbers of the 105 DIBs for vibrational sequences of the type  $0 \rightarrow v'$ . None of those found were very convincing.

Polyhedral carbon species have been suggested as possible candidates for the source of the absorption bands (Kroto 1987), as have their ions and various complexes (Léger *et al.* 1988). These theories were based on the supposed stability of these species and predicted electronic spectra. Several of the arguments that support PAH molecules as possible carriers of the DIBs can also be applied to the polyhedral carbon ions. However the ultraviolet and visible spectrum of neutral  $C_{60}$  recently observed in the laboratory (Leach *et al.* 1992) suggests that neutral  $C_{60}$  is not a carrier of the main DIBs. Astronomical searches in a restricted region have been unable to rule out the possibility that  $C_{60}$  is present in the ISM (Snow and Seab 1989). Webster (1992) proposes fullerenes which are partially ( $C_{60}H_n$ ) or completely ( $C_{60}H_{60}$ ) hydrogenated as the carriers of the DIBs. Their carbon skeleton structures are assumed implicitly or explicitly to be quasi-spherical. The hydrogen atoms covalently bonded to the surface of a fullerene change the structure of the  $\pi$ -electron system and thereby modify the optical properties, determining not only the diffuse band spectrum of the molecule but also the UV cross section. It is thought that the physical and chemical environment in the ISM controls the degree of hydrogenation so that changes in the environment give rise to spatial changes in the optical and ultraviolet properties of the medium. The theory goes some way to accounting the tendency of the 4430 Å family to be weak both in the diffuse clouds of the ISM and in directions in which the far ultraviolet extinction is high.

Edwards and Leach (1993) have calculated the rotational band contours of some predicted electronic spectra of the icosahedral molecule  $C_{60}$ . Reasonable molecular constants have been obtained from the experimentally measured geometry of the molecule in the ground electronic state and some assumed geometries for the excited state. The contours are calculated for a range of temperatures corresponding to

those which might be expected in the interstellar medium. The simulated contours are compared to the observed spectra of the DIBs from which they conclude that for rotational temperatures above 100 K the simulated profiles can reproduce the form and peak width of some of the interstellar bands and therefore the polyhedral carbon species cannot be excluded as a carrier of some of the DIBs. The contours are intended to augment the set of contours calculated for PAHs by Cossart-Magos and Leach (1990) for comparison with present and future observations of DIBs.

Webster (1993) presents a theory in which the carriers of the DIBs are members of an unspecified class of molecular hydrides denoted by  $XH_m$ , where  $m = 0, 1, \dots, m_{\max}$ ). The bands are carried by several species which differ in  $m$ , the number of hydrogen atoms they bear. Since the average number of hydrogen atoms is taken to be variable from place to place and to be determined by a dynamical equilibrium between photodetachment and chemical attachment reactions the difference between carriers will have observable consequences. Carriers with different numbers of hydrogen atoms are expected to have different interstellar habitats and they suggest that this underlies the observational partitioning of the bands into families. The carriers are assumed to be well mixed with the interstellar gas and dust but even so the equivalent width of any band is not simply proportional to the reddening; it also depends on what fraction of the population along the line of sight is in the form of the appropriate carrier. From their measurements of 5797 Å and 5780 Å they conclude that the fractional abundance of both carriers is low in dense gas and that the differences between the plots indicates that the carrier of 5780 Å bears more hydrogen atoms than that of 5797 Å. They argue for the fullerenes  $C_{60}H_m$  as the carriers. The correlation of the families of bands with Galactic latitude (McIntosh and Webster 1993) in terms of this theory implies that the carrier of the 4430 Å bears the most hydrogen atoms and that of 5797 Å bears the fewest.

## 1.5 Summary

### 1.5.1 ERE and the interstellar grains

ERE is a broad luminescence feature centered around  $6800\text{\AA}$ . Earlier in this chapter two main types of grains were discussed as the origin of this excess emission; HACs and PAHs. The major difference between these grains is their size; HACs being  $200 - 2000\text{\AA}$  compared to PAHs which are  $<10\text{\AA}$ .

Watanabe *et al.* (1982) have shown that HAC exhibits a broad luminescence band characteristic of ERE. The emission mechanism can then be explained in terms of electron-hole recombination. They also demonstrated how a reduction in the hydrogen concentration would cause the peak wavelength to increase as a result of a decrease in the band gap energy. This is in agreement with the observations of ERE where the peak wavelength is seen to vary according to the location. HAC is created in the ISM either via the accretion of C and  $\text{C}^+$  by silicate dust or by the rehydrogenation of hydrogen poor amorphous carbon. The latter was shown to take place in  $\text{H}_2$  photodissociation zones near bright stars. HAC contains both a component of 'graphite' like carbon ( $E_g = 0.3\text{ eV}$ ) and 'diamond' like carbon ( $E_g = 2.5\text{ eV}$ ), the ratio of which is normally 1. However newly formed HAC tends to be rich in the 'diamond' like carbon and therefore has a high band gap energy. As hydrogen is lost the ratio increases and emission shifts from the *R* waveband into the *I* and even into the infrared for older grains. The structure of HAC was also discussed in some detail. It is considered to be composed of clusters of aromatic rings aggregated to form a solid. The studies showed that only clusters with 5-7 rings would be able to survive. According to a formula derived by Robertson and O'Reilly (1987) this would produce  $E_g = 2 - 2.5\text{ eV}$ .

PAHs have already been accepted as the origin of the unidentified infrared features. Although they have also been suggested as the cause of the ERE there is still a lack of laboratory data and no molecule as yet has been found to identically resemble the spectrum of the ERE. Naphthalene has been discussed in some detail. As the

excitation energy increases the spectrum was observed to change from sharp separate emission peaks to a more diffuse and broad spectrum. This was interpreted in terms of a IVR process. The emission mechanism would then be explained in terms of fluorescence. Larger molecules like hexabenzocoronene produce similar results resembling the position and width of the feature observed in the Red Rectangle. However for larger molecules the mechanism of emission is best explained as due to phosphorescence. The main differences between fluorescence and phosphorescence is that phosphorescence has a much longer lifetime and involves the spin forbidden transition  $T_1 \rightarrow S_0$  whereas fluorescence only involves the singlet states. PAHs can be formed in a similar way to HACs by  $C^+$  accretion. The possibility of formation by the condensation in carbon rich envelopes was also mentioned although this process is not believed to be efficient enough. Three methods of destruction were briefly mentioned; erosion by collision with gas in shocks, photothermodissociation particularly in small PAHs and double ionization in large PAHs.

### 1.5.2 DIBs

DIBs arise in the diffuse ISM and over 100 bands have been identified so far. The lack of intrinsic profiles has made identification difficult. No fine structure has been found and together with the abundance considerations indicates that the origin is either due to molecular mantles or exotic molecules which do not depend on a supply of molecular hydrogen. The DIBs have been categorised into families which suggests that more than one carrier is responsible. This would explain the varying intensities of the families in different clouds, since the each carrier will prefer a different habitat. PAHs, which have already been discussed in connection with ERE, are also suggested as the origin of the DIBs, in particular the more stable condensed configurations. The rotational contours of the electronic spectra have been studied but proved inconclusive. However there are many PAHs which still need to be studied in a laboratory. The naphthalene cation  $C_{10}H_8^+$  is believed to match some of the DIBs in wavelength but problems arise in trying to match the width. Many

uncertainties exist in the relationship between the laboratory conditions and those in the ISM. Most of the arguments used for PAHs can also be used for polyhedral carbon species together with their ions. However the existence of  $C_{60}$  in the ISM is debatable, but calculations of the rotational contours for  $C_{60}$  have been shown to resemble DIBS for rotational temperatures  $>100$  K and therefore they cannot be ruled out. Fullerenes which are either partially or fully hydrogenated depending on their environment have also been proposed. This would relate to there being different families according to the amount of hydrogenation.

### **1.5.3 Relevance to ERE of observations on the Red Rectangle and on NGC 7023 and NGC 2023**

It is necessary to clearly identify the regions in which ERE exists and thus determine the level of contribution of ERE and any variations in peak wavelength and width in order to determine the interstellar grains responsible. It is also important to be able to establish any connection between ERE and the DIBs which might help explain the latter's origin. In the following chapters observations are described on the Red Rectangle and on NGC 7023 and NGC 2023 which provide evidence for the role of PAHs, HACs, fullerenes and DIBs. A re-examination of the spectra of the Red Rectangle obtained in 1981 by the Durham Polarimetry Group together with the analysis is presented in chapter 2 where evidence for DIBs and fullerenes is concluded. Polarimetry provides an important measure in astrophysics. By the use of colour maps a differencing technique is used which allows the ERE regions within NGC 7023 and NGC 2023 to be clearly identified. This is independent of information on the central star which is required in a technique used by Witt. A review of these two nebulae is presented in chapter 3 with the new data and new extended analysis in chapter 4.

# Chapter 2

## The Red Rectangle

### 2.1 Physical conditions

The Red Rectangle is a small reflection nebula illuminated by the bright star HD 44179, first discovered in 1975 as an infrared source in the AFCRL sky survey by Walker and Price. The nebula extends approximately 40" in a north-south direction, although wispy extensions can be traced out further. The system lies in the Milky Way at a distance of  $\sim 330$  pc (Cohen *et al.* 1975). In the blue waveband the nebula has the appearance of being very weak amorphous but generally centred on HD 44179. In the yellow waveband the star is surrounded by a small bright elliptical nebulosity. However in the red waveband the nebula appears to be a symmetrical bicone with the illuminating star at the apex and two extended 'spikes' or brightness enhancements emanating symmetrically from its corners, seen along the lines where the surface of the cone, viewed tangentially, is superimposed on lower surface brightness (Cohen *et al.* 1975). The limb-brightening implies that the nebula consists of an optically thin biconical surface instead of a filled biconical volume (Webster 1979). The narrowness of the neck of the bicone suggests that its axis is in the plane of the sky. In the near-infrared the spikes are only weakly visible (Cohen *et al.* 1975).

The following model has been proposed for the bipolar nebula. The central star is surrounded by an equatorial disklike structure of gas and dust in which the

inner edge of the toroid restricts the diffusion of light from the central object except into two cones of semiangle  $\sim 30^\circ$  around the normal to the disk. HD 44179 is a strong infrared source which implies there is considerable thermal emission by surrounding dust (Russell *et al.* 1978). Cohen *et al.* (1975) suggest that within the two cones starlight suffers local reddening by an admixture of small and large grains before escaping from the vicinity of the disk, eventually to be scattered in our direction by an extensive enveloping halo of gas and perhaps small dust grains. It is suggested that only quite cold grains can be present in the halo ( $T \leq 150$  K). The colour temperature of the infrared source is  $\sim 500$  K.

In 1915 Aitken discovered that HD 44179 was a visual binary which when resolved had components of nearly equal brightness with separation less than  $0''.3$ . Meaburn *et al.* (1983) made speckle observations of the double obtaining a separation of  $0''.29$  and speculating a period of 60 years. His results are treated with some scepticism since the presentation of his data is not completely convincing. Heintz (1990) however has made more recent observations and obtains much smaller measurements of  $0''.14$  and  $0''.17$  and concludes that the period is much greater, approximately 600 years. He also calculates that the distance of the binary is much further than previously thought falling between 450–600 pc. The lack of molecular absorption features in the near infrared rules out the companion being a late type secondary and the very weak atomic nebular emission precludes a hot companion. The two stars are therefore assumed to be identical of type B8 - A0 II - III (Cohen *et al.* 1975; Schmidt *et al.* 1980) with bolometric luminosities being  $\sim 360L_\odot$  each. Two alternative models of HD 44179 are provided by Greenstein and Oke (1977), one suggestion is a B star with an extended neutral shell, the other is an unusual Population II F giant.

The luminosity is somewhat large though for a normal A0 III or B8 III star. Another peculiarity is that the extinction derived from the colour excess in the visual indicates that  $E(B - V) \sim 0.4$  mag, which cannot provide enough absorption and re-radiation to explain the ratio of the infrared to stellar flux. Clearly this

object is not a normal star with a moderate standard of circumstellar extinction. Two possible solutions have been provided by Rowan-Robinson and Harris (1983). The first is that HD 44179 is at the centre of the Red Rectangle and a special geometry is required to provide sufficient amount of infrared radiation. In this case the distance would have to be reduced to 140 pc to fit the flux constraints. Secondly it was suggested that the central source was an A0 or late M star hidden behind 22 mag of visual extinction, the visible radiation being contributed by a companion star.

It is now generally accepted that the material which constitutes the nebula actually originates in another star, not HD 44179, perhaps a carbon star undergoing mass loss so that the dust is locally produced relatively young material sufficiently close and faint relative to the bright star to be unresolved. Recent speckle observations reveal two sources at near infrared wavelengths, a compact source  $0''.2$  across and an extended source  $1''$ . N/S by  $0''.4$  E/W (Dainty *et al.* 1985; Leinert and Haas 1989). Polarimetry in the *K* waveband, including both the central and extended source, revealed a low polarization suggesting that scattering off grains associated with the bipolar flow is not a plausible source of the infrared emission. The spatially resolved emission is elongated in the direction of the bipolar flow and is interpreted as thermal dust emission (Dainty *et al.* 1985). Leinert and Haas (1989) found a pronounced asymmetry of the Red Rectangle in the near infrared and the observations revealed a more complicated structure than in the earlier studies. Of the two components of different size known so far they resolve the smaller one into two, a narrow structure ( $0''.2$  in size) which is superimposed on the more extended infrared emission and an unresolved compact source. They identify the compact source with HD 44179 which is offset to the south by  $0''.15$  from the other two components. For the compact source the fraction of brightness remains constant with wavelength; the relative contribution of the narrow structure increases with wavelength as might be expected for an embedded source; the relative contribution of the larger structure decreases with wavelength as is typical for scattered light. They discuss the

possibility that HD 44179 is not at the centre of the Red Rectangle but that the source of the mass loss is an object deeply enshrouded at the core of the nebula with HD 44179 located slightly nearer to the observer. The two stars then probably form a binary.

Leinert and Haas suggest a very special geometry as shown in fig. 2.1. The larger envelope would be illuminated from both inside and outside by the compact infrared source and partly seen in the reflected light. Similarly visual light from HD 44179 would be reflected on a larger scale from material associated with the Red Rectangle. This would make the blue appearance of the nebula diffuse and almost circular. In the red where HD 44179 is weaker the structure might be dominated by the central object embedded in the envelopes. This geometry leads to a lower polarization because the light from the star in front is reflected by the more extended envelopes in backscattering. The light of the envelopes themselves will be unpolarized as far as it is thermal radiation and the light from the larger envelope should still be polarized by single or multiple scattering. The model is also able to explain the observed infrared to visual flux ratio. The weaknesses however are that there is no direct observational evidence available for the special arrangement of the stars and that two near infrared sources of nearly the same colour temperature would be required.

Cohen *et al.* (1975) in early studies considered HD 44179 to be a pre-main sequence star. Zuckerman (1976) however postulated with some reservation that HD 44179 is an evolved star, based on the molecular emission and the lack of connection with an interstellar cloud complex, perhaps a proto-planetary nebula. High resolution spectroscopic observations of HD 44179 were carried out by Waelkens *et al.* (1992) in order to determine photospheric abundances. The iron abundance is extremely low  $[\text{Fe}/\text{H}] = -3.2$  to  $-3.5$  with the CNO and S abundances being solar within an order of magnitude. The fact that C and/or He are overabundant compared with the sun confirms the theory that the star is a low mass object in the advanced stages of evolution since the enrichment in He and C of the outer stellar

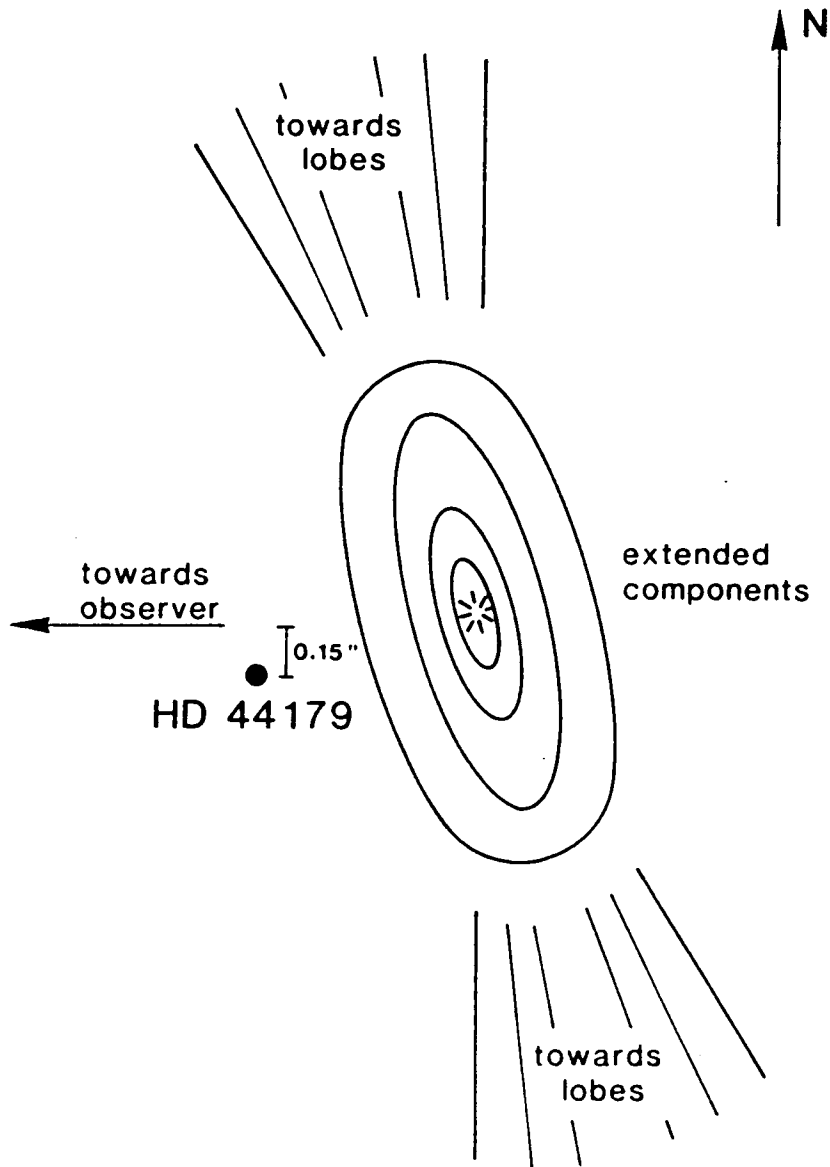


Figure 2.1: The model of the inner parts of the Red Rectangle, proposed by Leinert and Haas (1989), in which the central source is within the extended infrared structures. They have chosen the tilt (unknown) of the system to bring out HD 44179 into the equatorial plane.

layers is not normally thought to take place before the star reaches the asymptotic giant branch (AGB). However the abundance pattern does not agree with theoretical expectations from AGB nucleosynthesis. The fact that the star is a low mass object is also supported by its moderate to high galactic latitude. The high luminosity of the star leads to the idea that it is in the transition between AGB and planetary nebula phase. This post AGB theory is supported by the known infrared excess due to dust which is seen as additional evidence that the peculiar iron abundance is related to the presence of dust. The luminosity of the star, the apparent brightness and the fairly small reddening all indicate that the nebula is of a considerable size thus suggesting that the initial mass of the central star was not particularly low. It is therefore improbable that the low iron abundance is primordial. Waelkens *et al.* (1992) observations imply that the photospheric abundance of C and O is about the same and therefore the C/O ratio might be greater than one but only slightly. HD 44179 is assumed to be a carbon-rich object since the infrared emission features are normally attributed to C bonds which are only expected from clouds with a C/O ratio greater than one since only C atoms that are not locked in CO molecules are available.

Initial observations were made of the star and nebula by Cohen *et al.* (1975) and attention was drawn to a large Balmer jump. A normal B star atmosphere could not be fitted to this spectrum. In the ultraviolet the spectrum of HD 44179 is characterised by the virtual absence of the broad extinction bump at 2200 Å (Sitko *et al.* 1981). Duley (1985) thus precludes the presence of appreciable amounts of graphite dust since graphite particles with sizes  $\leq 40\text{nm}$  exhibit a plasmon resonance (Huffman 1977) in the vicinity of 2100–2200 Å even when coated with water ice or glassy carbon (Hecht 1981). The lack of the 2200 Å extinction also suggests that oxygen rich condensations are depleted in the Red Rectangle since a model for the interstellar dust attributes this feature to an electronic excitation of  $\text{O}^{2-}$  ions in small oxide or silicate particles (Maclean *et al.* 1982). Alternatively it means that the appropriate subset of grains that give rise to the feature have been modified in

some way. The spectrum shows a flat ultraviolet continuum and absorption due to gaseous CO has been observed between 1200–2000 Å with the possibility of emission due to either CO or a molecule containing C≡C, C≡N, C–C and C–H bonds, or both (Sitko 1983). The CO column densities in this object are high,  $N \sim 10^{18} \text{ cm}^{-2}$ . At wavelengths  $\leq 1600 \text{ Å}$  there is a precipitous decline in flux; the distribution of flux at wavelengths less than 1400 Å suggests that the star has spectral type  $\sim A0$ . The extinction curve for HD 44179 rises rapidly at wavelengths less than 1700 Å suggesting the presence of small grains. However such an effect might be caused to some extent by the absorption due to CO. Duley (1985) suggests that carbon dust in the Red Rectangle is amorphous since amorphous carbon produces a rapidly rising extinction for  $\lambda < 1700 \text{ Å}$  without the appearance of a 2200 Å band, similar to that seen in the spectrum of HD 44179. He points out that the amplitude of the rise in extinction between  $6\text{--}8 \mu\text{m}^{-1}$  may be larger than that produced from amorphous carbon alone. However the effect of absorption by gaseous carbon and possible emission may influence the apparent extinction by up to  $\pm 1 \text{ mag}$  at  $\lambda^{-1} = 6 \mu\text{m}^{-1}$  and perhaps  $\pm 2 \text{ mag}$  over the range  $7\text{--}8 \mu\text{m}^{-1}$ . The CO absorption also reduces the intensity on the  $\text{O}^{2-}$  absorption band and produces a shift to shorter wavelengths which is consistent with the extinction in HD 44179, which shows weak residual absorption peaking at  $4.7\text{--}4.8 \mu\text{m}^{-1}$ .

The nebular extinction towards HD 44179 has been compared with the interstellar curve towards a star in which the far ultraviolet extinction is very strong (Webster 1993). They are similar in that they both rise steadily from visible wavelength to a shallow peak ( $\sim 4.6 \mu\text{m}^{-1}$ ), fall slightly to a minimum ( $\sim 5.5 \mu\text{m}^{-1}$ ) and rise again beyond  $6 \mu\text{m}^{-1}$ . In both, the far ultraviolet extinction is very strong and the ‘bump’ is very weak. The only significant difference is that the extinction at higher frequencies is greater in HD 44179 and the ‘bump’ might be even weaker but overall the extinction curve does not differ greatly from the interstellar curves. Webster therefore adopts the hypothesis that the interstellar and the nebular extinctions have the same carrier which enables the testing of a new theory in which

the dominant component of the ultraviolet extinction is attributed to the fullerane molecules and their ions. The principle requirement is for the fullerane molecule to be found in a high concentration throughout the nebula and is therefore the only source of opacity that may be plausibly associated with emission phenomena energized by ultraviolet light. These fulleranes would also by astronomical standards have to be in an extreme condition bearing fewer hydrogen atoms than elsewhere, presumably as a consequence of the high rate of ultraviolet photolysis caused by the bright star HD 44179. The starlight would acquire the characteristic absorption signature of lightly hydrogenated fullerenes.

The study by Waelkens *et al.* (1992) of HD 44179 referred to earlier has revealed a set of emission lines near 4200Å but the carrier was not identified. Hall *et al.* (1992) have compared the reported wavelengths with known laboratory spectra and show that these lines arise from CH<sup>+</sup> which is an abundant astrophysical molecule, the reasons for this are still unknown. The six reported lines at 4225.82, 4227.14, 4229.45, 4232.70, 4237.67, and 4239.49 Å form an excellent agreement with the laboratory data (Carrington and Ramsay 1982). The observations of CH<sup>+</sup> in the Red Rectangle shows that the molecule is warmer than in diffuse clouds where only the absorption line at 4232.55 is detected, because the temperature is sufficiently low that only the lowest rotational energy level will be populated. Hall *et al.* (1992) determine a rotational temperature of CH<sup>+</sup> to be  $120 \pm 50$  K. This is rather low compared with the central temperature of the star. The line widths of CH<sup>+</sup> are two or three times narrower than those of the stellar absorption lines of atomic carbon. Their study confirms that the molecule is in the surrounding nebula rather than the star. Balma and Jura (1992) have also independently identified the new features with the presence of circumstellar CH<sup>+</sup> in the outflow. The features are assigned to emission from low lying rotational transitions in the (0,0) band of the A<sup>1</sup>Π - X<sup>1</sup>Σ<sup>+</sup> electronic system of the methyldyne ion. They claim that the presence of this molecule is probably a result of a photodissociation front produced by ultraviolet emission from the central star propagating through the circumstellar molecular

envelope. The most likely emission mechanism is radiative excitation followed by rapid fluorescent decay from the excited state. Observations of molecular ions in the envelope of the Red Rectangle are consistent with the proposal that carriers of the DIBs are also molecular ions.

The optical spectrum shows weak He I, C I and O I absorption lines and complex emission and/or absorption of  $H\alpha$ , Na I and Ca II at various low velocities. Moderate resolution near infrared spectroscopy of the Red Rectangle shows an almost featureless spectrum (Thronson 1982). No positively detected emission or absorption was found in the limit  $1.5-2.5\mu\text{m}$ , only a very red continuum. Considering the spectral type of the star the lack of hydrogen Brackett features was not surprising. A possible very weak CO absorption at  $2.3\mu\text{m}$ , which would suggest the contribution of a late type giant star to the emission, was noted. Since this is a low excitation star with little obscuring matter there was no reason to expect  $H_2$  emission.

The first spatial resolution observations (Low 1979) performed at  $5\mu\text{m}$  showed the Red Rectangle to be one of the few infrared sources which were clearly extended. High resolution infrared spectra of HD 44179 show strong unidentified infrared emission features located at  $8.7\mu\text{m}$  and  $11.3\mu\text{m}$  superimposed on a smooth continuum, first recognized by Merrill (in Cohen *et al.* 1975), which are attributed to mineral carbonates or sulphates. However the feature normally seen at  $9.7\mu\text{m}$ , which is a signature of silicates, was absent. The features are interpreted as being due to resonance bands in dust particles which implies that the emission is not optically thick. Merrill (1977) has since detected the other associate features at 3.3, 6.2, and  $7.7\mu\text{m}$  in great strength and Russell *et al.* (1978) has also detected the two emission features at 6.2 and  $7.7\mu\text{m}$ . The infrared emission was found to be rather flat between  $1-30\mu\text{m}$  and being broader than that of a single temperature blackbody they concluded that there is a significant range of temperatures in the dust cloud and that the cloud is optically thin throughout the infrared. The lack of any other emission in the near-infrared was noted by Cohen *et al.* (1975).

Tokunga and Young (1980) describe the feature at  $3.3\mu\text{m}$  as broad and smooth

and most likely to be caused by solid state resonance bands in grains. The data of Geballe *et al* (1985) showed that the 3.3–3.5  $\mu\text{m}$  spectrum displayed more variation than was previously thought clearly resolving two emission features one at 3.3  $\mu\text{m}$  and the other at 3.4  $\mu\text{m}$ . They also point out the existence of a third feature centered near 3.45  $\mu\text{m}$ . The fact that the features are resolved and smooth indicates that they are due to emission lines from atoms or simple gas phase molecules, unless the features are unresolved *Q*-branches. This is plausible for the relative narrow 3.4  $\mu\text{m}$  feature. However none of the likeliest simple molecules (CH, CH<sup>+</sup>, NH, NH<sup>+</sup>) has a *Q*-branch at that wavelength and therefore they conclude, as others, that the features have other origins. Geballe *et al.* (1989) detected 3.3  $\mu\text{m}$  emission 5" N of HD 44179 indicating that the region producing this emission is very extended. Contrary to previous observations Tokunaga *et al.* (1988) found that HD 44179 has 3.3  $\mu\text{m}$  emission but no 3.4  $\mu\text{m}$  feature. It should be noted that Geballe *et al.* (1989) centered on a region just off HD 44179 thus indicating a change in composition or excitation of emitting material surrounding the illuminating star. The spatial nature of the spectrum at 10  $\mu\text{m}$  has also been examined by Grasdalen *et al.* (1992). They find that at least two regions are producing 10  $\mu\text{m}$  radiation from HD 44179. One region produces nearly featureless continuum and is represented by the central source, the second region is much more extended than the central source and produces the unidentified infrared emission features and another feature at 12.8  $\mu\text{m}$  which may be related to these or may be Ne II. From the data they conclude that emission features are extended by at least 1". Very weak CO( $J=1 \rightarrow 0$ ) line emission at 4.7  $\mu\text{m}$  was observed in the spectrum of HD 44179 (Knapp 1986; Bachiller *et al* 1988). The CO outflow velocity from this source is unusually small perhaps only 5  $\text{kms}^{-1}$ . The CO feature is probably of circumstellar origin and the weakness of this line and its small width indicate a small CO density.

Cohen *et al.* (1975) note that there are no diffuse interstellar bands seen in the spectrum of this object. They also found that there is no radio or X-ray emission. Geldzahler and Cohen (1983) made a high sensitive search at 1.465 GHz and

4.885 GHz in an attempt to find evidence of radio emission in the Red Rectangle. They were unsuccessful and concluded that it was unlikely that HD 44179 was another example of an SS433 type object giving a  $3\sigma$  upper limit of 0.09 mJy. Alternatively if the Red Rectangle was a bipolar nebula then any radio emission would be thermal. They suggest that the absence of thermal radio emission in the Red Rectangle could result from either optical thickness or a variety of conditions in both temperature and electron density. They therefore conclude that their findings were not unusual.

## 2.2 Polarization

Observations initially made by Cohen *et al.* (1975) suggest the existence of large grains which dominate the polarization near  $1\ \mu\text{m}$ . The result supports the suggestion of a disk around the central star. They interpret their results as requiring the dust disk to be viewed nearly edge on.

If the broad bump seen in the visible spectrum of the nebula (see section 2.3.1) is due to an emission processes then it would be expected to reduce the polarization within the feature. Schmidt *et al.* (1980) measured the polarization at two positions  $10''$  N and  $10''$  S of HD 44179. The results obtained were  $P_B \sim 7\%$  and  $P_R \sim 2\%$  which showed that there was indeed a reduction in polarization, but a constant position angle, through the bump which indicated that the emission originates within the nebula itself and dilutes the scattered starlight. Perkins *et al.* (1981) also tested to see if the emission feature was due to scattered light and made linear polarization maps in the red and blue wavebands. A centrosymmetric pattern of polarization vectors was found around HD 44179 proving that the apex star was indeed the illuminating source. The percentage polarization was found to be significantly less in the red than in the blue within the bicone and on the spikes with typical values in the blue of 20%. The reduction in the red polarization was found to be a factor of four but outside the bicone the blue and red polarizations were approximately equal. Their results were therefore consistent with those of Schmidt *et al.* (1980).

Unlike the intensity images, spikes were found in both the red and the blue polarized intensity maps (Perkins *et al.* 1981). They therefore concluded that there was enhanced dust density on the biconical surface together with a favourable scattering geometry in order to explain this. This gives support for Schmidt *et al.* (1980) theory that the red emission arises on the surface of the bicone and is unpolarized. It does not originate from scattering of starlight even by grains with a peculiar albedo.

## 2.3 The Nebula Spectrum

### 2.3.1 The Optical Features

Cohen *et al.* (1975) were the first to show that the spectrum of the nebula and star appeared to have a very broad emission feature centred at  $6900 \text{ \AA}$ . Low resolution ( $50 \text{ \AA}$ ) spectrum of the Red Rectangle taken in the brightest parts of the nebula within  $10''$  of the central star show a scattered stellar spectrum on which is superposed a smooth and symmetrical broad bump which extends over  $\sim 2500 \text{ \AA}$  (FWZI) with FWHM  $\sim 800 \text{ \AA}$  (Greenstein and Oke 1977). It is centered approximately on  $H\alpha$ , at  $6500\text{--}6600 \text{ \AA}$ , has a comparable intensity to the scattered light and peaks about 1.5 mag above the continuum. This feature is not seen in the spectra of the star. The broad feature itself consists of a large amount of structure which includes groups of strong emission lines superposed on the diffuse components, seen more clearly on the moderate resolution spectra ( $10 \text{ \AA}$ ) of Schmidt *et al.* (1980). The unidentified features are recorded in table 2.1.

Warren-Smith *et al.* (1981) have taken high resolution ( $1 \text{ \AA}$ ) spectra of the nebula in several places and spectra of the central star covering the wavelength range  $3400\text{--}6600 \text{ \AA}$ . They identify three distinct types of emission features in addition to the previously mentioned broad feature.

- Narrow emission lines of NaD (strong),  $H\alpha$  (weak), and CaII H and K (strong) from very low excitation plasma. These lines are intrinsic emission from the

Peak Wavelength (Å) Schmidt <i>et al.</i> (1980)	Peak Wavelength (Å) Warren-Smith <i>et al.</i> (1981)	Profile
5800	5799	R-type
5826	5828	M-type
5853	5855	R-type
5885	5880	R-type
5914	5913	M-type
5940	5938	M-type
	6109	M-type
	6208	M-type
6378	6378	M-type
6394		
	6420	M-type
	6563	M-type
6615	6615	R-type

Table 2.1: Unidentified emission features in the spectrum of the Red Rectangle. The results are from Schmidt *et al.* (1980) and Warren-Smith *et al.* (1981).

nebula and not scattered starlight since the central star spectrum shows narrow emission lines of NaD (strong),  $H\alpha$  (strong) but no detectable H or K emission. It might even show weak K line absorption. The NaD lines varies in ratio across the nebula from  $\sim 2:1$  just within and outside the bicone where it is optically thin and  $\sim 1:1$  on the spikes where it is optically thick. This confirms the hollow structure of the nebula. These lines do not broaden or split across the nebula.

- ‘R-type’ band-like features. These are characterized by a sharp rise on the shorter wavelength side and gradual degradation on the longer wavelength side. These features occur at 5799, 5855, 5880 and 6615 Å, with the third one being less prominent than the rest. The degree of red degradation appears to be reduced on the spikes of the bicone apart from which the features seem to have very similar structure with their relative intensities remaining constant with position in the nebula.

- ‘M-type’ diffuse features which are broad (10–20 Å FWHM) and roughly symmetrical, centered on 5828, 5913, 5938, 6109, 6208, 6378, 6420, 6563 Å. There is also the possibility that there might be weak features in the blue spectrum which they were unable to detect except maybe a feature at 4044–4053 Å.

Witt and Boroson (1990) provide two profiles of the Red Rectangle, one at 10" S of the star and one 6" S. The central wavelength/bandwidth values for these profiles are shown in Table 2.2. They find that the sharp lines near 5800 Å are visible as a single feature on the short-wavelength wing of both the band spectra which they present. Most remarkable is the drastic change in the relative strengths of the 6380 Å and the 6617 Å features between the two offsets. At 10" south, the 6617 Å feature is barely detected, whereas at 6" south, the same feature dominates the centre of the band. The ERE band intensity is as much as 25 times larger than it is found in any other reflection nebula. They conclude that the ratio of  $I_{ERE}/I_{SCA}$ , where  $I_{ERE}$  and  $I_{SCA}$  are the ERE and scattered intensities respectively, increases with decreasing angular offset from the star HD 44179. The ERE band strength varies with position in this nebula even more than the scattered light intensity. Their observations are consistent with a geometry where most of the dust is beyond HD 44179 as seen from earth. ERE is emitted isotropically whereas dust scattering is strongly forward directed at visible wavelengths, hence only material predominantly behind HD 44179 will show the observed ratio of  $I_{ERE}/I_{SCA}$ .

Long slit spectroscopy throughout the nebula shows that the intensity ratios of the five sharp features 5800, 5826, 5855, 5880, 5938 Å are constant across the face of the nebula which suggests a common emitter for all five features (Schmidt and Witt 1991). These sharp features however exhibit a measurably different spatial intensity distribution from that of the broadband ERE indicating distinct but possibly related origins. The sharp emission features are most intense either at or slightly inside ( $\sim 1''$ ) the biconical interfaces, which are formed by an apparent bipolar outflow from a central object through the surrounding nebula. The ERE is more broadly distributed across the equatorial regions and reaches a maximum intensity

Slit PA	Slit Position	$\lambda_c$ ( $\text{\AA}$ )	$\Delta\lambda$ ( $\text{\AA}$ )	$I(\text{ERE})$ ( $\text{ergs cm}^{-2} \text{s}^{-1} \text{sr}^{-2}$ )	ERE/Scat
NS	Slit 6" E of HD 44179	6643	770	$2.6 \times 10^{-3}$	0.53
EW	Slit 10" S of HD 44179	6590	760	$2.0 \times 10^{-3}$	1.00
EW	Slit 6" S of HD 44179	6839	920	$7.1 \times 10^{-3}$	1.06
EW	Slit 7" N of HD 44179	6581	740	$3.0 \times 10^{-3}$	1.25
EW	Slit 14" N of HD 44179	6522	700	$4.0 \times 10^{-3}$	0.70

Table 2.2: Extended red emission detections by Witt and Boroson (1990), where  $\lambda_c$  is the central wavelength and  $\Delta\lambda$  is the bandwidth.

in the walls of the biconical structure beyond the contact surface. The line width is interpreted as due to rotational structure broadening, so the fact that the central wavelengths of the sharp features exhibit blue shifts of 2–5  $\text{\AA}$  with increasing distance from the central star coupled with an observed decrease in width of the sharp features is interpreted as due to a decrease in the population of high rotational states of the emitting molecules with increasing distance from the source of excitation.

### 2.3.2 The Emission Source

Searches have been made through compilations of molecular band information by Schmidt *et al.* (1980) who found no single species to be able to convincingly explain the spectrum of the Red Rectangle. Any molecule that was able to produce a system similar in appearance to the group observed were also expected to produce strong features elsewhere in the spectrum which were not detected.  $\text{H}_2\text{O}^+$ , a strong emission component in cometary spectra (Wehinger *et al.* 1974), produces a good agreement in its (0,9,0) transitions with several of the 5800  $\text{\AA}$  lines but there is no sign of the (0,8,0) or (0,7,0) bands which are just as prominent in comets. Likewise CaCl shows some agreement in the 5800–6370  $\text{\AA}$  range. FeO produces strong diffuse emission in the orange as well as bands near the 5600, 5800, 6050, 6225  $\text{\AA}$  groups but the matches are only approximate both in wavelength and strength agreement. The  $\text{C}_3$  molecule produces the best fit with phosphorescent lines at 5856, 5874, 5911, 5969

and  $6308 \text{ \AA}$  in a neon trapping with a  $50 \text{ \AA}$  shift to the red in argon (Weltner and McLeod 1964). Additional support also came from the presence of strong absorption due to CI toward HD 44179 in both optical and ultraviolet. The  $C_3$  as well as  $C_2$  features have already been seen in another bipolar nebula, GL 2688. However the  $4050 \text{ \AA}$  system of  $C_3$  which is prominent in the spectra of GL 2688 is not seen in the Red Rectangle, neither is the strong  $5 \mu\text{m}$  band detected in HD 44179 seen in GL 2688 (Merrill 1977). They pointed out though that many detailed laboratory studies of a large number of molecules had not at this stage been made. There was also the possibility that the observed emission arises from a common molecule under conditions which had yet to be reproduced in the laboratory since molecular signatures are often shifted and altered in structure by the laboratory conditions. If the simple molecules were trapped on grains abundant within the nebula the mode of attachment could well modify the emission wavelength. They therefore conclude that the overall feature which strongly resembles an emission spectra of some molecules remains unidentified.

Warren-Smith *et al.* (1981) support the theory that the red emission feature is due to free molecules in the nebular medium. They propose that if the  $C_3$  series were shifted  $57 \text{ \AA}$  to the blue then they would be able to identify most of the lines with transitions in the Red Rectangle. However they would not be able to identify the third strongest band at  $6615 \text{ \AA}$ . Maier (1980) has studied the spectrum of some open shell organic cations which produce spectrum with a general similarity to that of the Red Rectangle. These produce broad ( $\sim 2000 \text{ \AA}$ ) dissociation spectrum in the red,  $5000\text{--}8000 \text{ \AA}$  region, and red-degraded or middle peaked bands which are strongest on the blue end of the broad feature. Many of these linear organic molecules are built up of  $C\equiv C$  and  $C\text{--}C$  bonds. The vibrational frequency of the stretching fundamentals of these two bonds are  $2119 \text{ cm}^{-1}$  and  $629 \text{ cm}^{-1}$  respectively for the ground molecular state of dicyanoacetylene (Maier 1980). Other linear cations or even neutral molecules expected in the Red Rectangle have very similar frequencies ( $\pm 20\%$ ). Warren-Smith *et al.* (1981) point out that the strong

bands in the spectrum of the Red Rectangle at 5799 Å and 6615 Å have an energy difference of  $2127\text{ cm}^{-1}$  and that the bands at 5880 Å and 6109 Å have a difference of  $638\text{ cm}^{-1}$ . They thus conclude the high chance that the unidentified constituent which causes the ERE is constructed of  $\text{C}\equiv\text{C}$  and  $\text{C}-\text{C}$  bonds.

They suggest that the organic material might be carbyne which is made up of strings of  $\text{C}-\text{C}\equiv\text{C}$  which has been proposed as a constituent of the interstellar material and connected with the unidentified infrared bands (Webster 1980). Carbyne is stable between 2600 and 3800 K (Whittaker 1978). This is consistent with the temperature of the narrow line plasma which is seen in the bicone. Whittaker suggests that above  $\sim 3000\text{ K}$  carbyne might be produced from  $\text{C}=\text{C}=\text{C}$  ( $\text{C}_3$  molecule) by the transfer of one bond and/or from graphite grains by fracturing the hexagonal planes of which it is composed. They point out the possibility that the environment might be one of graphite and also oxygen deficient since the absence of the  $9.7\ \mu\text{m}$  feature in the spectrum of HD 44179 indicates the absence of silicate grains (Aitken 1979; 1981).

In an attempt to understand the origin of diffuse interstellar bands Wdowiak (1981) conducted matrix isolation experiments and produced a species that not only correlated with the principle absorption bands but also exhibited four fluorescent features having characters similar to those seen in the Red Rectangle. He states that one of the features is probably just *R*-line fluorescence of chromium ions as impurities in sapphire substrate, but the other features at 5740 Å and 5675 Å are related to the reaction product or products of the discharge. The first of these is the stronger feature and shows the same profile as the *R*-type emission features observed in the Red Rectangle. In some experiments Wdowiak suggests a similar behaviour for the second of these features. He also found an occasional third emission feature at 6382 Å which correlates with the *M*-type feature at 6378 Å. The strengths of the features seem to correlate well with the absorption features attributed to  $\text{C}_2^-$ . The two emissions at 5740 Å and 5675 Å are suggested as being due to a single species existing at two different kinds of site, resulting in the splitting of what would have

been one feature. The experiment suggests that either the same or similar ions and radicals are matrix isolated in the mantles of grains in the Red Rectangle which are exposed to the illumination by HD 44179. The difference in wavelength is explained by the species in the matrix having different characteristics than those of Ar, used in the experiment.

Duley (1985) suggests that hydrogenated amorphous carbons (HAC) are responsible for the extended red emission. In the mantles of the outflow cones appears to be the locations where there are short wavelength photons and the availability of atomic hydrogen for the hydrogenation of amorphous carbon. Laboratory experiments show that HAC films formed at temperatures  $T \leq 500$  K exhibit a broad luminescence band with a peak wavelength of 6400 Å. The width and shape of this emission band is strikingly similar to broad visible emission seen in the Red Rectangle. Precursor molecules for the formation of HAC via plasma deposition in the nebula could be the source of the discrete emission features superimposed on the continuum, which would explain why the emission is only seen in the nebula spectrum. Large polycyclic aromatic molecules such as coronene and hexa-benzo coronene phosphoresce between 5000 Å and 7000 Å (Clar and Zander 1956; Clar and Stephen 1965). Large polyaromatics would also exhibit the infrared emission features.

D'Hendecourt *et al.* (1986) attribute the observed emission in the Red Rectangle to the emission of highly vibrationally excited isolated PAH's molecules. They claim that the diffuse nature of the observed luminescence is a characteristic of large isolated molecules as a result of intramolecular vibrational energy randomization. Isolated molecules can be invoked to reproduce the observed spectrum. Due to the high emission efficiency of the molecules they can also explain the infrared emission bands. They calculate that the luminosity of the nebula can be reproduced by assuming that about 10% of the cosmic abundance of C is present in these molecules, assuming a quantum efficiency of 0.5 for the luminescence. This is compatible with the abundance required to explain the infrared bands.

Continuing from the previous studies Wdowiak *et al.* (1989) have subjected

mixtures of CO, CH<sub>4</sub>, N<sub>2</sub>, H<sub>2</sub>O and Ar with 42% and 8% argon to an electrical discharge, frozen out the reaction products at  $T \sim 20$  K and then subsequently warmed the sample to room temperature. This resulted in a stable residue which showed a broad fluorescence similar to that observed in the Red Rectangle. They made the composition of mixtures to be fairly consistent with cosmic abundances and proposed that the grain mantles in the Red Rectangle/HD 44179 are composed of a similar complex residue. The samples however fluoresce with the peak emission several 100 Å lower than that seen in the nebula spectra. They claim that the emission depends upon the sample characteristics and that by varying the method of preparation a residue could be produced that would match the spectrum of the nebula more closely. These residues are suggested as having formed by reactions on the grain surface induced by irradiation of absorbed species (Greenberg 1982). The optical properties of the particles present in the nebula suggest a carbonaceous material resulting from the polymerization of a cosmic mixture of elements which need not necessarily be HAC. Carbonaceous films rich in hydrogen have already been suggested as the sources of many observed interstellar and circumstellar features. The results of Wdowiak *et al.* (1989) support the hypothesis that grains or mantles primarily of H, C, N, and O composition are the source of many spectral features.

The species responsible for the sharp emission features are molecules which are themselves produced through the interaction of plasma flowing outward through the cones, chemically eroding HAC grains in the cone walls leading to the formation of molecular fragments and radicals, excited to fluorescence by radiation from the associated central star (Schmidt and Witt 1991). Laboratory experiments have shown that HAC films are readily eroded by a thermal and energetic hydrogen impact yielding molecular ions like CH<sub>3</sub><sup>+</sup>, C<sub>2</sub>H<sub>3</sub><sup>+</sup>, C<sub>2</sub>H<sub>4</sub><sup>+</sup>, C<sub>3</sub>H<sub>3</sub><sup>+</sup>, C<sub>3</sub>H<sub>5</sub><sup>+</sup>, and more massive species (Rye 1977; Vietzk *et al.* 1987).

Webster (1993) in considering the ultraviolet extinction curve proposes that all peculiarities in the spectrum can be attributed to the strong presence of fullerenes in the nebula and the high ultraviolet flux upon them. The energy absorbed from

the starlight would excite the electronic and vibrational degrees of freedom of the molecules which would then reradiate it in the visible and infrared bands as ERE and the unidentified infrared emission respectively. The ERE in the Red Rectangle would owe its exceptional brightness not only to the high density of carriers but also to the great abundance of ultraviolet energy.

### 2.3.3 The Emission Mechanism

It has been proposed that the ERE might either arise from unknown nebular emission process or in the peculiarity of the scattering cross-section of the nebular grains.

Greenstein and Oke (1977) proposed an explanation in terms of a special wavelength dependence of albedo of dust in reflection nebula since they believed that the velocity spread required to broaden the  $H\alpha$  line to its observed width was improbable. However their theory is questionable since a similar feature is absent in reflection nebula surrounding Messier 82 (Visvanathan 1974), which contains dust with the same infrared emission spectrum and therefore presumably the same material as dust in the Red Rectangle (Willner *et al.* 1977; Russell *et al.* 1978). Webster (1979) has compared the Red Rectangle with SS433 and consequently reconsidered the possibility that the red emission feature could be broadened  $H\alpha$  radiation which acquires great width as a result of kinematic process and is similar to that which gives rise to two anomalous spectral lines in SS433. These lines in SS433 are reliably identified as  $H\alpha$  emission from precessing relativistic jets ( $\beta \sim 0.27c$ ) emanating from a central object that ejects material into a cone (Abell and Margon 1979) and scattered by dust. This precession cone is reminiscent of the bicone of the Red Rectangle. However if the jets were in the nebula spectrum then due to projection effects they would be expected to vary from place to place. In fact the feature was found to vary very little with direction (Greenstein and Oke 1977).

The total luminosity radiated in the bump rules out emission due to the thermal excitation in dust grains, as proposed by Dwek *et al.* (1980) for the unidentified infrared features. Grains at a distance of  $10''$  from the central star are quite cool.

Collisional excitation of transitions by thermal electrons is also ruled out since the output of A0 III stars shortward of  $912\text{\AA}$  is only  $0.2 L_{\odot}$  (Münch 1968) and the majority of this appears as hydrogen recombination radiation in the nebular and stellar spectrum. For the same reason direct radiative pumping of fluorescent cascade in some molecules by ultraviolet emission is discarded.

Schmidt *et al.* (1980) proposed that the most likely explanation is fluorescence which occurs as a result of absorption of an optical photon where there is abundant flux from the illuminating star. They also postulated that the sharp emission features e.g.  $5800\text{\AA}$  lines, may arise in gaseous molecules as a result of transitions between vibrational states of different electronic states, whereas the more diffuse underlying component corresponds to the same transitions, but perturbed, in molecules attached to grains. The two electronic states involved would be the ground and first excited states. Another explanation of the sharp features could involve the transition ions associated with structural defects in grains. Duley (1979*a*; 1979*b*) has used this method to try and account for the diffuse interstellar bands and certain unidentified emission lines in the spectra of gaseous nebulae. There is also the possibility that the unidentified infrared emission features arise in the same emission process as the extended red emission. Warren-Smith *et al.* (1981) expanded on the theory of Schmidt *et al.* (1980) and suggested that the diffuse or degraded structure might correspond to rotational broadening and changes in the degradation from place to place correspond to a difference in excitation temperature. Linear carbon chain molecules have low transverse vibrational frequencies which could also contribute to the detailed structure of the spectrum.

Sitko (1983) has suggested that the absorption of dust in the region  $\lambda < 1600\text{\AA}$  removes sufficient ultraviolet light to enable the red emission to occur via fluorescence from HACs. D'Hendecourt *et al.* (1986) claimed that when considering PAHs as the emitter that since the emission peaks at relatively long wavelengths then phosphorescence rather than fluorescence should be considered. This argument is supported by experiments on an isolated pyridine molecule.

The emission features when produced in molecules arise from the transitions between states in which the rotational inertia of the molecule in the upper state is greater than that in the lower state, subject to the selection rule  $\Delta J = 0, \pm 1$ , individual transitions occur at lower frequencies for increasing  $J$  values. A change toward conditions of low rotational excitation thus leads to a sharpening and apparent blueward shift of the band center when observed with a spectral resolution insufficient to resolve the rotational substructure. Such shifts observed in diatomic or simple linear molecules amount to several angstrom units (Herzberg 1966). The existence of states with a broader range of rotational quantum number near HD 44179 supports the idea that free molecules or radicals are involved as opposed to matrix embedded species.

### 2.3.4 The Association with the Diffuse Interstellar Absorption Bands

The studies of Wdowiak (1981) were the first to connect the emission features with the diffuse interstellar bands but it was Sarre (1991) whom first pointed out that a set of four emission features in the Red Rectangle wavelength corresponded well with those of a recently classified subgroup of diffuse interstellar bands (DIBs) (Krelowski and Walker 1987). It is thought that at least one of the diffuse band carriers is formed in the Red Rectangle region. Table 2.3 shows the good agreement with peak wavelengths of the emission features in the nebula, which have typical widths of 6 Å and the family of DIBs, with widths of about 1 Å.

Sarre (1991) attributes the greater widths and small wavelength shifts of the Red Rectangle bands relative to the DIBs as due to the higher temperature close to the star. He also claims that the lack of emission at 5780 Å and 6284 Å might simply be due to low fluorescence quantum yield. The emission bands probably arise due to electronic transitions of one or more gas phase molecules. Sarre (1991) proposes that the  $C_{60}$  entity might be responsible for the common set of absorption and emission bands observed. Kroto *et al.* (1985) have already suggested that the  $C_{60}$

Peak Wavelength ( $\text{\AA}$ )		Profile
Red Rectangle	DIBs	
5799	5797	steep blue sided
5855	5850	
	5376	approximately symmetrical
6380	6379	
6615	6614	

Table 2.3: A comparison of the emission (Red Rectangle - Warren-Smith *et al.* 1981) and absorption (DIBs - Sarre 1991) features in the Red Rectangle

molecule or derivative is responsible for the DIBs. Preliminary simulations of the contours of unresolved *R*-branch molecular rotational lines of a  $C_{60}$  entity at various temperatures show that a small change in the rotational constant is sufficient to cause the contour to form a band head i.e. steep blue side and a red degraded tail.

Fossey (1991) has also independently noted the near correspondence in wavelength between a group of DIBs and some of the discrete emission features observed in the Red Rectangle. He suggests that the more symmetrical features at 5828  $\text{\AA}$  and 6615  $\text{\AA}$  and a shoulder on the red wing of the 6615  $\text{\AA}$  feature correspond to the blended contours of the *Q* and *P* branch rotational lines. He calculates the rotational constant of the molecule in the excited electronic state from the energy separation of the strongest *R* and *P* branch rotational lines. For a molecular temperature in the range 3000–7000 K the values obtained are typical of carbon-chain molecules of about 3–7 atoms in length or small PAH containing between 1 and 3 rings. This would rule out  $C_{60}$  and large PAH as possible candidates for the emission.

### 2.3.5 Summary

The Red Rectangle nebular spectrum is characterised by a broad luminescence feature centered around 6600  $\text{\AA}$  on which is superimposed two types of emission band-like features; red degraded and symmetrical. These bands are seen to vary in relative strength and the ratio of  $I_{ERE}/I_{SCA}$  increases with decreasing offset from the central

star. Some of the sharp features are seen to exhibit a blue shift and become narrower in width as the cooler regions away from the central star are entered. No single species has yet been found to explain the spectrum. Molecules which are able to produce a similar system are also expected to show strong features elsewhere. There is however evidence that the molecules are built up of  $C\equiv C$  and  $C-C$  bonds since their vibrational frequencies can be matched to differences in wavelengths of some of the observed features. This led to a suggestion that the material was carbyne. A good correlation has been found between the fluorescent features of  $C_2^-$  and those in the Red Rectangle indicating that either the same or similar ions might be present. Both HACs and PAHs are proposed as possible sources. HAC produces a very similar spectrum in terms of shape and width and the conditions in the Red Rectangle would appear to support its formation. An explanation for the discrete emission features would be in terms of molecular fragments and radicals. Tests have been carried out on grains or mantles of H, C, N and O composition, however the complex residue was found to fluoresce  $\sim 100\text{\AA}$  lower than required. Finally a case for fullerenes is also discussed.

The original theories for the emission mechanism were in terms of a special wavelength dependant dust albedo, broadening of  $H\alpha$  radiation, thermal excitation in dust grains or collisional excitation of transitions by thermal electrons. All of these proved to be unsatisfactory. The most likely explanation is in terms of either the fluorescence of HACs or the phosphorescence of PAHs. The sharp emission features may result as the transitions between vibrational states of different electronic states in gaseous molecules. The broad feature is then due to the same transition but in molecules attached to grains. This latter idea was developed further in terms of rotational broadening. Finally the emission features were connected with one of the families of DIBs with the  $C_{60}$  entity proposed as the common source. The following section examines in detail the association between the band-like emission features in the Red Rectangle and the DIBs in order to then identify a possible carrier.

## 2.4 New Results

### 2.4.1 Observation and Reduction Details

Observations were made at the Cassegrain F/8 focus of the 3.9 m Anglo Australian Telescope (AAT) using the Royal Greenwich Observatory (RGO) spectrograph and CCD as detector in December 1980. High resolution ( $1 \text{ \AA}$ ) spectra were taken of the Red Rectangle nebula with the slit positioned along both the spikes (PA191 and PA162) and centred on the central star. A third position (PA120) was chosen such that the slit was centred  $7''$  N of the central object and ran across the previous two positions as shown in fig. 2.2. The measurements covered the spectral range  $5700 \text{ \AA}$  to  $6660 \text{ \AA}$ . Spectra were also taken of the central star. Flatfields were observed as were a Cu-Ar lamp and a standard star for calibration purposes.

The data was re-reduced using the Figaro software package. The spectra were first flatfielded to correct for pixel to pixel variations using the average flatfield image. The sky correction was done two dimensionally by selecting two regions along the slit which were free from the nebular light, one at either end. An average value was then determined for each wavelength and subtracted from each pixel in that column of the frame. One dimensional spectra were extracted by selecting a particular region along the slit and then summing the counts along each column from the rows that made up the selected region. The calibration lamp spectra were made in the same way. Both the nebula and star spectra were wavelength calibrated and rebinned to a common wavelength scale.

### 2.4.2 Analysis of the spectra

Some of the work carried out by the author which is presented in this section has already been published in Scarrott *et al.* (1992). Fig. 2.3 shows the integrated spectrum for all the data with the slit at a position angle  $162^\circ$ . The ERE can clearly be seen to extend over the entire spectral region with the maximum occurring at  $\sim 6660 \text{ \AA}$ . Superimposed on this broad emission are many of the features which have

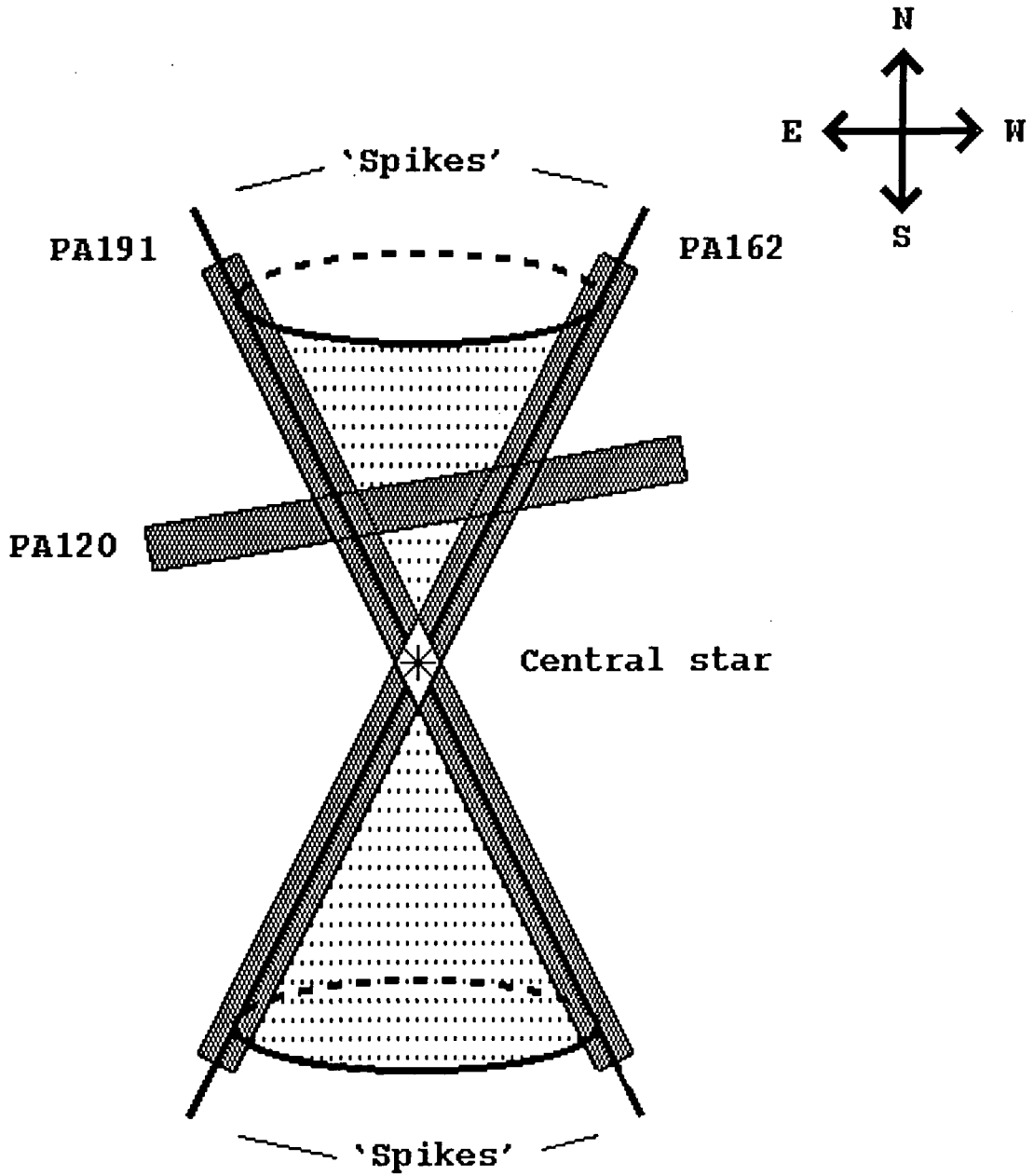


Figure 2.2: The three positions of the slit with respect to the Red Rectangle.

Peak Wavelength ( $\text{\AA}$ )	Corresponding DIBs ( $\text{\AA}$ )	Band profile
5800 (5797)	5797	red-degraded
5827		symmetrical
5853 (5850)	5850	red-degraded
5884		symmetrical
5913		symmetrical
6105		blue-degraded
6380	6379	symmetrical
6395		symmetrical
6578 (6577)	6576	red-degraded
6615 (6614)	6614	red-degraded

Table 2.4: The peak wavelengths ( $\pm 2 \text{\AA}$ ) and band type of the observed features in the summed spectra of the Red Rectangle (fig. 2.4). The peak wavelengths of the features depends on the position in the nebula. For the red-degraded bands the wavelength of the half maximum of the blue leading edge is given in brackets

already been described in section 2.3.1. Almost identical spectra were found for the other slit positions, PA191 and PA120. It should be noted that the spectrum of PA120 has already been published by Warren-Smith *et al.* (1981). When comparing the integrated spectra at the different slit positions it can be seen that some of the bands have marginally different widths which probably arises since each spectrum originates from different regions of the nebula. The variations thus reflect the different conditions. In order to emphasize the various band features a linear background representing the ERE has been subtracted, fig. 2.4, and the nominal peak wavelengths of the labelled features together with the band type are listed in table 2.4.

In order to determine if the carrier molecules have line shapes that are temperature dependent spectra of the lines at different positions along the slit, either side of the central star, were produced and are shown in fig. 2.5 for the spectral region  $5700 \text{\AA}$  to  $5920 \text{\AA}$  and in fig. 2.6, of the single feature at  $5800 \text{\AA}$ . In both cases the slit was at a position angle of  $162^\circ$  i.e. NW to SE. These individual spectra are much

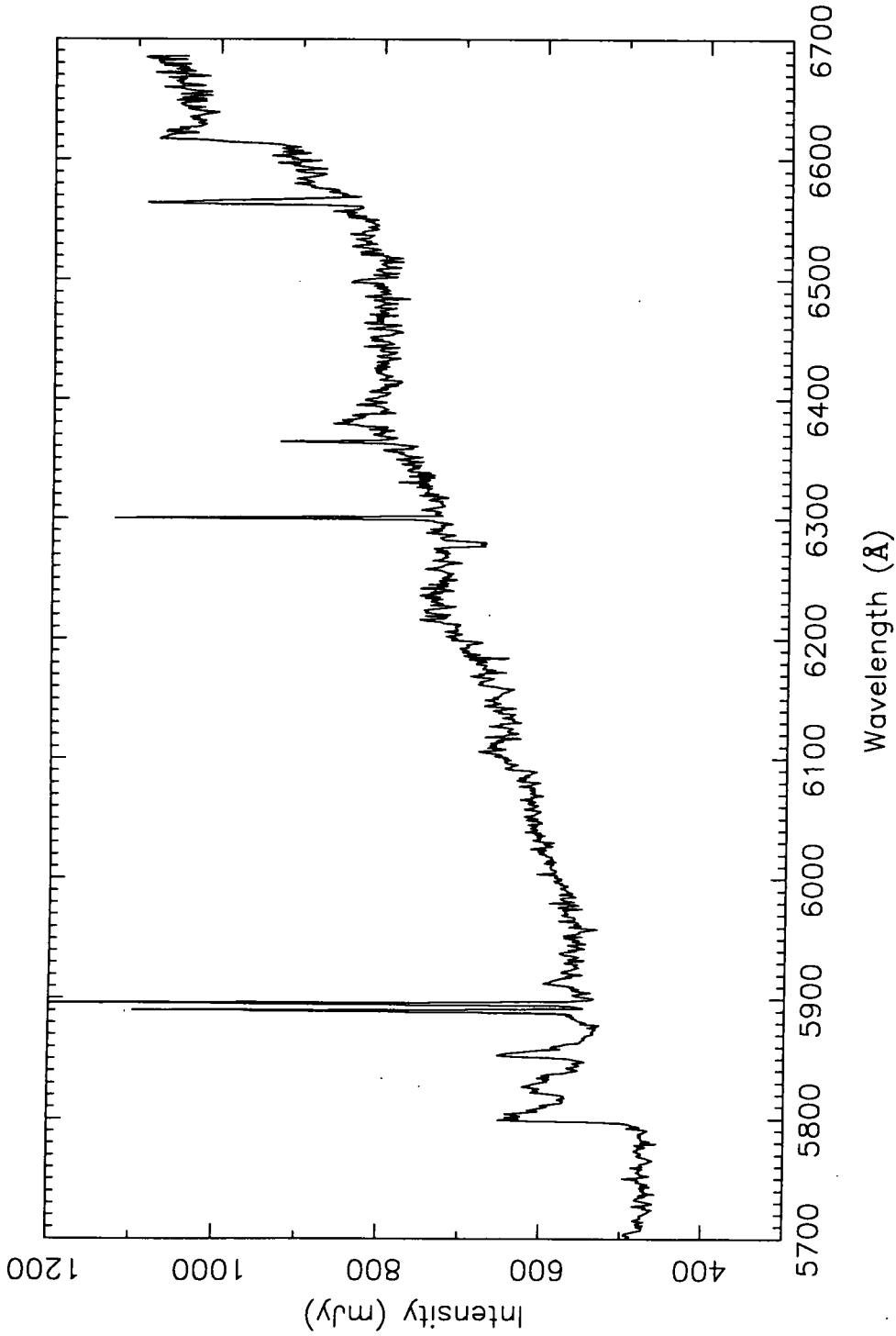


Figure 2.3: The summed spectra of the Red Rectangle with the slit at a position angle of  $162^\circ$ . This corresponds to the NW - SE spike. The integrated data represents the inner  $\pm 3''$ , excluding those that contain the central star.

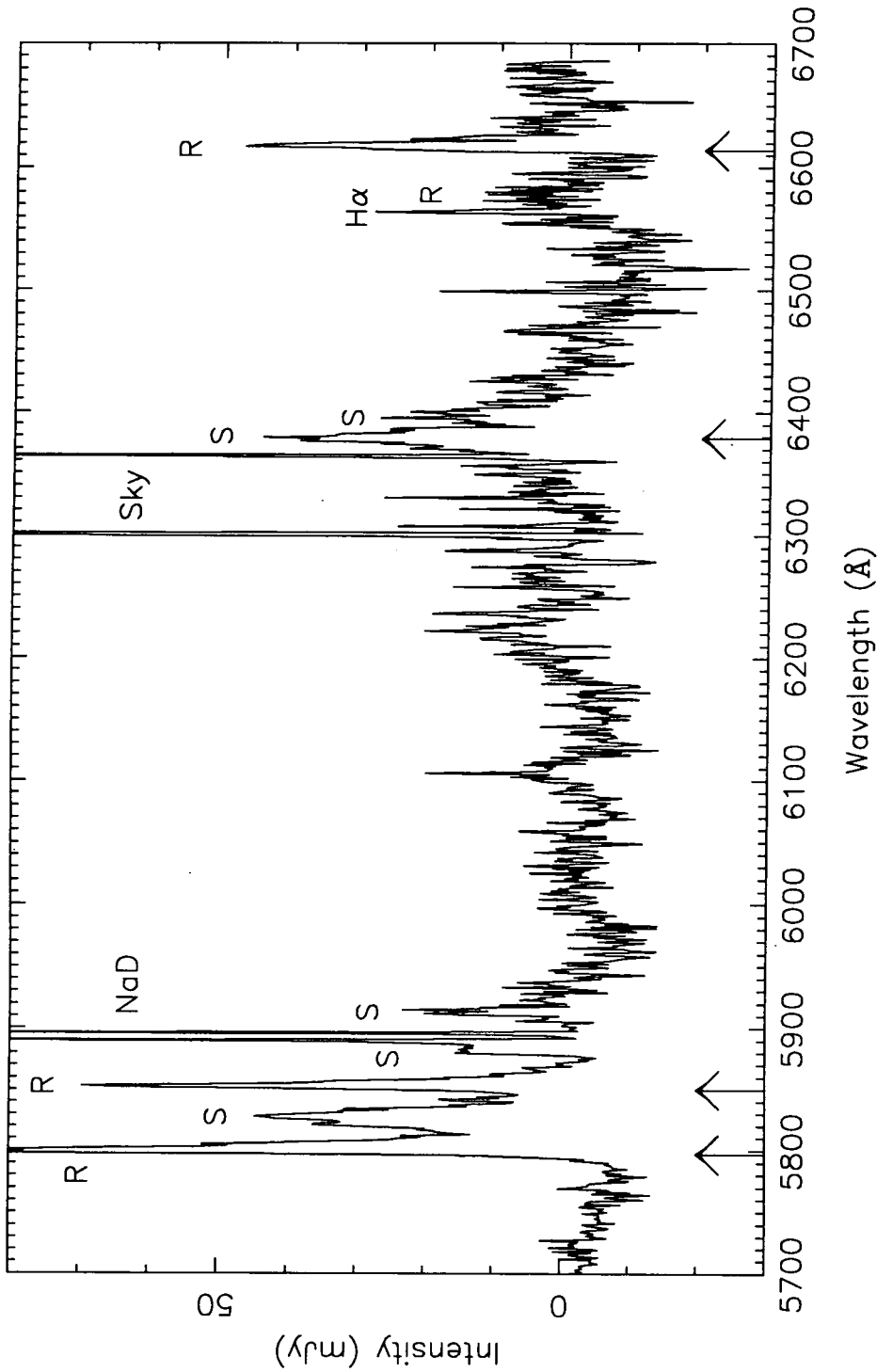


Figure 2.4: The summed spectra of the Red Rectangle with the slit at a position angle of  $162^\circ$ . This corresponds to the NW - SE spike. The integrated data represents the inner  $\pm 3''$ , excluding those that contain the central star. A polynomial fit was made to the background representing the ERE which was subtracted in order to highlight the small scale emission features. The bands are tabulated in table 2.4, the four tick marks indicate the positions of the DIBs associated with the emission bands.

noisier than the integrated spectrum and therefore do not show the fainter features which have become incorporated in the background. The spectra are numbered according to their position along the slit with the higher numbers corresponding to the SE and the lower ones to the NW. The offset between adjacent spectra is  $2.7''$ . In fig 2.5 the spectra have been added together at the edges in order to increase the signal to noise ratio. The central star would have appeared at positions 33 and 34.

As observed by Schmidt and Witt (1991), in data of lower spectral resolution, it can be seen that the bands appear to alter in shape with offset from the central star in a manner which is symmetrical about the central star. This is observed in both sets of data taken along the spikes. However in the data with the slit at position angle  $120^\circ$  no such behaviour was found as can clearly be seen in fig 2.7, which shows spectra for different positions along the slit with PA120 for the region  $5700 \text{ \AA}$  to  $5920 \text{ \AA}$ . The spectra correspond to the region of the slit inside the bicone and are numbered according to their position along the slit such that the higher numbers correspond to the E and the lower ones to the W. Almost identical spectra can be seen since one corresponds to an almost equal distance from the central star and therefore to a similar temperature.

The band width systematically increases from  $\sim 3 \text{ \AA}$  at large offsets to  $\sim 7 \text{ \AA}$  nearer the central star i.e. the width increases with increasing temperature. This property is most noticeable in the lines at  $5800$ ,  $5853$  and  $6614 \text{ \AA}$ . The peak of each band,  $\lambda_{\text{Max}}$ , shifts towards shorter wavelengths at larger offsets with the wavelength value changing by  $\sim 5 \text{ \AA}$  over the range of offsets measured. However as clearly demonstrated in fig. 2.6 the wavelength at half maximum of the blue leading edge  $\lambda_{\text{Blue}}$  of the red-degraded bands remains constant to within the measurement of accuracy ( $1 \text{ \AA}$ ) for all offsets. Also clearly seen in fig. 2.6 is the reduction in strength of each band as one moves away from the central star.

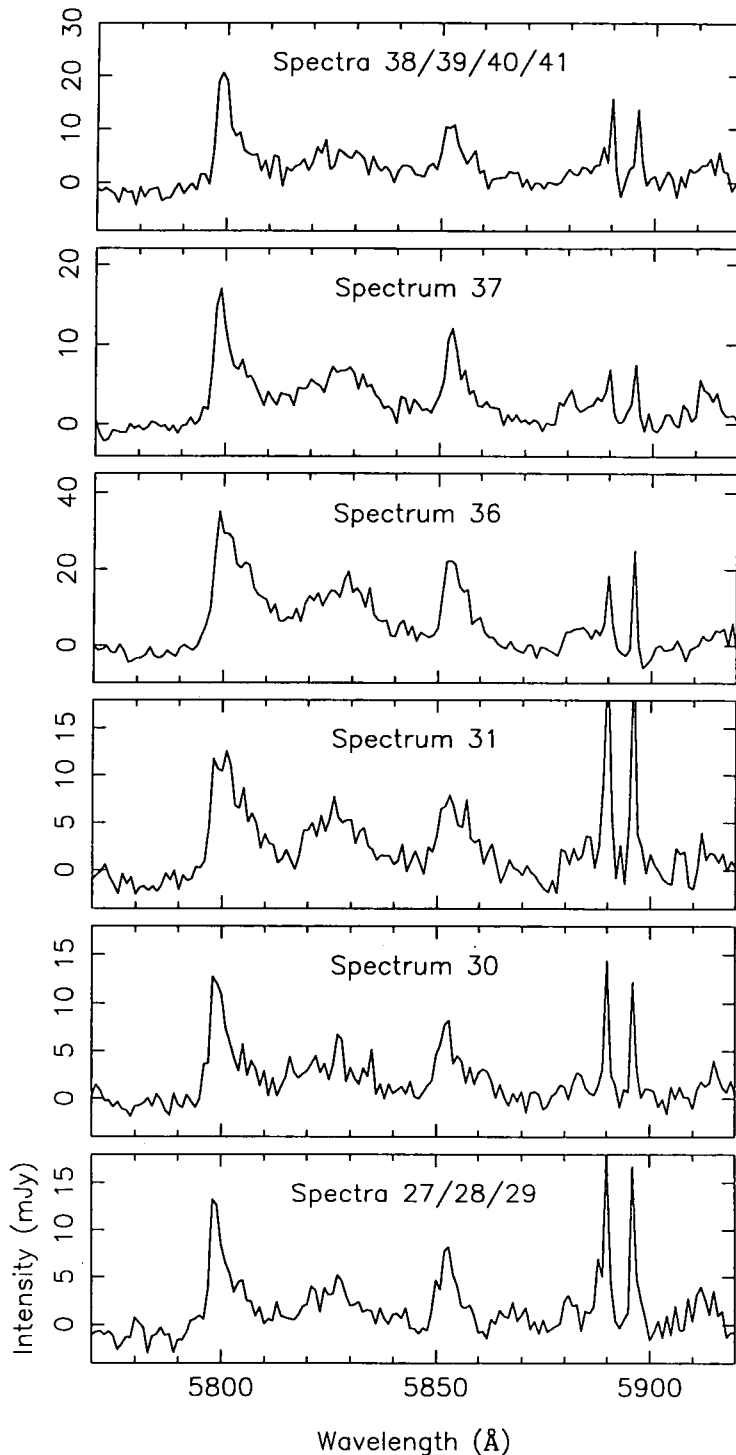


Figure 2.5: Spectra for the region 5700–5920Å with the slit at a position angle of  $162^\circ$ . The spectra are numbered from 27 to 41 according to their position along the slit, with the highest number referring to the south-east and the lowest to the north-west. Each spectrum is offset by  $2''.7$  from the adjacent spectra. The central star would appear in spectra 33 and 34. The end spectra have been summed in order to lower the noise.

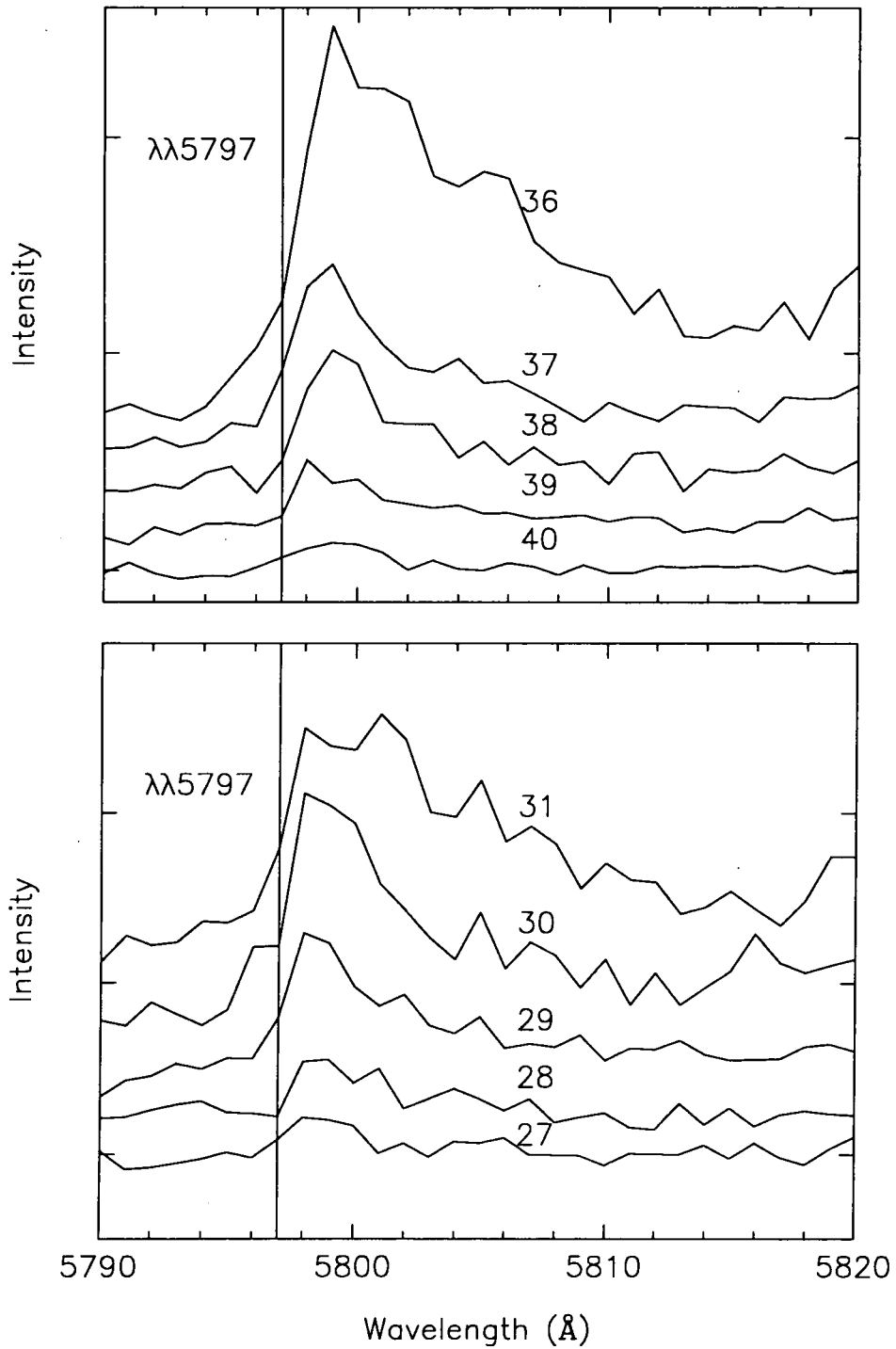


Figure 2.6: The spectra of the 5800Å feature at increasing offsets from the central star for the slit at a position angle of 162°. The top and bottom diagrams correspond to the north-west side and the south-east side respectively. The relative intensities of the spectra have been retained. The spectra are numbered as in fig. 2.5.

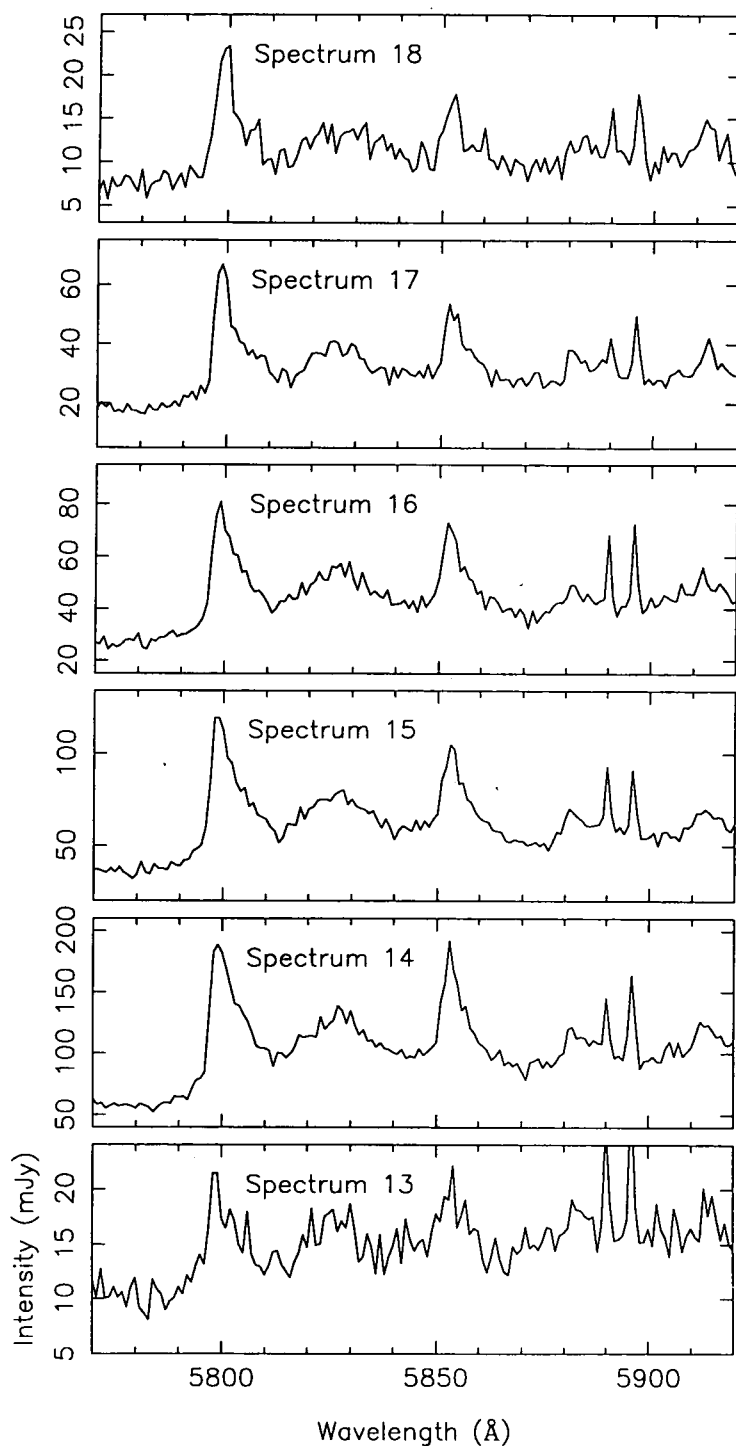


Figure 2.7: Spectra for the region 5700–5920Å with the slit at a position angle of 120°. The spectra are numbered from 13 to 18 according to their position along the slit, with the highest number referring to the east and the lowest to the west.

## 2.5 Discussion

### 2.5.1 The link with the DIBs

It has been shown in the previous section that the unique emission features in the Red Rectangle at 5795, 5850 and 6614 Å alter in both shape and peak wavelength with distance from the central star. As the temperature decreases the features become narrower ( $\sim 3$  Å), almost as narrow as the DIBs (1 Å). The peak wavelength converges towards that of the corresponding DIB and the blue leading edge of the red-degraded bands at 5797, 5850 and 6614 Å agree within the limits of the experimental errors with the value of the DIBs. Furthermore both the feature at 5800 Å and 6615 Å in the Red Rectangle have the same profiles as the absorption features; a steep blue side and a red-degraded tail. These DIBs form part of a recognised family (Krelowski and Walker 1987). The remaining members at 6376/9 Å might correspond to an unresolved diffuse emission feature at 6380 Å. There is clearly a link between the emission features of the Red Rectangle and the absorption features of the interstellar bands. Due to the similarity of their characteristics it is possible to conclude that each emission/absorption pair arises as a consequence of the same carrier. Other families of DIBs that have now been identified e.g. 5780, 6196, 6203, 6269, and 6284 Å, and 4430 Å and 6180 Å (Krelowski and Walker 1987), appear to be missing. Likewise the remaining features observed in emission do not have corresponding features in absorption. This could suggest that there is more than one carrier responsible.

### 2.5.2 The emission mechanism

It has already been discussed that the spectra have the appearance of electronic transitions of gas phase molecules (see section 2.3.3). The widths and shapes of the bands are believed to arise from the unresolved rotational contours. The decrease in population of the higher rotational energy levels with a reduction in temperature is reproduced in the changing profiles of the bands when passing from the center of the

nebula through the bicone to the interstellar medium where the band wavelengths converge towards the DIBs. The red-degraded bands with steep blue sides probably originate from rotational *R*- (or *Q*-) type branch heads which arise when one of the excited state rotational constants is smaller than that in the ground state. One can therefore interpret the Red Rectangle bands in terms of vibronic structure of an electronic transition. Fossey (1991) has already suggested a rotational branch structure. The  $155.5\text{ cm}^{-1}$  difference in the  $5797\text{ \AA}$  and  $5850\text{ \AA}$  DIBs indicates that this might just be an energy level separation in the excited electronic state e.g spin-orbit splitting. There are perhaps other regions of the DIB spectrum in which two narrow lines occur with comparable relative intensities and separation. The Red Rectangle bands near  $5827\text{ \AA}$  and  $5884\text{ \AA}$  have as yet no corresponding counterpart in absorption. This is perhaps not surprising if these features involve vibrationally excited levels of the ground electronic state.

### 2.5.3 A possible carrier

While it remains fairly clear that the  $5797\text{ \AA}$  and  $5850\text{ \AA}$  band pairs are due to the same carrier the other members of the family mentioned earlier need not necessarily result from the same carrier. It has already been noted in section 2.3.1 by Witt and Boroson (1990) that the relative intensities of the  $6380\text{ \AA}$  and  $6615\text{ \AA}$  band alter with offset distance suggesting different carriers. Scarrott *et al.* (1992) have compared a calculated rotational contour of the  $\text{C}_{60}$  entity using a value of a 3% reduction of  $\Delta B$  on electronic excitation with the DIB at  $5797\text{ \AA}$ . These profiles are shown in fig. 2.8. We claim the behaviour of the wavelength and width of the unidentified molecular emission features and the DIB may be modelled by a variation in temperature alone. The optimal rotational temperature being 40 K (DIB) and 170, 250, 450 K (Red Rectangle). However the observed band was recorded as relative transmission of radiation and not as absorbance. This was not taken into account in the simulation. The transformation of an absorption spectrum to a transmission spectrum will lead to a reduction in the width of the resulting band contour so a slight increase

in the rotational temperature would be needed to reproduce the observed band. It is clear though that a  $C_{60}$  species can give rise to an electronic spectrum similar to this particular DIB. Therefore a  $C_{60}$  entity can not be ruled out.

A 3% change in the rotational constant might be considered rather large for the excitation of a single valence electron in a large organic molecule, but could possibly occur for a charge transfer transition, maybe involving an included or surface atom (Kroto 1990). A cold absorption spectrum of neutral  $C_{60}$  molecule (Hauffer *et al.* 1991) has shown that this molecule is not a carrier of the principal DIBs. In principle though a large molecule can give rise to both the DIB and Red Rectangle profiles but further laboratory data is still required.

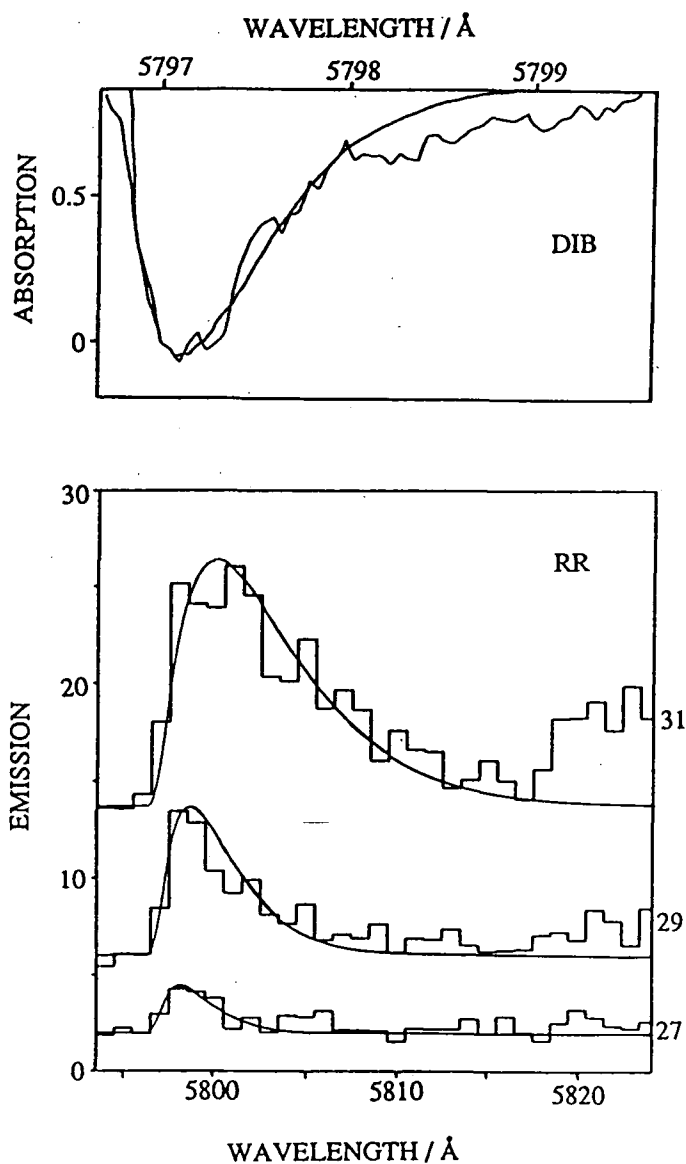


Figure 2.8: The smooth curve represents the profiles generated from the  $C_{60}$  entity contour calculations with a 3% reduction in rotational constant on electronic excitation. These are superimposed on the observational data for the DIB and Red Rectangle band at 5797 Å. The DIB band is an intrinsic profile taken from Westerlund and Krelowski (1988). The resolutions are 0.05 (DIB) and 1 Å (Red Rectangle, with the optimal temperatures 40 K (DIB) and 170, 250, 450 K (Red Rectangle)). The calculations are based on the band origin at 5796.8 Å and theoretical predictions have been matched to the data by including a shift and normalization (Scarrott *et al.* 1992).

# Chapter 3

## Review of NGC 7023 and NGC 2023

### 3.1 Introduction

#### 3.1.1 Physical Conditions in NGC 7023

NGC 7023 is a reflection nebula located in Cepheus (see fig. 3.1), extensively studied as a consequence of its high surface brightness and large size. The Palomar observatory sky survey red print shows a bright  $2' \times 3'$  diameter core with fainter tenuous filaments visible up to  $6'$  away from the central star, the surrounding area being devoid of any other nebulosity within a  $5^\circ$  radius. Less heavily exposed photographs show that the core itself also consists of knots and filaments. Clear evidence of this filamentary structure can be seen in the blue and red images photographed by Ney *et al.* (1980). NGC 7023 is imbedded in the northern end of a large  $30' \times 60'$  dark cloud whose luminosity extends over some  $15'$ . The exact shape and size of the nebula has still to be fully portrayed. There is a highly obscured region  $\sim 7'$  to the east and a “hole” in the cloud  $\sim 5'$  to the west where there is also a large clustering of faint variables (Weston 1953). These stars appear to have no common proper motion and are therefore an unrelated background group seen through a “window” in the nebula, or a lane of relatively high transparency between the individual clouds and filaments that form the nebula.



Figure 3.1: NGC 7023 in blue light. North is at the top and east is to the left (Moore 1982).

NGC 7023 is illuminated by the central star HD 200775, an emission-line star whose spectral type is still a matter of considerable debate. Herbig (1960) was the first to categorize it as one of the Be stars thus suggesting that HD 200775 represents a pre-main sequence star of moderately large mass. Subsequent identifications have varied from B5e to B2IVe (Mendoza 1958; Van den Bergh 1966; Aveni and Hunter 1967; Guetter 1968). Further evidence for the pre-main sequence nature of this star is provided by Strom *et al.* (1972). In their search for further evidence of protostellar activity, in which they photographed the central 75" squared region around HD 200775 at  $1\ \mu\text{m}$ , they found a number of probable embedded stars. It was first noted by Weston (1953) that HD 200775 is the centre of a T association containing some 14 stars including LkH $\alpha$ 275, 276, and 427 (Herbig 1962; Herbig and Rao 1972), as well as several irregular variables and 6 far-infrared emitters, (Gezari *et al.* 1984). At least three T Tauri stars appear to be members of binary systems (Romano 1975). The total stellar mass content of the this central area is estimated to be about  $100 M_{\odot}$  (Aveni and Hunter 1969).

In the ultraviolet the stellar spectrum was found to be anomalous with the principal difference being a much weaker  $2175\ \text{\AA}$  feature than normal (Walker *et al.* 1980). The ultraviolet extinction curve (Witt and Cottrell 1980*b*; Walker *et al.* 1980; Witt, Bohlin and Stecher 1981) shows no indication of abnormal reddening in the near infrared. The level of ultraviolet extinction in HD 200775 is however uncertain since intrinsic reddening contributes to the colour excess ( $B-V$ ) of this star. The differences between independent determinations of the spectral type and extinction of HD 200775 lead to rather large uncertainties in its distance and luminosity. The distance varies from 350 pc (Witt and Cottrell 1980*a*) to 600 pc (Aveni and Hunter 1967) with a range of values in between from different observers. Modern observations tend to prefer the less distant evaluations but it remains unresolved. The luminosity is estimated to be  $4000 L_{\odot}$  by Whitcomb *et al.* (1981).

HD 200775 has a variable spectrum (Rush and Witt 1975) and shows strong infrared excess between  $1\ \mu\text{m}$  and  $20\ \mu\text{m}$  (Gillet and Stein 1971; Strom *et al.* 1972;

Milkey and Dyck 1973). Gillet and Stein first attributed the excess to a hot circumstellar disc, later analyses however favour free-free emission from dense circumstellar plasma (Milkey and Dyck 1973; Strom *et al.* 1975). The energy distribution of the star is approximately constant, with a value of 10 Jansky, and therefore does not resemble a blackbody characteristic of a stellar photosphere (Ney *et al.* 1980). HD 200775 is most likely to be a newly formed star of less than  $10 M_{\odot}$  which has ejected the plasma and dust of the cocoon from which it formed as the star begins its nuclear burning stage, or even during the late stages of gravitational collapse. Combined ultraviolet, optical and infrared observations (Altamore *et al.* 1980) provide further evidence for an extended shell of dust and gas around this star.

Far-ultraviolet observations of NGC 7023 show that the nebular brightness is consistent with the dust having a relatively high albedo ( $a \approx 0.6$ ) and a nearly isotropic phase function ( $g \approx 0.2$ ), or with a low albedo dust ( $a \approx 0.3$ ) with forward throwing phase function ( $g \approx 0.6$ ) (Witt and Cottrell 1980*b*). An average grain albedo in the ultraviolet of  $a \approx 0.54$  was found for the spectral range 1300–3100 Å by Witt *et al.* (1982) in their investigation of the scattering properties of nebular dust grains. The asymmetry factor  $g$  declined monotonically with decreasing wavelength with a value of  $g = 0.25$  at 1400 Å. The dust albedo increased to a level of  $a \approx 0.6$  near 1400 Å after reaching a minimum  $a \approx 0.4$  near 2200 Å. The dust properties derived for the far-ultraviolet were found to suggest that isotropically scattering particles of high albedo contribute significantly to the interstellar scattering in the far-ultraviolet.

Keenan (1936) was the first person to investigate the variation of colour with distance in the nebula. From photographs taken in red and blue light he found that the nebula was bluer than the star by 0.03 mag at  $r = 0.5'$  and increased to a red excess of 0.47 mag at  $r = 1.0'$  before dropping to a red excess of 0.28 mag at  $r = 1.7'$ . On average the nebula was white in colour, as expected if the particles were fairly large, but in some directions the nebula was slightly redder than the star, particularly along a curved bright filament which crosses a wedged shaped dark

region  $\sim 40''$  NW of the center. This filament was much more conspicuous on the red plate than on the blue and showed a strong red excess of the order of 0.3 mag. Keenan's result of the nebula colour has been interpreted in terms of scattering from an embedded star by metallic particles whose diameter was between 0.1 and  $0.05 \mu\text{m}$ . These results have as yet to be repeated, however the regions studied by different observers do not coincide. There is a unanimous agreement that the nebula is bluer than the star in all regions within  $2.5''$  of HD 200775 and that a region about  $1'N$  of the star is almost neutral in colour, otherwise the agreement in the photometric data is generally rather poor. For similar regions the measurements of Elvius and Hall (1966) closely agree with those of Martel (1958), but those of Vanysek and Svatos (1964) are often systematically redder.

An attempt was made to account for the high surface brightness of NGC 7023 by continuous fluorescence of dust grains, but was found not to exist and could not explain more than 10% of the total surface brightness (Rush and Witt 1975). Witt and Cottrell (1980a) have investigated the colour and surface brightness at more positions than any other observer in 4 radial directions covering the wavelength range  $3500-4700 \text{ \AA}$ , at a range of offsets from  $30''$  to  $300''$ . They conclude that near the star, less than  $30''$  away, the nebula is only slightly bluer than the star but that the further away from the star the bluer it becomes with the maximum occurring at somewhere between  $100''$  and  $150''$  depending on the direction. After which the colour varies with wavelength, with the exception of a region  $100'' N$  which is redder than the star over observed spectral range. The onset of the colour trend divergence is approximately at a distance of  $100''$  from the star. They explain the behaviour by the existence of a cavity with an angular radius of  $\sim 100''$  existing within NGC 7023 and centered on the illuminating star. The nebula does not exhibit a smooth surface brightness distribution with the intensity decreasing monotonically with increasing angular distance from the illuminating star. Details of the irregularities vary systematically with wavelength. The measurements indicate that the nebular intensity, in general, increases slowly with decreasing wavelength when compared with the stel-

lar flux. The general behaviour of the nebular surface brightness as a function of offset is approximately represented by a power law with the exponent essentially wavelength independent:-

$$S \propto r^p$$

where  $S$  is the surface brightness,  $r$  is the radial distance and  $p$  is a constant which was found on average to be  $-1.44$ . The irregularities consist of a bright ridge at  $\sim 175''$  E of HD 200775 and a prominent brightness enhancement  $125''$  and  $200''$  N. This structure is most apparent in the ultraviolet. They also observe a brightness plateau around an average offset distance of  $125''$  in all directions except west, coinciding with the colour trend divergence. They also suggest that these changes in colour and brightness are related to the presence of an HII region of similar radius to the cavity. Ney *et al.* (1980) conclude from the thermal bremsstrahlung spectrum that there is a compact HII region but the diameter is  $< 4''$ .

Whitcomb *et al.* (1981) found that the infrared emission ( $40-400 \mu\text{m}$ ) from NGC 7023 was consistent with thermal emission expected from the equilibrium heating of nebular grains by ultraviolet and visible radiation, from the illuminating star, in a  $\sim 4'$  diameter region around the star. The nebula shows substantial variations in density, with a spatial scale of  $< 1'$ , increasing steeply northwest of the illuminating star with the maximum occurring at  $\sim 50''$  NW. The spatial structure of the infrared emission correlates well with the distribution of reflected visible radiation. Since the dust temperature shows a maximum at the position of HD 200775 and then decreases towards the position of greatest dust density they conclude that there is no evidence for any other significant source of dust heating other than by direct and scattered stellar radiation from HD 200775.

Chokshi *et al.* (1988) studied the far-infrared fine structure lines OI ( $63 \mu\text{m}$ ) and CII ( $158 \mu\text{m}$ ) and interpreted their emission as arising in a warm atomic photodissociation region produced by the interaction of the ultraviolet radiation of the illuminating star with the molecular cloud. The photodissociation region occurs near where Whitcomb *et al.* (1981) found the maximum dust density to be. The

strongest emission lines were found  $20''$  W,  $30''$  N from the star. From the infrared luminosity they estimated that the ultraviolet intensity in HD 200775 is a factor of  $2.6 \times 10^3$  larger than the interstellar ultraviolet flux. The intensities of the infrared lines could be explained if they arise in a region with maximum kinetic temperature  $\sim 200$  K located at the position of peak far-infrared line and continuum surface brightness. The observed spatial dependence of the emission suggests that both the temperature and density fall off away from this position. Observations are found to imply equal column densities of warm atomic and molecular gas in the vicinity of HD 200775.

Ammonia maps around HD 200775 reveal filamentary structures, with size of  $120'' \times 60''$ , which breaks up into substructures, typical sizes being  $< 30''$  (Fuente *et al.* 1990). The peak emission was found at  $\sim 120''$  N of the central star; toward the star the emission is at least a factor of 33 lower. A gradient in the gas kinetic temperature was found ranging from 14 K, typical temperature for dust and warm molecular clouds, at an offset of  $120''$  to  $\sim 31$  K at  $60''$ , occurring at the edge of the  $\text{NH}_3$  filament. The ammonia abundance in the cold condensations of NGC 7023 is  $1 - 3 \times 10^{-8}$ . Their data suggests that the abundance decreases gradually as a function of distance to the star, being a factor of 20 smaller toward the star position than in the cold condensations. They conclude from their results that the ammonia emission arises from clumps in an adjacent zone to the photodissociation region. The model could then explain both gradients, kinetic temperature and ammonia abundance if the  $\text{NH}_3$  emission came from a region with visual extinction from the star between 4.8 and 6.8 mag.

The first millimeter detection of NGC 7023 was made by Loren *et al.* (1973) in a survey of Herbig Ae and Be stars. They detected  $^{12}\text{CO}$  with a temperature of 12.8 K centered on HD 200775. Elmegreen and Elmegreen (1978) did extensive low resolution mapping over an area  $0.5^\circ \times 1^\circ$  in  $^{12}\text{CO}$  at 115 GHz. Emission from  $^{12}\text{CO}$  was observed over most of the the dark cloud, with an antenna temperature of 10–14K in the northern region of the cloud and 6–8K in the southern region. In addition

they also detected the  $^{13}\text{CO}$  isotope at 110 GHz and CS emission at 146 GHz. They combined their observations of  $^{12}\text{CO}$  and  $^{13}\text{CO}$  to obtain an average column density of  $600\text{ cm}^{-3}$ . The  $^{12}\text{CO}$  emission has two “hotspots”, one in the highly obscured region east of NGC 7023, which coincides with the detection of a 6cm source and leads them to suggest that some young stars are still embedded in neutral material, and one  $\sim 5'$  south of the “hole” with there being a distinct minimum at the location of the “hole”. The detection of CS emission also coincides with the 6cm source and they cite this as additional evidence for a rather dense spot in this area. According to the results of Liszt and Linke (1975) and Penzias *et al.* (1971) the CS emission implies a much larger density of the order of  $10^4\text{ cm}^{-3}$ . They also made a crude estimate of the gas contained in the core region of  $\sim 600 M_{\odot}$ . Comparing with the result of Aveni and Hunter for the stellar mass there is a large fraction of stellar mass relative to gas suggesting that low mass star formation is probably occurring throughout the cloud, not just at the edges as appears to be true in the case of high mass stars in giant clouds.

Watt *et al.* (1986) mapped the nebula in  $^{12}\text{CO}$  and  $^{13}\text{CO}$   $J=1 \rightarrow 0$  covering an area  $0.5^{\circ} \times 1^{\circ}$ . Their results indicate a large extended low density molecular cloud and they suggest that the region is characteristic of a bipolar outflow source, the outflowing lobes being directed along the minor axis. They find a higher density clump at the ends of the flows where the interaction of the ambient cloud has resulted in heating and compression. The northern peak is found adjacent to a “hole” in the optical extinction. Their spectra however show little indication of high velocity wings arising from the material within the lobes. The total column density of gas inferred from the  $^{13}\text{CO}$  observations implies that the nebula is optically thin everywhere at  $1.65\text{ }\mu\text{m}$  and  $2.2\text{ }\mu\text{m}$ . They derive a density of  $\sim 5 \times 10^4\text{ cm}^{-3}$  for a clump which they observe in both  $^{12}\text{CO}$  and in  $^{13}\text{CO}$ . Chokshi *et al.* (1988) derive a density of around  $4 \times 10^3\text{ cm}^{-3}$  from their observations of the far infrared fine structure lines, while mapping of clumps of  $\text{NH}_3$  emission (Fuente *et al.* 1990) indicates densities of  $(1-2) \times 10^4\text{ cm}^{-3}$ . The two orders of magnitude variation in gas density derived

by different techniques, as well as clumpy structure seen in  $^{13}\text{CO}$  and  $\text{NH}_3$  maps, clearly indicate the presence of strong density variations. The photodissociation model suggests that the observed CO emission arises predominantly from low density molecular cloud material surrounding the dense clumps responsible for the OI and CII emission. Fuente *et al.* (1992) provide the results of observations made of the  $J = 2 \rightarrow 1$  line of  $^{13}\text{CO}$  which they claim shows a cavity around HD 200775 which is filled by high velocity molecular gas. The  $\text{NH}_3$  condensations are located just at the edges of this cavity and might therefore be related to the interaction of the molecular outflow and ambient clouds.

Lépine and Nguyen-Quang-Rieu (1975) made a weak detection ( $\geq 0.2\text{ K}$ ) of OH near HD 200775 at 1667 MHz possibly associated with the star itself. The shell surrounding the star may interact with the surrounding nebula producing OH emission. There is an indication of both a narrow and wide ( $\Delta v \geq 20\text{ km s}^{-1}$ ) component at this frequency. The narrow component is probably due to emission from material at a distance greater than eight stellar radii consistent with FeII line observations (Weston 1949). The broad component is possibly due to the rotation of a disc shaped envelope within eight stellar radii of HD 200775. Radio line observations made by Pankonin and Walmsley (1978) have produced C158 $\alpha$ , C110 $\alpha$  recombination spectra and OH 1667 MHz emission from the position of the central star. The detected CII region may not be associated with the reflection nebula. They also detected  $\text{H}_2\text{CO}$  in absorption east of HD 200775 peaking where they found a weak 6cm continuum source. They suggest that this coincidence could imply that the continuum source is embedded in the cloud. CO emission also peaks at this position. Two radio continuum sources have been detected in the dark cloud surrounding NGC 7023, both sources are probably background radio sources which are not associated with the nebula or the surrounding dark cloud (Haslam *et al.* 1978). Haslam *et al.* believes the radio source which is coincident with the 6 cm source, the peak CO emission and the CS emission is just 4 C 67.34, a background source.

### 3.1.2 Physical Conditions in NGC 2023

NGC 2023 first studied in 1922 by Hubble, is an almost spherical reflection nebula which is found in Orion (see fig. 3.2) towards the eastern edge of the dark cloud complex, L1630; which extends from roughly the Horsehead nebula and NGC 2024 to the reflection nebulae NGC 2068 and NGC 2071, covering an area of  $\sim 6$  square degrees with a visual extinction of  $\sim 4$  mag (Lynds 1962). NGC 2023 is approximately  $10'$  in diameter which agrees closely with the value obtained from the Hubble (1922) relationship

$$m + 5 \log a = 11.02$$

giving a radius of  $4.5'$  if  $V = 7.83$  mag for HD 37903, the central star. Photographs of the nebula taken by Witt, Bohlin and Stecher (1984) reveal deviations from the approximate circular symmetry. They claim that the west boundary appears to be more abrupt than is observed to be the case in the other three directions, from which they conclude that a ridge of foreground obscuring matter overlies the western extensions of the nebula resulting in the apparent asymmetry. The extent and shape of the nebula implies that the illuminated edge of the cloud is primarily face-on to the observer. The nebula reveals the presence of wispy filamentary structure, and measurements of the infrared energy distribution suggest inhomogeneities in the dust distribution (Evans 1981). Stars in NGC 2023 appear to cluster on the nearside of the dust cloud.

NGC 2023 is illuminated by the central star HD 37903, R.A. =  $05^h 39^m 07^s$ ; Dec =  $-02^\circ 17' 19''$  (1950). This is a B1.5V star (Sharpless 1952) at a distance of 450–500 pc (Racine 1968; Lee 1968; de Boer 1983). The reddening,  $E_{B-V} = 0.36$  (Lee 1968), to HD 37903 confirms that the star is partially embedded in the L1360 cloud. The low visual extinction toward the star ( $A_V \sim 1$ ; Lee 1968) shows that HD 37903 lies on the near side of the molecular cloud. Colour photographs show the nebula to be distinctly bluer than the illuminating star with the possible exception of the south-west sector. Photometric studies made by Lee (1968) of HD 37903 reveal the presence of anomalously high ultraviolet extinction, thus provoking ex-

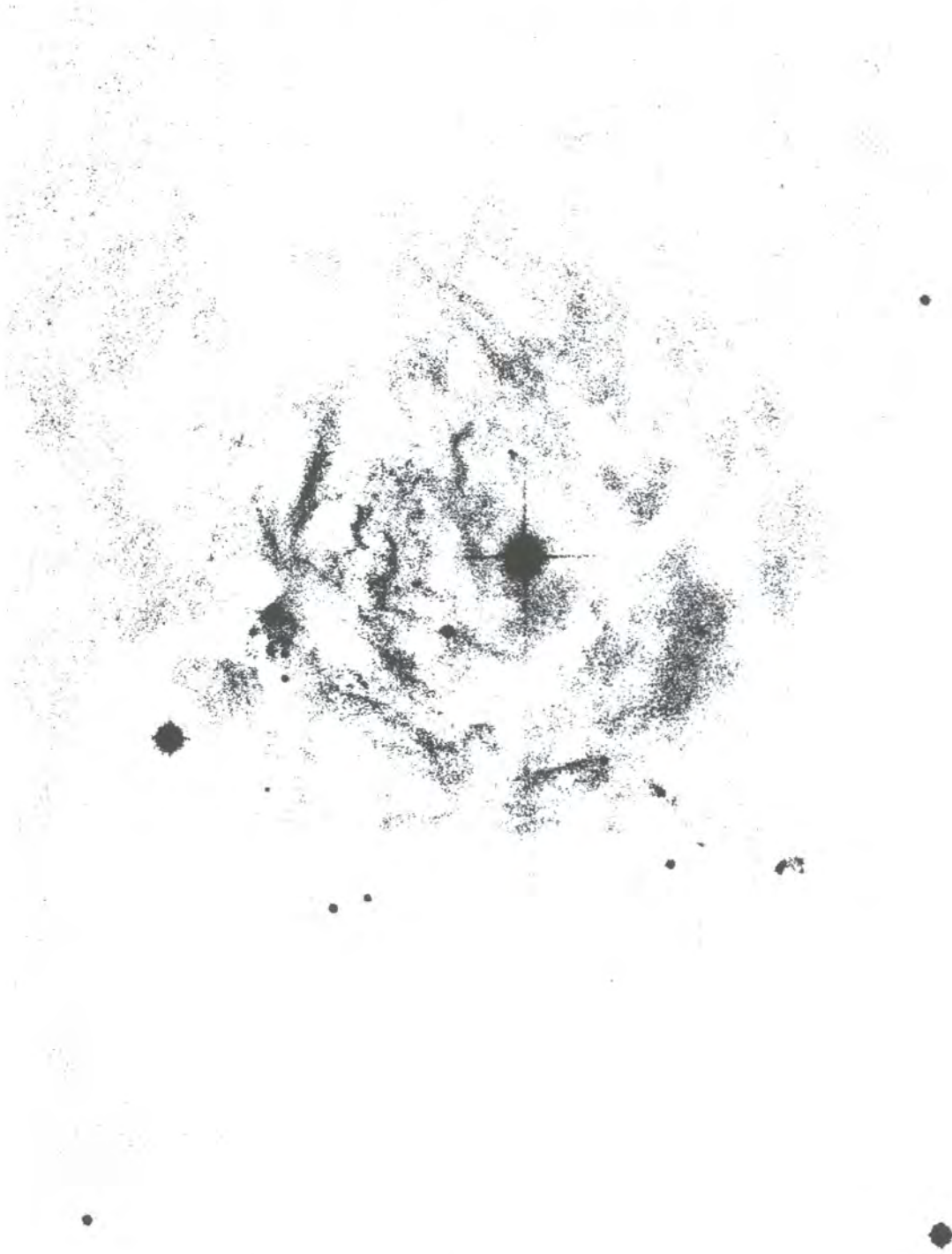


Figure 3.2: NGC 2023 in red light. The image scale is  $2''.5\text{mm}^{-1}$ . North is at the top and east is to the left. The central star is HD 37903 (Witt and Malin 1989).

tensive studies of the ultraviolet extinction curve (de Boer 1983; Witt, Bohlin and Stecher 1984). De Boer (1983) finds that the extinction is excessive by as much as 0.4 mag, between 2700 Å and 5000 Å, and is almost normal for wavelengths less than 2500 Å. However the results of Witt, Bohlin and Stecher indicate that a high level of extinction is reached only in the 2200 Å band at  $\lambda \leq 1340$  Å. The extinction curve is known to exhibit a peculiar wavelength dependence, characteristic of larger than normal dust grains with an abundance ratio of smaller to larger grains also lower than normal.

The whole region appears to be an area of very active star formation. Within  $\sim 2'$  of NGC 2023 is an emission line star LKH $\alpha$ 287 (Herbig and Kuhl 1963), just one of the T-Tauri stars discovered in the dark cloud. Strom *et al.* (1975) identified a cluster of ten reddened stars from NIR surveys of selected regions of L1630, which are probably late B to early A type stars deeply embedded in the dust, of which several are within a few arcminutes of NGC 2023. The dust density increases towards the south where coincidentally Sellgren (1983) has found a young cluster of stars with  $K > 10$  mag formed within the NGC 2023 molecular cloud, as concluded from their spatial distribution and reddening centred 67" S and 60" E of HD 37903. She estimated that between 30–60% of the stars were pre-main sequence. Spectrophotometry on two of these stars showed H $\alpha$  emission lines due to either a circumstellar shell or a stellar wind. Witt, Schild and Kraiman (1984) carried out photometry on eleven probable pre-main sequence stars south of HD 37903 in the spectral range 350–1000 nm and found that they were not major contributors to the illumination of the reflection nebula. From Sellgren's results DePoy *et al.* (1990) predict that there should be  $\sim 50$  additional stars brighter than  $K = 15$  mag present. However no additional cluster members were found. They therefore suggest that either no low-mass stars have formed or that they are still hidden in molecular "cocoon" remaining from the star formation stage. Of the sixteen stars detected in the cluster only the illuminating star itself was observed without overlying extinction by dust. This might be due to the star having destroyed its primeval covering of dust with

a stellar wind, common in such early-type stars. Malin *et al.* (1987) has discovered two groups of Herbig-Haro objects in the southern vicinity of NGC 2023. The more northerly group, i.e. that closest to the nebula, showed proper motions which indicated movement away from the ionized regions of NGC 2023 and concluded that these objects may have been accelerated outwards from this centre of activity, suggesting that star C, (see section 3.2.3), is the most likely candidate for the exciting star of the H-H objects. The H-H complex situated  $\sim 8.5'$  SW of NGC 2023 contains two separate groups of objects whose proper motion suggests that they are moving in mutually opposite directions, ruling out the possibility that NGC 2023 is responsible for their acceleration. However there may be deeply embedded T-Tauri stars which might be the sources of the H-H objects.

Emerson *et al.* (1975) carried out a far-infrared ( $40 - 350 \mu\text{m}$ ) photometric study of NGC 2023. By comparing the energy absorbed in the ultraviolet to the total integrated energy in the infrared excess they concluded that the excess results from emission by dust. The surrounding dust absorbs the ultraviolet photons ( $1350 - 2900 \text{ \AA}$ ) emitted by HD 37903 and re-emits in the far-infrared; this emission was found to peak at the position of HD 37903. Observations made by Harvey *et al.* (1980) between  $40 - 160 \mu\text{m}$  show there are two peaks in the far-infrared emission; at the shorter wavelength the far-infrared emission peaks on or close to HD 37903, while the longer wavelength emission peaks  $1'$  S of HD 37903 coincident with the CII recombination line peak. The dust temperature also peaks at or close to HD 37903 confirming that the star is the dominant heating source for dust seen in the infrared, thus concluding there are probably no obscured stars of earlier spectral type and higher luminosity than HD 37903 within the NGC 2023 cloud. The size of the far-infrared emission is  $5'$ , similar to the optical size, indicating that the same dust is probably responsible for both. The far-infrared data implies a roughly uniform dust mass density within  $0.1 \text{ pc}$  of the star with no significant density increase toward the star. Most of the infrared emitting dust is greater than  $0.1 \text{ pc}$  away from HD 37903 with an increase by a factor of four in the dust  $1'$  S of HD 37903. This is consistent

with the lack of any  $10\ \mu\text{m}$  circumstellar dust emission, i.e. no strong dust density gradient increase toward smaller radii. This suggests that HD 37903 is not closely surrounded by local density enhancement from which it presumably condensed and is therefore probably old enough to have disrupted its 'placental' cloud.

Tucker *et al.* (1973) and Milman *et al.* (1975) detected CO  $J = 1 \rightarrow 0$  line emission and found an enhanced region towards NGC 2023, with a peak gas temperature 35 K from a survey of L1630. The gas temperature is 0.6 times the temperature of the dust, a ratio which is consistent with the interpretation that the gas is heated by the dust in the vicinity of the exciting star (Goldreich and Kwan 1974). Milman *et al.* (1975) showed that both the  $^{12}\text{CO } J = 1 \rightarrow 0$  (115.2712 GHz) and  $^{13}\text{CO } J = 1 \rightarrow 0$  (110.2014 GHz) emission peak near the position of NGC 2023 though not at the same position, and fall off sharply to the west. To the east of NGC 2023 there is a secondary peak in the  $^{12}\text{CO}$  emission. The enhanced CO emission signifies the presence of very young stars. White *et al.* (1981) made high resolution  $J = 3 \rightarrow 2$  CO (345 GHz) measurements of NGC 2023 and found a single molecular hotspot centred at the position of the optical nebula with a peak excitation temperature  $T = 39$  K. It appears to be the case of an isolated molecular condensation which has collapsed to form a single symmetrically shaped core, lying inside an extensive plateau of cooler gas. The CO peak excitation temperatures for the CO transitions  $J = 1 \rightarrow 0$ ,  $J = 2 \rightarrow 1$  are 51 K and 40 K respectively. Maps taken in  $^{12}\text{CO}$  by Gatley *et al.* (1987) reveal a bright ridge of emission lying immediately outside the brightest portion of the fluorescent molecular shell (see section 3.3.2) thus demonstrating density variations. The bulk of the molecular material is believed to lie behind the exciting star and reflection nebula with the CO emission most likely to come from the relatively thin layer of gas on the nearside of the molecular cloud (Harvey *et al.* 1980).

White *et al.* (1990) has observed the NGC 2023 region in the CO  $J = 2 \rightarrow 1$  and  $J = 3 \rightarrow 2$  lines. Again the CO emission is brightest around the reflection nebula concentrated into a region of diameter  $\sim 6'$  (0.8 pc) where the gas kinetic

temperature may be at least 50K. Outside this region the line intensities suggest the gas kinetic temperature decreases to 15–25K. The model that has emerged is that the CO gas is in a shell which is being compressed and excited by some mechanism e.g. radiation pressure. Pre-existing condensations in the parent molecular cloud may result in density variations across the ionization front causing the shell to have a broken irregular appearance. White *et al.* (1990) find clear similarities between their CO  $J = 2 \rightarrow 1$  contour maps and the CO  $J = 1 \rightarrow 0$  by Gatley *et al.* (1987). The data is consistent with the emerging model.

Jaffe *et al.* (1990) present measurements of the CO  $J = 2 \rightarrow 1$ , C<sup>18</sup>O  $J = 2 \rightarrow 1$ , and CO  $J = 3 \rightarrow 2$  to trace the bulk of the molecular gas. They also observe the 372  $\mu\text{m}$  CO  $J = 7 \rightarrow 6$  line to trace the distribution of warm molecular gas and the 158  $\mu\text{m}$  C<sup>+</sup>  $^2P_{3/2} \rightarrow ^2P_{1/2}$  fine-structure line to trace warm neutral atomic gas in the same region. They found that the photodissociation region southwest of HD 37903 contains both atomic and excited molecular material and lies closer to the exciting star than does the bulk of the molecular cloud. The bright narrow line CO  $J = 7 \rightarrow 6$  emission peaks 1' SE of the exciting star, at a ridge in NGC 2023. The 158  $\mu\text{m}$   $^2P_{3/2} \rightarrow ^2P_{1/2}$  line emission from C<sup>+</sup> is also bright and extended and peaks southeast of HD 37903. The peak surface brightness corresponds to a C<sup>+</sup> column density of  $8 \times 10^{17} \text{ cm}^{-2}$ . The very good agreement between the CO  $J = 7 \rightarrow 6$ , H<sub>2</sub>, and C<sup>+</sup> distribution strongly favours a common heating mechanism for the atomic and molecular PDR gas. The narrow CO  $J = 7 \rightarrow 6$  lines almost completely rule out shock excitation of the CO. The incident far ultraviolet ( $91\text{nm} < \lambda < 200\text{nm}$ ) flux is  $\sim 1000$  times the interstellar radiation field value, or an order of magnitude below the fluxes incident on sources where the CO  $J = 7 \rightarrow 6$  line has previously been observed. There is still a significant amount of CO  $J = 7 \rightarrow 6$  emission arising from regions with  $T_{gas} > 85 \text{ K}$ , which is substantially greater than  $T_{dust}$ . The CII line flux distribution peaks 0'.7 SE of the exciting star, close to the peak of the H<sub>2</sub> emission. The C<sup>18</sup>O  $J = 2 \rightarrow 1$ , which traces the molecular column density, has its emission peak  $\sim 4 \times 10^{17} \text{ cm}$  beyond the C<sup>+</sup> peak.

Howe *et al.* (1987) mapped the spatial distribution of the  $158\ \mu\text{m}$  CII fine structure line in NGC 2023. The peak emission was found  $\sim 30''$  SE of the central star, with the FWHM of the emission  $\sim 3'$ . The low-level emission however extends  $\sim 5'$  east-west and  $\sim 8'$  north-south. The bulk of the CII emission appears to arise just inside the fluorescently excited  $2\ \mu\text{m}$   $\text{H}_2$  emission shell discovered by Gatley *et al.* (1987), see section 3.3.2. Howe *et al.* explain the CII emission in terms of arising from warm ( $100\text{--}300\ \text{K}$ ) dense ( $n_{\text{H}} > 10^4\ \text{cm}^{-3}$ ) photodissociation regions at the surface of the molecular cloud. The extent of the low-level emission is partly due to the geometry of the nebula.

The other rotational molecular lines observed in NGC 2023 include HCN (Morris *et al.* 1974)  $\sim 1'$  SE of HD 37903. The line brightness temperature is quite low which may indicate, unless HCN emission is optically thin, that densities of  $\geq 10^5\ \text{cm}^{-3}$ , which are needed to thermalize HCN, are not common in this cloud. Pankonin and Walmsley (1976) observed  $6\ \text{cm}$   $\text{H}_2\text{CO}$  ( $4829.66\ \text{MHz}$ ), which peaks to the south of HD 37903 and  $18\ \text{cm}$  OH .

Knapp *et al.* (1975) looked for  $\text{H}109\alpha$  and  $\text{H}76\alpha$  towards NGC 2023. They failed to detect any recombination lines. They claimed that the HII region is too small to give rise to detectable recombination line emission from H or He. They estimated that there should be an HII region immediately surrounding HD 37903 of the order  $0.5'$  in diameter with a quite low mean density, of the order  $500\text{--}1000\ \text{cm}^{-3}$ . Most photons emitted by HD 37903 between  $912\text{--}1100\ \text{\AA}$  ionize the carbon. Pankonin and Walmsley (1976) expected a  $6.2'$  diameter region but calculated that H recombination line flux would be too weak to detect although they did detect a point source of radio continuum centred on HD 37903. HD 37903 might not be hot enough to produce a sizeable HII region but it has given rise to an extended CII region and to carbon recombination line emission detected by Brown *et al.* (1975), Knapp *et al.* (1975), Pankonin and Walmsley (1976), Pankonin and Walmsley (1978) and Van Gorkom *et al.* (1979). Knapp *et al.* (1976) detected the carbon recombination line emission at  $\text{C}166\alpha$  ( $\sim 1425\ \text{MHz}$ ),  $\text{C}167\alpha$  ( $1400\ \text{MHz}$ ),

C142 $\alpha$  (2273 MHz), C110 $\alpha$  (4874 MHz) and C76 $\alpha$ . They propose a model for the CII region which consists of a “halo”, with a diameter of  $\sim 2$  pc, with a mean  $n_e \sim 0.2 \text{ cm}^{-3}$  and a mean  $T_e \sim 20$  K. The electron density increases exponentially near the star HD 37903. The carbon emission lines arise in the cold gas region surrounding the central star. The carbon ionization is provided by stellar photons 912–1100 Å emitted by HD 37903 which escape the highly compact HII region surrounding the star and are absorbed in the more extended surrounding medium. The coexistence of CII region with a region of enhanced CO emission suggests that CO in NGC 2023 may be excited by electron collisions. From examination of the widths of the emission lines from different parts of NGC 2023 it appears that the illuminating star imparts no expansion or turbulent motion to the surrounding gas.

Pankonin and Walmsley (1976) searched for the C157 $\alpha$  (1684 MHz), C110 $\alpha$  and C138 $\beta$  (4900 MHz) lines. Their observations support the belief that HD 37903 is the primary source of ionization of carbon toward NGC 2023 but S108 may also contribute. The peak CII emission is close to where there is a peak in the CO emission, 1' S of HD 37903. They believe that Knapp *et al.* (1975) have over estimated the source size due to the poor quality of their data. They present evidence for two velocity components to the CII based on the evidence of double peaked carbon recombination line, a compact, high density “core” ( $n_e \approx 10 \text{ cm}^{-3}$ ) and a lower density, more extended “halo” ( $n_e \approx 1 \text{ cm}^{-3}$ ). The radius of this “halo” is  $\sim 0.3$  pc, the electron density  $\sim 1 \text{ cm}^{-3}$  and a temperature in the range 20–50 K. Pankonin and Walmsley (1978) present C91 $\alpha$ , C110 $\alpha$ , C138 $\alpha$  and C157 $\alpha$  data from the compact component from which they fit a model of a source with uniform density and temperature. They estimate the size of the core region to be  $< 0.15$  pc; with the electron density  $\sim 10 - 25 \text{ cm}^{-3}$  and a temperature in the range 20–50 K. Van Gorkom *et al.* (1979) also found relatively strong Cn $\alpha$  line emission in the nebula. Their C109 $\alpha$ , C110 $\alpha$  spectrum support the theory by Pankonin and Walmsley.

Radio emission over the whole of the Orion region has been mapped at 2.7 GHz

where approximately the same areas have been observed there is quite good agreement. However none of the faint areas where the extremely high values of Gliese and Walter were reported have been observed. Elvius and Hall found that the percentage polarization was found to increase linearly and fairly steeply with increasing wavelength in different parts of the nebula. The polarization was also found to increase with increasing radial distance from the central star which reaches a maximum and then decreases again. The maximum polarization was reached at a variety of distances from the star depending on the different direction. This was assumed to be due to the complicated three dimensional structure of NGC 7023. Gehrels (1967) measured polarization in three regions in the ultraviolet (3600 Å), green (5500 Å), and red (8300 Å) light. He studied regions 38" from HD 200775 in an east, north-east and north direction. A typical region was found to have 13%  $P$ , 19%  $P$  and 22%  $P$  with these filters respectively. Zellner (1970) observed the one region that both previous sets of data included, a region centered 38" NE of the central star. Both Zellner and Gehrels found their values to be 0.7 times higher than those of Elvius and Hall, but the wavelength dependence remains the same. It should be noted however that Zellner was collaborating with Gehrels and therefore should not be considered as an independent observer.

The discrepancy does not lie within the given boundaries of error. Gehrels (1967) attributes it to the fact that Elvius and Hall performed sky measurements at greater distances than those of Gehrels' whose regions were well inside the nebulosity. Indeed it is possible that the residual luminosity could account for most of the disparity but not all. Gehrels was convinced that this meant that the grains exhibited the same wavelength dependence as interstellar grains. This statement is contrary to the findings of Elvius and Hall. If the large difference between the values of polarization are assumed to be due to variations in the apertures used and the amount of sky background deducted, therefore presuming that the relative discrepancies are correct, then it can be concluded that since density fluctuations could not explain the variation alone the grain properties must differ throughout the nebula.

Ney *et al.* (1980) photographed NGC 7023 in polarized light ( $\lambda_{eff} = 6500 \text{ \AA}$ ). Their maps plot the magnetic vector  $H$  which shows that the nebula is radially polarized. The most recent polarization observations have been made by Moore (1982) in the  $B$  (4400  $\text{\AA}$ ),  $VV$  (5200  $\text{\AA}$ ), and  $R$  (6500  $\text{\AA}$ ) wavebands, using an electronographic camera. The polarization maps show a centrosymmetric pattern around HD 200775 confirming again that this star is the only important light source in the nebula. The percentage polarization is seen to increase with radial distance and then decrease for all wavelengths. There is also a tendency for the degree of polarization to increase with wavelength. A general fall in intensity occurs with distance from the star, which is slightly asymmetrical north-south. Other irregular variations in the brightness are noted.

While processes other than scattered light dominate the near infrared emission of NGC 7023, a detectable scattered light component remains, as is demonstrated by the polarization measurements at 1.25, 1.65, 2.2  $\mu\text{m}$  made by Sellgren, Werner and Dinerstein (1992) in their study of the infrared scattering properties of dust. Their results are given in table 3.1. They found very high polarization measurements up to 26% at  $J$ . The percentage polarization is at a maximum near 1  $\mu\text{m}$ , of typically 20%, and then decreases with increasing wavelength at the observed positions, resulting in rather low percentage polarizations at 2.2  $\mu\text{m}$ , up to a factor of 4 lower than the visual polarization. Grain model calculations would predict it to be a factor of 2 higher than the visual polarization (White 1979), this suggests that reflected light can account for only  $\sim 20\%$  of the 2.2  $\mu\text{m}$  emission. This could be much smaller though if the continuum emission which dominates the near infrared spectrum is itself intrinsically polarized. This increase in percentage polarization with wavelength in the visible and then decrease in the infrared is interpreted as being due to two components with different energy distributions, the polarized scattered starlight and the unpolarized small particle emission contributing to the observed surface brightness. The polarization position angles are consistent with the polarized component of emission being due to scattered starlight from a single

star, HD 200775. The position angles are all observed to be perpendicular to the line between the illuminating star and the observed nebular position.

The percentage polarization does not increase monotonically with wavelength as expected for pure scattered light, the scattering in the nebula must therefore be diluted by other radiation which is intrinsically less polarized or unpolarized. The contribution of this diluting radiation must increase with increasing infrared wavelength since the polarization steadily decreases. The obvious candidate is the emission from small particles which dominate the total near infrared emission from NGC 7023 (Sellgren, Werner and Dinerstein 1983; Sellgren *et al.* 1985). Sellgren, Werner and Dinerstein (1992) place an upper limit of  $\sim 6\%$  on the polarization of the emission which dilutes the polarized scattered light from NGC 7023 based on the lowest observed polarization values at  $2.2 \mu\text{m}$ . This upper limit is in agreement with other determinations of the polarization of emission presumed due to small particles. Sellgren, Rouan and Léger (1988) place an upper limit of  $2\%$  on the polarization of the  $3.3 \mu\text{m}$  emission feature in the Orion Nebula, and upper limits of  $3\% - 4\%$  on the polarization of the  $11.3 \mu\text{m}$  feature in the Orion and the planetary nebula NGC 7027. These features are associated with the near infrared continuum emission in visual reflection nebulae. The centrosymmetric pattern of infrared polarization observed and the good agreement between the position angles at visual and infrared wavelengths are strong arguments against magnetic field alignment of small particles in NGC 7023. Therefore polarization due to aligned small grains or PAHs is unlikely.

### 3.2.2 NGC 2023: Visible and Infrared Wavelengths

The first work was done by Khachikyan, described briefly by Minin (1965), which showed that the visible nebula has a mean polarization value of  $13\%$ . Mannion (1987) shows a centrosymmetric pattern of polarization vectors centred on HD 37903. He obtained electronographic data in the  $B$ ,  $V$ , and  $Z$  wavebands and CCD data in the  $R$ ,  $I$ , and  $Z$  wavebands. Polarization traces through HD 37903 in the E-W direction on the electronographic data were asymmetric rising steeply and monotonically to

Position	U	B	V	R	J	H	K
Percentage Polarization							
70''S	11.2 ± 0.9	15.8 ± 1.0	19.1 ± 1.2	...	15.8 ± 1.4	11.1 ± 1.3	7.1 ± 1.2
35''S	4.3 ± 0.4	8.2 ± 0.9	12.9 ± 1.4	...	26.1 ± 6.7	7.4 ± 3.3	...
30''W, 20''N	...	...	18.3	...	25.9 ± 1.5	10.8 ± 0.6	4.4 ± 0.5
30''N	...	13.9	13.2	14.1	21.3 ± 1.5	7.4 ± 0.5	4.6 ± 0.4
60''N	...	...	...	...	...	...	13.1 ± 4.5
70''N	11.8 ± 1.4	13.4 ± 1.2	18.1 ± 1.2	...	21.8 ± 5.4	17.8 ± 3.6	...
Polarization Position Angle							
70''S	92	92	91	...	96 ± 3	87 ± 4	84 ± 5
35''S	91	88	87	...	94 ± 8	90 ± 13	...
30''W, 20''N	...	...	27	...	36 ± 2	32 ± 3	43 ± 3
30''N	...	84	91	88	89 ± 3	87 ± 3	99 ± 3
60''N	...	...	...	...	...	...	68 ± 18
70''N	81	86	85	...	99 ± 7	97 ± 6	...

Table 3.1: Polarization measurements in different region of NGC 7023 (Sellgren, Werner and Dinerstein 1992).

the west and less steeply to the east. The degree of polarization was found to increase with wavelength and offset distance but it was not found to be constant with position angle for various radii from HD 37903. The polarized intensity traces have a similar profile with the highest intensity recorded between 40–50" E with a sharp fall off from the maximum to 100" E. A rather low intensity was recorded to the west of HD 37903. The total intensity traces are also asymmetric about HD 37903 with the highest value recorded to the east of the central star. There was a smaller maximum to the west followed by a sharp decline in intensity.

Traces made in a north-south direction through the CCD data show that the degree of polarization is seen to increase with offset distance and wavelength; there is a steady increase between 6" S–100" S in the *R* and *I* wavebands and a rather sharp increase in the *Z* waveband. Polarized intensity falls sharply in *R* and *I* but there is a peak at 60" S, while in the *Z* it is fairly constant over the 6–100" S range. In all three wavebands the total intensity decreases sharply between 16–50" S then there is a small decrease from 50–70" S followed by a gradual fall off in intensity between 80–150" S and a plateau region at greater than 150" S.

While nonequilibrium emission from small particles dominates the near infrared emission from NGC 2023 (Sellgren, Werner and Dinerstein 1983, Sellgren 1984) the near infrared polarization was found to be high throughout the near infrared and not to decrease to longer wavelengths as does the polarization of NGC 7023 (Sellgren, Werner and Dinerstein 1983). There is also no clear pattern of polarization with wavelength nor are the position angles constant with wavelength. In the *I* and *Z* wavebands Mannion (1987) noticed a perturbed region of polarization around star C (Sellgren 1983), also known as S108 (Strom *et al.* 1975). He describes a polarization jet-like filament seen near S108 extending some 30–35" and since the near-centrosymmetric region that surrounds the star S108 is only visible in these two filters it indicates that S108 is embedded in dense nebula dust and produces a reflection nebula only in the near infrared. Scarrott *et al.* (1989) also noticed this small scale structure in the *I–R* colour image and a distortion region in the

near infrared polarization map in the vicinity of star C which is absent in data at shorter wavelengths. They conclude from polarization imaging at *I* that this star illuminates a small bipolar reflection nebulae located deep within the L1630 cloud, although more distant regions of NGC 2023 continue to be illuminated by HD 37903 at *I*. They conclude that at *B*, *V*, and *R*, HD 37903 is the sole illuminating star of NGC 2023; star C begins to contribute significantly only at *I*. The position angles rotate with wavelength apparently due to the increasing importance of star C at the infrared wavelengths. For the southern nebular positions, the observed *K* position angle suggest illumination primarily by star C (Sellgren, Werner and Dinerstein 1992). For the southern position angles at *J*, there appear to be contributions both from HD 37903 and star C to the polarized reflection nebulosity. For the northern nebula positions the position angles are such that they cannot distinguish between HD 37903 and star C as the dominant illuminating star; if each star is equally intrinsically bright in the near infrared then HD 37903 would be expected to illuminate primarily the northern part of the reflection nebula, simply because it is closer.

### 3.2.3 Star C in NGC 2023

Star C is a pre-main sequence star with an infrared excess and is typical of T-Tauri star, being of late spectral type and showing strong  $H\alpha$  emission. This star has also been suggested by Malin *et al.* (1987) to be the probable exciting source of a group of Herbig-Haro objects to its southwest, and may be associated with a molecular outflow in the region detected by Bally and Lada (1983). Star C is about 1 mag fainter than HD 37903 at  $2.2\ \mu\text{m}$  (Sellgren 1983; DePoy *et al.* 1990), but star C is actually 0.3 mag brighter than HD 37903 at  $3.8\ \mu\text{m}$  (DePoy *et al.* 1990). Witt, Schild and Kraiman (1984) conclude from visual photometry that star C is very reddened and may have a dereddened  $2.2\ \mu\text{m}$  magnitude brighter than HD 37903. The fact star C is brighter than HD 37903 at  $3.8\ \mu\text{m}$  while the reverse is true at  $2.2\ \mu\text{m}$  is probably due to a combination of increasing infrared ex-

Position	U	B	V	R	J	H	K
Percentage Polarization							
60"S	...	14.0 ± 2.4	...	...	13.4 ± 1.6	10.7 ± 1.6	10.7 ± 1.0
12"W, 57"S	7.8 ± 0.5	...	...	...	...	...	...
45"W, 46"S	...	...	8.0 ± 1.5	...	...	...	...
34"W, 46"S	6.3 ± 0.2	...	8.5 ± 1.1	...	...	...	...
45"W, 42"S	...	7.8 ± 0.9	...	11.3 ± 2.0	...	...	...
34"W, 42"S	...	8.6 ± 0.9	...	...	...	...	...
40"W, 40"S	...	7.7 ± 2.0	...	...	4.8 ± 1.5	8.8 ± 1.8	7.5 ± 1.8
45"W, 35"S	...	...	8.6 ± 1.2	...	...	...	...
34"W, 35"S	6.9 ± 0.3	...	9.9 ± 0.8	...	...	...	...
60"N	...	9.3 ± 2.2	...	...	19.4 ± 2.9	4.4 ± 4.9	6.8 ± 5.4
12"W, 64"N	7.0 ± 0.8	...	...	...	...	...	...
60"W, 120"N	...	...	...	...	...	...	24 ± 9
Polarization Position Angle							
60"S	...	87 ± 6	...	...	123 ± 4	134 ± 5	141 ± 3
12"W, 57"S	107 ± 2	...	...	...	...	...	...
45"W, 46"S	...	...	131 ± 5	...	...	...	...
34"W, 46"S	129 ± 1	...	123 ± 4	...	...	...	...
45"W, 42"S	...	155 ± 3	...	155 ± 5	...	...	...
34"W, 42"S	...	149 ± 3	...	...	...	...	...
40"W, 40"S	...	127 ± 8	...	...	82 ± 10	65 ± 6	72 ± 5
45"W, 35"S	...	...	142 ± 4	...	...	...	...
34"W, 35"S	136 ± 1	...	135 ± 2	...	...	...	...
60"N	...	83 ± 8	...	...	121 ± 5	111 ± 32	82 ± 25
12"W, 64"N	82 ± 3	...	...	...	...	...	...
60"W, 120"N	...	...	...	...	...	...	95 ± 15

Table 3.2: Polarization measurements in different regions of NGC 2023 (Sellgren, Werner and Dinerstein 1992).



cess and decreasing dereddening at the longer wavelength in star C. This supports the conclusions of Witt, Schild and Kraiman (1984) that star C is comparable in intrinsic brightness to HD 37903 and is therefore likely to be a significant source of illumination for the reflected light in the near infrared, particularly for positions south of HD 37903. The star is also close to the peak in the far-infrared emission (Emerson *et al.* 1975; Harvey *et al.* 1980) and the CII recombination line emission (Knapp *et al.* 1975; Pankonin and Walmsley 1976; Pankonin and Walmsley 1978).

### 3.3 Extended Emission

#### 3.3.1 Infrared Excess

The visual reflection nebulae NGC 7023 and NGC 2023 have been found to emit strong infrared emission (Sellgren, Werner and Dinerstein 1983). They found that the emission from each nebula consisted of a smooth relatively flat continuum which could be characterized by a greybody with a high colour temperature of 1000 K with strong emission features at  $3.3 \mu\text{m}$  and a broad emission wing centred at  $3.4 \mu\text{m}$ . Both nebulae show a constant  $3.3 \mu\text{m}$  feature to continuum ratio of  $\sim 6$ , which is amongst the highest value ever observed, and indicates that both the continuum and feature are associated and may even have a common physical basis. For the positions that were observed by Sellgren, Werner and Dinerstein the continuum colour temperature and the  $3.3 \mu\text{m}$  feature to continuum ratio appear to be the same in both nebulae. At  $3.8 \mu\text{m}$  the surface brightness was observed to be far in excess of what could be explained by reflected light alone. Sellgren (1984) extends the previous spectrophotometric observations to shorter wavelengths and also increases the number of positions studied. The observations strengthen the conclusions formed earlier. The continuum is seen to extend from at least  $1.25 \mu\text{m}$  to  $4.8 \mu\text{m}$ . Despite the widely different colours of the illuminating stars both NGC 2023 and NGC 7023 were found to have similar infrared colours and both nebulae showed an excess surface brightness at  $2.2 \mu\text{m}$ , again which could not be explained by reflected light.

The infrared emission is shown to extend over a region  $3' \times 6'$  in diameter with the spatial distribution closely resembling that of the visual reflected light.

Allamandola, Greenberg and Norman (1979) claimed that the infrared fluorescence was a result of ultraviolet induced vibrational excitation of small molecules e.g. CH, H<sub>2</sub>O, NH<sub>3</sub>, and CO frozen on 0.1  $\mu\text{m}$  sized grains at low ( $\sim 10$  K) temperatures. This model requires a multicomponent mantle that is not going to change composition under a wide variety of interstellar conditions. The model also requires too high an ultraviolet fluorescence efficiency particularly if a common emission mechanism was to be adopted, considering that the feature to continuum ratio is constant in different reflection nebula and at different locations within each nebulae. Dwek *et al.* (1980) proposed equilibrium thermal emission from small (0.01  $\mu\text{m}$ ) grains coated with an unspecified polymeric material heated by the ultraviolet radiation. The problem with this model is that it is unable to account for the high brightness temperature of the 3.3  $\mu\text{m}$  emission (190 K) in these sources which is higher than the maximum temperature (70–150 K) of a dust grain in radiative equilibrium with the central star of the nebula. This model would also require values for the infrared oscillator strength near unity, when typical values vary from  $10^{-5}$ – $10^{-3}$  for vibrational transitions. The previous emission models are thus unable to explain the infrared excess and 3.3  $\mu\text{m}$  emission feature in reflection nebulae. It is not possible to explain the continuum emission as a result of free-free emission due to the lack of associated radio emission from these nebulae. Field stars are also ruled since the infrared colours of stars in the vicinity of these nebulae (Sellgren 1983) are very different from the observed colours of the nebular emission. There are also too few a number to explain the extended emission. Reflected light as well as being unable to explain the infrared surface brightness of the nebulae, cannot account for the 2.2  $\mu\text{m}$  polarization which is observed to be too low. Nor can reflected light account for the nebulae infrared colours being similar while the central stars have differing infrared colours.

Sellgren (1984) proposed that the observed continuum is produced by thermal

emission from very small grains  $\sim 10 \text{ \AA}$  of unspecified composition which momentarily reach high temperatures  $\sim 1000 \text{ K}$  following the absorption of a single UV photon, or after collisions (Harwit 1975; Purcell 1976). The peak temperature would then depend only on the energy of the UV photon and not on the distance of the grains from the star thus explaining the lack of radial colour temperature gradient from the central star in these sources. Both the infrared emission and the visual reflected light are proportional to the amount of incident starlight which would therefore account for the good agreement between the visual and infrared surface brightness distributions. This model also successfully predicts the fraction of the nebular luminosity,  $\sim 10^{-2}$ , involved in the  $1-5 \mu\text{m}$  near infrared emission, and requires only a small fraction,  $\sim 10^{-3}$ , of the total mass of grains to be  $\sim 10 \text{ \AA}$ . This model may also apply to the emission features as well as to the continuum. The problem however is that it relies on the assumption that the  $10 \text{ \AA}$  sized grains can be treated as if they have bulk thermal and optical properties.

The  $3.3 \mu\text{m}$  and  $3.4 \mu\text{m}$  features are just two of six unidentified infrared emission features between  $3.3 \mu\text{m}$  and  $11.3 \mu\text{m}$  that have been seen in many other sources, such as HII regions, planetary nebulae, and galaxies (Aitken 1981). The breadth of the features indicates that the emitting material is in a solid phase (Tokunaga and Young 1980; Grasdalen and Joyce 1979; Bregman and Rank 1975). Sellgren *et al.* (1985) carried out spectrophotometric observations of NGC 7023 and NGC 2023 from  $4$  to  $13 \mu\text{m}$  to search for the companion features which were found at  $6.2$ ,  $7.7$ ,  $8.6$ , and  $11.3 \mu\text{m}$ . They also searched for the continuum emission at longer wavelengths which enabled them to test the predictions of their thermal fluctuation model. They concluded that the continuum emission extends from  $1$  to  $13 \mu\text{m}$ . The feature to continuum ratio for the  $11.3 \mu\text{m}$  feature was also found to be  $\sim 5-7$  as well as that for the  $3.3 \mu\text{m}$ . The relative strengths and shape of the features are identical to those seen in other sources. This indicates that the same nonequilibrium emission mechanism operates in all sources showing these features. No evidence was found for  $10 \mu\text{m}$  silicate emission.

The single temperature blackbody model was shown to be too narrow and provided a poor fit to the 1–13  $\mu\text{m}$  continuum observations. If the nebular flux is due to thermal emission then a range of grain temperatures must be required. The shape of the predicted flux distribution with wavelength can be fit well to the continuum observations in the reflection nebulae. At the shortest wavelengths, 1–2  $\mu\text{m}$ , the predicted flux begins to fall below the observed spectrum. This is in qualitative agreement with the polarization observations of NGC 7023 which show that the fraction of near infrared emission due to reflected light is small at 2.2  $\mu\text{m}$  but becomes increasingly important as the wavelength decreases to 1.25  $\mu\text{m}$ . The quiescent environment of reflection nebulae implies that the features are associated with the interstellar medium rather than with a particular source of excitation. The feature emitting material must be hardy, ubiquitous and easily produced. Unidentified emission features apparently dominates the near infrared spectrum of ordinary interstellar material illuminated by ultraviolet radiation.

Léger and Puget (1984) built on the ideas of Sellgren (1984) and proposed that the feature emission is due to nonequilibrium thermal emission from large aromatic molecules, in the gas phase, excited by ultraviolet photons. They found good spectroscopic agreement between the calculated emission spectrum of the polycyclic aromatic hydrocarbons (PAH), coronene, and the features. They argued that only lines should be emitted and therefore they cannot account for the continuum emission. However Puget, Léger, and Boulanger (1985) derived continuum emission from 1 to 3  $\mu\text{m}$  from electronic transitions and they argue that the longer wavelength continuum emission is due to a superposition of weaker lines. Allamandola, Tielens, and Barker (1985) used the single photon excitation process suggested by Sellgren (1984) to calculate the emission spectrum expected from one PAH, chrysene, and found spectroscopic agreement with the features. They claimed that Léger and Puget (1984) were incorrect in treating emission from PAHs as a thermal phenomenon. In Allamandola, Tielens and Barker's model the continuum could be produced in two ways. Firstly by emission from the lowest lying electronic states or

secondly by emission from the vibrational quasi-continuum e.g low lying continuum produced by the overlap of all the various overtone and combination bands . However their theory did not make any predictions as to the shape of the continuum. In these gas phase fluorescent mechanisms there are no nonradiative mechanisms competing for the de-excitation of the molecules unlike in the original case of fluorescence of molecules in grain mantles. The emission features have also been identified with other carbonaceous substances (Sellgren 1990). There is a small contribution from the emission from ultraviolet excited vibrational fluorescence of molecular hydrogen, but this does not dominate the  $2.2 \mu\text{m}$  broadband emission of the reflection nebulae (see Section 3.3.2).

### 3.3.2 Molecular Hydrogen

Sellgren (1986) observed strong molecular hydrogen emission in the Q-branch at  $2.41 \mu\text{m}$  in NGC 2023, however she found no evidence for hydrogen emission in NGC 7023 at the positions searched. She concludes that  $\text{H}_2$  provides between 30% and 35% of broadband  $2.2 \mu\text{m}$  emission in NGC 2023 at  $80''$  S of the central star and at  $60''$  S hydrogen emission contributes  $\sim 20\%$ . For NGC 7023 an upper limit of 10% is placed. From the observations of NGC 2023 she concludes that  $\text{H}_2$  emission in reflection nebulae is due to ultraviolet fluorescence. The observed surface brightness of  $\text{H}_2$  emission is consistent with the predictions of the ultraviolet model. Internal nebular absorption or multiple pumping by ultraviolet photons may explain why there is less observed  $\text{H}_2$  emission than is predicted from the available stellar ultraviolet luminosity for NGC 7023.

Near infrared emission lines of vibrationally excited molecular hydrogen in NGC 2023 have also been observed by Gatley *et al.* (1987). The relative intensities of the lines is in excellent agreement with the theoretical predictions for ultraviolet pumped fluorescence model, which also accounts for the resultant spatial distribution of the neutral gas observed. Maps of the  $\text{H}_2$  lines show fluorescent emission originating from a thin shell of radius  $\sim 75''$  which surrounds the central star. The emission

is strongest to the southeast and lies just within a similar arc structure seen in integrated CO ( $J = 1 \rightarrow 0$ ) and CO ( $J = 2 \rightarrow 1$ ) emission (Gatley *et al.* 1987; Jaffe *et al.* 1990). Within the shell the hydrogen is radiatively dissociated. Density variations within the nebula cause the shell to appear nonspherical broken and clumpy. This shell of fluorescent  $H_2$  lies at the edge of Sellgren's nebula. Near the star the intense radiation field destroys the molecular hydrogen and heats the dust. The very small grains produce a near-infrared emission nebula, while the larger grains radiate away the bulk of the power from the star in the far-infrared (Harvey *et al.* 1980). At the interface between the dissociated region and the quiescent molecular cloud, where the radiation field is severely attenuated by the dust,  $H_2$  continues to be excited and destroyed by ultraviolet radiation. However the observed strength of the  $H_2$  emission suggests that only  $\sim 1\%$  of the stellar ultraviolet flux is presently absorbed in the molecular gas, thus the dust slows the predicted rate of growth of the dissociation sphere. The fresh material may be supplied either from the quiescent cloud or by the formation of  $H_2$  on grain surfaces (Tielens and Hollenbach 1985). Gatley *et al.* also mapped the emission at  $3.3 \mu\text{m}$ , which was found to be very different from the  $H$  ( $1.65 \mu\text{m}$ ) and  $K$  ( $2.2 \mu\text{m}$ ) maps. This is interesting since they all measure dust emission. The emitting grains which form Sellgren's nebula are not responsible for a large fraction of the emission in the  $3.3 \mu\text{m}$  feature. The similarity of the  $3.3 \mu\text{m}$  map to that of  $H_2$  suggests that either the carrier of the  $3.3 \mu\text{m}$  feature is absent or depleted within the volume where the  $H_2$  is dissociated or that the conditions favourable to the production of the  $3.3 \mu\text{m}$  feature occur where the  $H_2$  is excited.

NGC 2023 shows two separate sequences of energy levels corresponding to the ortho and para forms of molecular hydrogen (Hasegawa *et al.* 1987). If it was newly formed  $H_2$  then the para/ortho ratio would be expected to be 1:3, however a ratio of 1:(2.0–1.4) was found. The ratio is determined by the formation process of  $H_2$  on the grain surface, and therefore depends on the grain chemical composition, surface condition and temperature, the ratio is also dependent on the conversion reaction in the gas phase. Both sequences are characterised by a high

vibrational excitation temperature ( $T_v > 3600$  K) and a low rotational excitation temperature ( $T_r \approx 900 - 1500$  K). This is as expected from theoretical calculations (Takayanagi *et al.* 1987). This supports the identification of  $H_2$  emission in the nebula as due to fluorescent cascade after the absorption of an ultraviolet photon (Gatley *et al.* 1987). The fluorescence results in vibrationally and rotationally excited states in the electronic ground state. These radiative transitions do not alter the para/ortho ratio. The two sequences of population in NGC 2023 show similar excitation characteristics suggesting that the para/ortho ratio measured from the separation of the two sequences may represent the ratio of the total abundance of para- $H_2$  and ortho- $H_2$ .

### 3.3.3 Visible and Near-infrared Excess

Witt, Schild and Kraiman (1984) reported the findings by Gorodetskii and Roshkovshii (1978) of their photographic survey of NGC 2023, which covered the wavelength range  $3700 - 9000 \text{ \AA}$  in four broad bands. The results indicated at the longer wavelength end an unusual high nebular surface brightness. However the first detailed photometric study of NGC 2023 was carried out by Witt, Schild and Kraiman (1984) who showed that the nebula did indeed exhibit an unexpectedly high surface brightness in the spectral range  $0.65 \leq \lambda \leq 1 \mu\text{m}$ . The onset of the excess radiation appears quite suddenly around a wavelength of  $6000 \text{ \AA}$ . The  $R$  and  $I$  excess in the nebula emission was found to require a nonscattering mechanism while the radiation in the  $3500 - 5500 \text{ \AA}$  range is simply due to dust scattered starlight from HD 37903. Since the extended emission has a very similar spatial correlation to that of the infrared emission (see Section 3.3.1) together with the fact that the  $(R - I)$  colour shows no variation with distance from the central star suggests that there is a common nature and origin. This has led Witt, Schild and Kraiman to interpret this extended red emission in terms of a high frequency tail of the  $2 - 5 \mu\text{m}$  emission observed by Sellgren, Werner and Dinerstein (1983). However in order to fit in with Sellgren's model still smaller grains approaching temperature spikes near

the evaporation temperature of grains ( $T \sim 2000$  K) would have to be invoked to produce substantial emission in the  $R$  and  $I$  bands with possible additional contributions from molecular band emission. They propose that the fluorescence by solid grain material due to the irradiation by ultraviolet is a possibility.

Imaging of NGC 7023 was performed by Witt and Schild (1985) covering the spectral region  $B, V$  and  $I$ . The nebula was also found to exhibit a substantial  $I$  excess with very similar characteristics to that previously observed in NGC 2023, again beyond any explanation from dust scattering alone even with a maximum albedo of unity. The individual nebulae show a wide range of  $(V-I)$  colour differences. The relative strength of the extended emission in the  $I$  band reaches a maximum when the  $(B-V)$  colour difference is bluest in both NGC 2023 and NGC 7023. This is most readily understood if one considers that the range of  $(B-V)$  values results from differences in the internal reddening of the nebular radiation. Thus the largest  $(B-V)$  values in a given nebula arise where the reddening of stellar radiation before and after scattering is a minimum. Witt and Schild therefore conclude that the maximum relative strength of the  $I$  excess occurs where the radiation arriving from the illuminating star is spectrally least altered. They successfully explain their observations in terms of a simple colour-colour model whereby between 30% and 50% of the observed  $I$  intensity of the reflection nebulae arises due to a luminescence process excited by ultraviolet radiation from the illuminating stars. The fit of their model to the data identifies photons in  $1800 < \lambda < 2500$  Å region probably absorbed through the broad 2200 Å extinction band as the likely source of the excitation energy since the 2200 Å feature if considered as a possible energy channel is more than sufficient to power the observed  $I$  excess.

In a survey of the photometry of fourteen bright reflection nebulae Witt and Schild (1986) also present measurements in the  $B, V, R$  and  $I$  photometric bands for NGC 7023, concentrating on the prominent filaments in the central part of the nebula which exhibit unusually wide range of colours. They found the maximum surface brightness in  $V$  to be  $19.5 \text{ mag arcsec}^{-2}$  at about  $40''$  northwest of HD 200775

whereas from a detailed investigation of the scattering properties of the nebulae particles in NGC 7023 in the spectral range  $1400 \text{ \AA} \leq \lambda \leq 5500 \text{ \AA}$ , Witt *et al.* (1982) reported an average  $V$  surface brightness of  $18.5 \text{ mag arcsec}^{-2}$  in a narrow annulus of  $18''$  mean radius centered on HD 200775. The observed level of absolute nebular surface brightnesses in  $V$  and the radial gradients could be explained satisfactorily if the illuminating stars were embedded in extended clouds of moderate density by an amount corresponding to an optical depth of about 0.5 to 1. The dust must be of high albedo  $\sim 0.7$  and scattering must be strongly forward throwing. Bright reflection nebulae are therefore the result of near optimal scattering geometries. The relative surface brightness demonstrates the overwhelming fraction of the reddening seen in the illuminating stars must be produced directly within the nebulae and not by general interstellar dust.

The spectroscopic data obtained by Witt and Schild (1988) confirms that the source of the previous photometrically detected extended red emission (ERE) in reflection nebulae is indeed emission in the form of a broad luminescence band. The  $R$  excess extends from no excess at some locations to more than 30% excess at other locations. Both nebulae demonstrate similar correlations between an excess in  $R$  and an excess in  $I$ . Their results strongly suggest that the  $I$  excess is made up of two separate parts. The first being directly proportional to the  $R$  excess and is probably due to the long wavelength wing of the luminescence feature and the second being independent of the  $R$  excess, which is most likely to be a separate continuum emission component with a spatial distribution similar to the scattered light at  $I$  and is therefore probably related to the excess near infrared continuum in these nebula. In the spectral region  $6200-8100 \text{ \AA}$  all the features present in the spectra of the individual nebular were also present in the illuminating stars spectra. However a very broad emission feature was made obvious when the nebular energy distribution was divided by that of the respective illuminating star, with the excess radiation being greater than 25% above the level predicted for scattering alone. On average the wavelengths of the peak emission were found to be  $6740 \text{ \AA}$  and  $6640 \text{ \AA}$  for NGC 2023

and NGC 7023 respectively with FWHM  $\approx 1200 \text{ \AA}$  and a secondary peak near  $7200 \text{ \AA}$  seen at the limit of detectability in all spectra. The spectra are characterised by a relatively sharp rise at the short wavelength end and a more gradual decline at the long wavelength wing. Duley (1985) was the first to suggest that the fluorescence of hydrogenated amorphous carbon (HAC) was responsible for the broad luminescence feature which he detected in the Red Rectangle, peaking near  $6400 \text{ \AA}$ . Witt and Schild (1988) suggest that the feature is the same as that seen in NGC 2023 and NGC 7023, although weaker and peaking at a longer wavelength and are thus also due to the same basic process in a slightly more disordered carbonaceous material. Further support is shown by the band shape which is characteristic of amorphous materials with a high density of localized tail states at the band edges (Bodart and Feldman 1985). The variations of the band's intensity, shape, and peak wavelength can be interpreted as resulting from varying the concentration of the hydrogen in the amorphous carbon. Witt and Schild (1988) suggest the possible connection between a sideband at  $7150 \text{ \AA}$  detected by Lin and Feldman (1982) in the luminescence band of a-C:H and the weak secondary feature detected near  $7200 \text{ \AA}$ .

More extensive surface photometry in the *B*, *V*, *R*, and *I* photometric bands for NGC 2023 and NGC 7023 has enabled better spatial distributions of the ERE to be determined. Enhanced filamentary structure can be seen with greater contrast in the *R* and *I* images. In NGC 2023 a region of enhanced band emission is found in a system of narrow filaments apparently forming segments of a spherical shell about  $60''$  in radius surrounding the illuminating star. The intensity is greatest towards the east and south of HD 37903, while there is a distinct weakness of band emission in a  $50^\circ$  sector north of HD 37903. The strongest and sharpest bands are associated with a molecular hydrogen dissociation zone. This has led to the suggestion that the presence of hot atomic hydrogen produced in this photodissociation process, by the influence of ultraviolet stellar radiation (Stecher and Williams 1967; Dalgarno and Stephens 1970), provides the conditions necessary for the hydrogenation of amorphous carbon which leads to the exceptionally large

photoluminescence efficiency. The efficiency reaches a sharp peak for a hydrogen concentration of  $6.5 \times 10^{22} \text{ cm}^{-3}$  and falls by a factor of 2 when the hydrogen concentration decreases by 20% (Watanabe *et al.* 1982). A similar spatial correspondence has been suggested for NGC 7023. The measurements obtained on the filaments visible in NGC 2023 and NGC 7023 have a ratio of  $R$  excess to  $I$  excess greater than average. This is what they predicted from laboratory results, that in bright  $R$  filaments the carbon luminescence band would sharpen shifting towards shorter wavelengths and reducing the power in the long-wavelength tail as the hydrogen concentration in the amorphous carbon increases thus increasing the correlation between the  $R$  excess and  $I$  excess. The region of ERE filaments in NGC 2023 spatially coincides with the a region of near-infrared  $\text{H}_2$  fluorescence at  $3.3 \mu\text{m}$  observed by Gatley *et al.* (1987). Since the  $3.3 \mu\text{m}$  band is characteristic of aromatic compounds (Bellamy 1958) and is possibly attributed to polycyclic aromatic hydrocarbon (PAH) molecules (Léger and Puget 1984) the observations suggest the coexistence of a-C:H and PAHs in the same environment. This could be understood if solid a-C:H in the form of small grains and mantles on surface of mineral grains coexists in equilibrium with a population of free PAHs.

The examination of the ( $R-B$ ) colour image reveals the presence of strong ERE relative to the scattered nebular continuum in two major filaments in NGC 7023, one approximately  $50''$  northwest and one about  $70''$  southwest of HD 200775, assuming that the nebular light in the photometric  $B$  band is entirely due to scattering. The former filament represents the edge of a strong density enhancement facing the illuminating radiation from HD 200775, as suggested by the map of NGC 7023 at  $125 \mu\text{m}$  by Whitcomb *et al.* (1981) and the second filament is coincident with a region of steeply increasing optical depth at  $125 \mu\text{m}$ . These filaments represent environments where a substantial fraction of the incident stellar radiation must be intercepted by dust within a very short distance and are thus similar to that of the regions in NGC 2023.

An unsharped masked  $R$  photograph of NGC 2023 by Malin *et al.* (1987) shows

Object	Position	$\lambda_c$ (Å)	$\Delta\lambda$ (Å)	$I(\text{ERE})$ ( $\text{ergs cm}^{-2} \text{s}^{-1} \text{sr}^{-2}$ )	ERE/Scat
NGC 2023	62"ENE of HD 37903	6673	620	$1.2 \times 10^{-4}$	0.29
NGC 2023	84"ENE of HD 37903	6822	800	$1.4 \times 10^{-4}$	0.42
NGC 7023	20"W, 0"N of HD 200775	6862	820	$1.6 \times 10^{-4}$	0.04
NGC 7023	20"W, 50"N of HD 200775	6871	760	$2.1 \times 10^{-4}$	0.15
NGC 7023	20"W, 50"S of HD 200775	6568	620	$4.0 \times 10^{-5}$	0.04
NGC 7023	20"W, 70"S of HD 200775	6902	780	$1.3 \times 10^{-4}$	0.12
NGC 7023	S end of slit (lying NS) just W of HD 200775	6884	980	$1.3 \times 10^{-4}$	0.12
NGC 7023	S end of slit (lying NS) just W of HD 200775	6946	840	$1.1 \times 10^{-4}$	0.14

Table 3.3: Extended Red Emission Detections (Witt and Boroson 1990).

the ERE filaments. Witt and Malin (1989) photographed high resolution maps of NGC 2023 for the photometric  $B$  and  $R$  bands which clearly show the distribution of the ERE predominantly in filaments. The ERE filaments arise because the abundance of luminescing material is locally strongly enhanced and not due to any connection with localized nebular density enhancement. In order for the nebular material to be photoluminescent in the extended red emission band the necessary conditions must be optimal in the location of the filaments and less than optimal elsewhere. These conditions include the presence of an exciting radiation field, the luminescence efficiency of the nebular material and the orientation of the luminescent surface to the line of sight. A high resolution image of the southeast quadrant of NGC 2023 of  $H_2$  at  $2.12 \mu\text{m}$ , provided by Gatley, shows the  $H_2$  fluorescence concentrated in filaments which are identical in width and location to those of the ERE (Witt and Malin 1989). This provides further evidence for the association of the ERE with the dissociation of molecular hydrogen, the width and location of the ERE being dependent on the range in depth over which the stellar photons, responsible for the  $H_2$  dissociation, are actually absorbed by the nebular region. However the original  $H_2$  map of Gatley *et al.* (1987) shows an extended region of  $H_2$  emission about  $120''$  N of the illuminating star. Witt and Malin find no counterpart on the ERE map. The association is therefore incomplete.

Witt and Boroson (1990) obtained spectra with a more extended wavelength coverage of NGC 2023 and NGC 7023. The onset of the ERE band was determined to be at a wavelength of  $\sim 5400 \text{ \AA}$ . The central wavelengths/bandwidths of the profiles presented of NGC 2023 and NGC 7023 are given in table 3.3. For the two profiles of NGC 2023 the total band intensity was found to be the same in both, but the band appears to shift toward the longer wavelength side with an increase in offset from the star. The offset distance does not however take into account projection effects so the relationship between band shift and location is inconclusive. The profiles of NGC 7023 correspond to a featureless region adjacent to HD 200775, the red edge of a globule illuminated by HD 200775, a blue filament and a red filament. The second

DIB ( $\text{\AA}$ )	Equivalent Width ( $\text{m\AA}$ )
5705	27
5778	170
5780	155
5797	25
5844	<5
5849	3

Table 3.4: Diffuse Interstellar Absorption Bands and their measured equivalent widths in the spectrum of HD 37903 (Josafatsson and Snow 1987)

and fourth regions are distinctly visible as features on the ( $R-B$ ) colour map. Witt and Boroson found that the ERE band intensities for the featureless region and the red filament are essentially identical despite a difference in offset distance by a factor 3.6 and a difference in scattered light intensity of nearly a factor of 4. Variations in the bandwidth and wavelength of the peak emission can be seen not only between different objects but also as one moves from region to region within an object, a weak positive correlation exists between the band width and the central wavelength. There was however no correlation found between the nebular colour and the strength of the ERE band in either nebula.

### 3.3.4 Diffuse Interstellar Bands

Josafatsson and Snow (1987) obtained the spectra of HD 37903, the central star of the nebula NGC 2023, over the wavelength range 5695  $\text{\AA}$  to 5870  $\text{\AA}$ . They were able to measure six of the diffuse interstellar absorption bands (DIB's). These are recorded in table 3.4.

### 3.3.5 Summary

In both NGC 7023 and NGC 2023 a strong infrared continuum emission has been found covering the range 1 - 13 $\mu\text{m}$ . There are also discrete features at 3.3, 3.4, 6.2, 7.8, 8.6, and 11.3 $\mu\text{m}$ . Explanations of the infrared emission include UV induced

vibrational excitation of small molecules, equilibrium thermal emission from small grains and field stars. However none of these have been proved satisfactory. It has been proposed that the features are in fact due to nonequilibrium thermal emission from PAHs in the gas phase. There are however arguments about the treatment of the emission as a thermal phenomenon and that instead the continuum is produced either from the low lying electronic states or from the vibrational quasi-continuum. The possible contribution due to molecular hydrogen is also discussed.

Excess radiation has been found in both NGC 7023 and NGC 2023 in the red and near-infrared wavebands. The origin of this excess is believed to be connected with that of the infrared excess, with the ERE being the high frequency tail. Observations reveal that the maximum relative strength of the *I* excess occurs where the radiation arriving from the illuminating star is spectrally least altered. The ERE arises due to a luminescence process excited by ultraviolet photons. The intensity of the excess in the *R* has been seen to vary depending on location. A correlation was formed between the *R* and *I* excess. The peak of the ERE was found to be 6740Å in NGC 2023 and 6640Å in NGC 7023. Variations in the bandwidth are also seen to occur in both nebulae. HAC, already proposed as the source of ERE in the Red Rectangle is again associated with the ERE in NGC 7023 and NGC 2023. The differences that occur are interpreted in terms of a varying concentrations of hydrogen. The ERE is shown to occur in particular filaments within the nebulae. In NGC 2023 a connection is made with a molecular hydrogen dissociation zone suggesting that this could provide the ideal conditions necessary for the formation of HAC. In the following chapter new results are examined in order to clearly identify the locations of the ERE and thus identify the source. It is also necessary to find if there are any links with the DIBs as in the case of the Red Rectangle.

## Chapter 4

# New Observations of NGC 7023 and NGC 2023

### 4.1 The Observation and Reduction Details of NGC 7023

The data was obtained at the F/15 focus of the 1m JKT on La Palma in 1989 over a period of 7 nights from July 28 to August 3 using the Durham imaging polarimeter with a GEC coated CCD as detector. The author was not one of the observers. Observations were made in four filters  $B$  ( $\sim 4400 \text{ \AA}$ ),  $V$  ( $\sim 5520 \text{ \AA}$ ),  $R$  ( $\sim 6630 \text{ \AA}$ ), and  $I$  ( $\sim 8090 \text{ \AA}$ ). The image area was centered on HD 200775 and an opaque mask was used to block out the central starlight in order to prevent the CCD from saturating during long exposures. Six overlapping field positions in the region of NGC 7023 were recorded in the  $V$ ,  $R$ , and  $I$  wavebands in order to obtain a complete field and four overlapping field positions were recorded in the  $B$ . Each field position consisted of a set of four exposures lasting 500s in which two orthogonal polarization states were recorded. The image scale of the telescope is  $1.23'' \text{ pixel}^{-1}$ . The data was reduced using the procedure described by Warren-Smith (1979) and Scarrott *et al.* (1983) whom also discuss the possible errors. Common field stars were used in order to align the images. The main source of error is in the sky subtraction. Since the observations record both object and surrounding sky simul-

taneously an area in the vicinity of the object must be chosen which is representative of the sky-background uncontaminated by the object. However the nebula is so extensive that it almost completely covers the image area and therefore there was little sky in the field of view. Thus any area chosen for the sky subtraction inevitably contained some faint nebulosity. Since each field was reduced separately the regions used for sky subtraction were different and could therefore have contained varying amounts of nebulosity.

## 4.2 Polarimetry Results of NGC 7023

Some of the data presented in this section has already been published by Watkin *et al.* (1991). In all diagrams north is at the top and east is to the left, with the position of the central star being marked by a cross. Fig. 4.1 shows a greyscale intensity or brightness image of NGC 7023 in the  $R$  waveband with the field being  $8'.1 \times 6'.6$ . The intensity is clearly inhomogeneous and asymmetric with the faint nebulosity quite extensive and wispy; the main wisps running approximately N-S  $\sim 3'.2$  E and  $\sim 3'.5$  SSW from the central star. The nebula appears to be slightly elongated along an axis at position angle  $30^\circ$ . One of the most pronounced features of the nebula is a high intensity forked tongue  $\sim 130''$  WNW of HD 200775 which projects into a low intensity region. It would therefore appear that the nebula varies in either a structural manner or due to changes in density. The presence of dust is indicated by the visibility of stars which are more numerous and brighter in the red than in the blue. Fig. 4.2 and 4.3 are also brightness images of NGC 7023 in the  $B$ , and  $R$  wavebands scaled in order to show the structure of the central region with the field being  $2'.7 \times 4'.3$ . The nebula shows many small scale variations. A close examination of the  $R$  and to a lesser extent the  $I$  images reveal the presence of filamentary structures not seen with similar contrast on the  $B$  image. The most prominent features are: two E-W lying filaments at an offset of  $\sim 65''$  S and the other, a "northern horn"  $\sim 53''$  N from HD 200775, running NE-SW there is a filament  $\sim 37''$  S, a "forked-tongue" filament  $\sim 32''$  SW and a curved filament

~ 55" NW.

The polarization and intensity contour maps are shown in fig. 4.4, 4.5, 4.6, and 4.7 for the *B*, *V*, *R* and *I* wavebands respectively. A low level intensity cut off was specified in order to prevent contamination from random and chaotic vectors from low intensity regions which are simply due to noise. In all the wavebands studied a centrosymmetric pattern of polarization vectors can be seen which confirms that HD 200775 is the only light source of the reflection nebula. The percentage polarization varies according to position in the nebula but the overall behaviour is identical on all four maps. That is there appears to be no structural variation only apparent in one wavelength. The common features are a region 76" ESE of HD 200775, roughly perpendicular to the axis of elongation, where the polarization is markedly decreased, also a region ~ 141" WNW where the polarization is again slightly decreased. Other features include a relatively high region of polarization to the north-east and also to the south-west.

The percentage polarization and position angle were measured at 70" S, 35" S, 30" W 20" N, 30" N, 60" N and 70" N, using an aperture size of 10".5 which coincides with the positions and aperture size used by Sellgren, Werner and Dinerstein (1992) for measurements made in the *J*, *H* and *K* wavebands. The results are given in table 4.1 and plots of the wavelength dependence including Sellgren's results are given in fig 4.8. The general trend appears to a monotonic increase in polarization with wavelength in the visible and near-infrared followed by a decrease in polarization with wavelength in the infrared, with the maximum polarization occurring somewhere between ~ 0.81  $\mu\text{m}$  and ~ 1.25  $\mu\text{m}$ . The position angles remain approximately constant with wavelength.

The presence of a nonscattering contribution to the surface brightness of a nebula is easily demonstrated through three colour surface photometry, with three filters chosen such that two of the three bandpasses are dominated by scattering, while the third is centered on the nonscattering contribution, such as an ERE feature. The presence and relative contribution due to the ERE in the third band can then

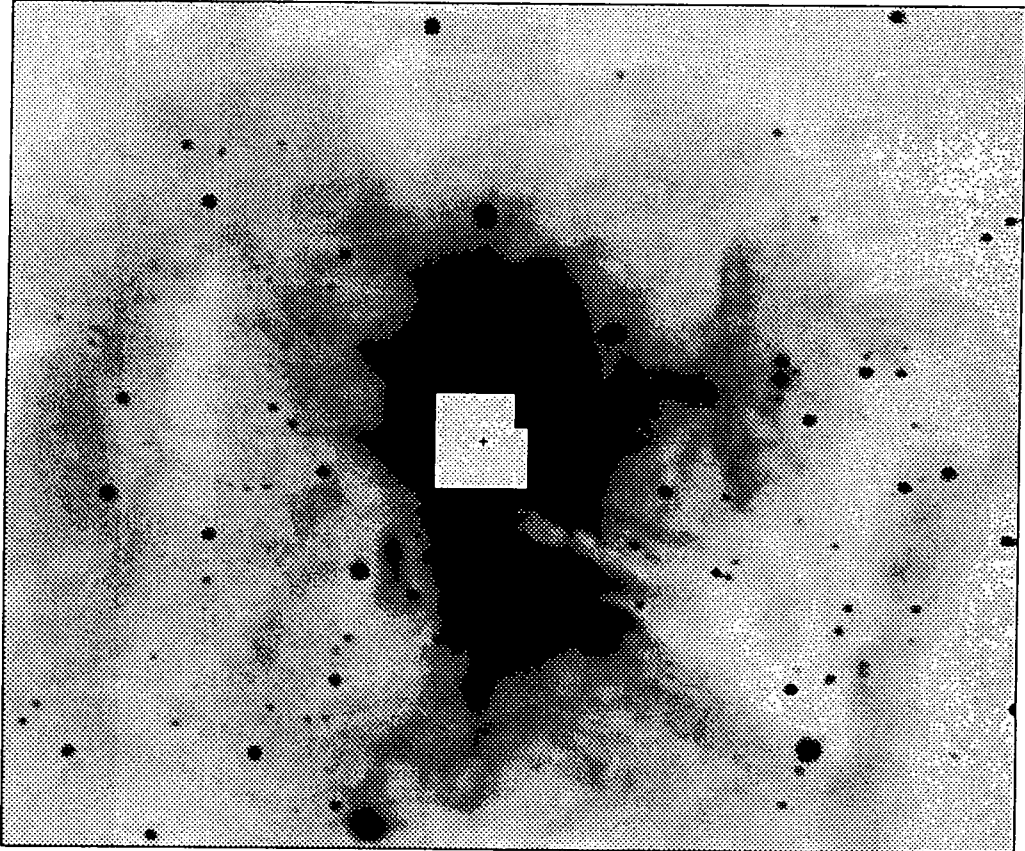


Figure 4.1: Intensity image of NGC 7023 in the  $R$  waveband. The field is  $8'.1 \times 6'.6$  in size.

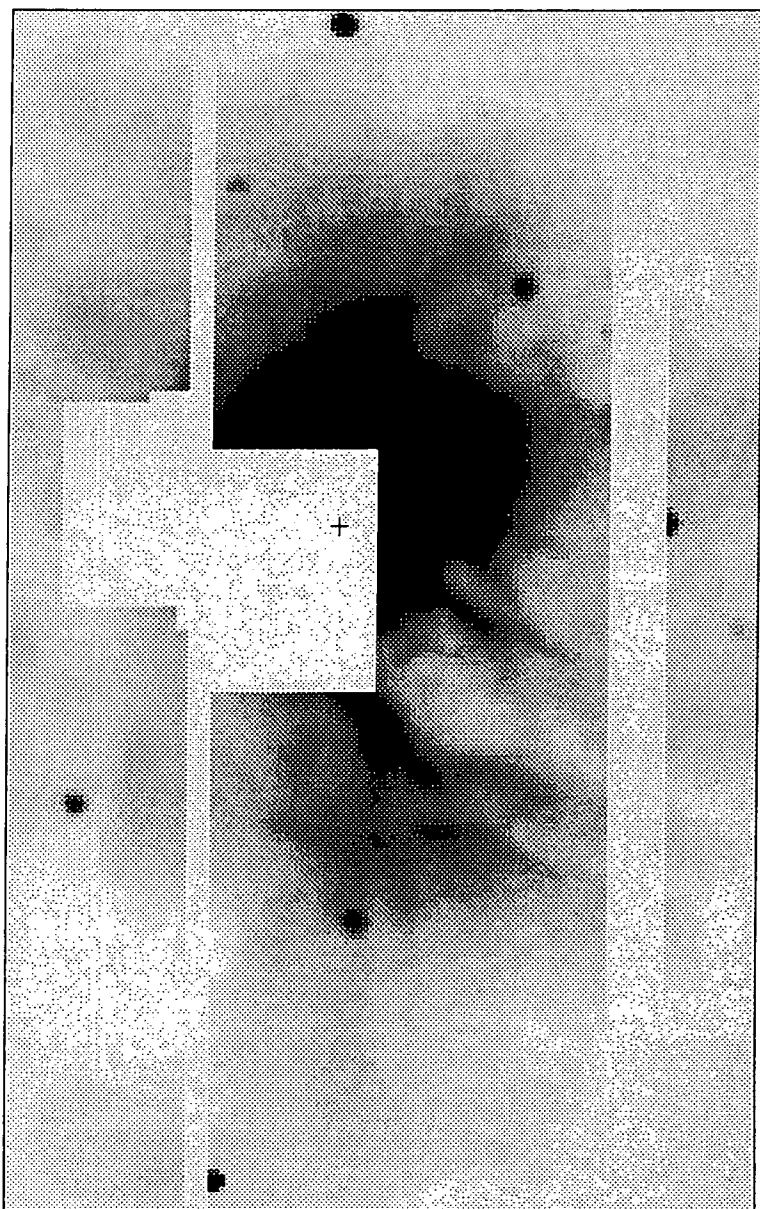


Figure 4.2: Intensity image of NGC 7023 in the *B* waveband. The field is  $2'.7 \times 4'.3$  in size.

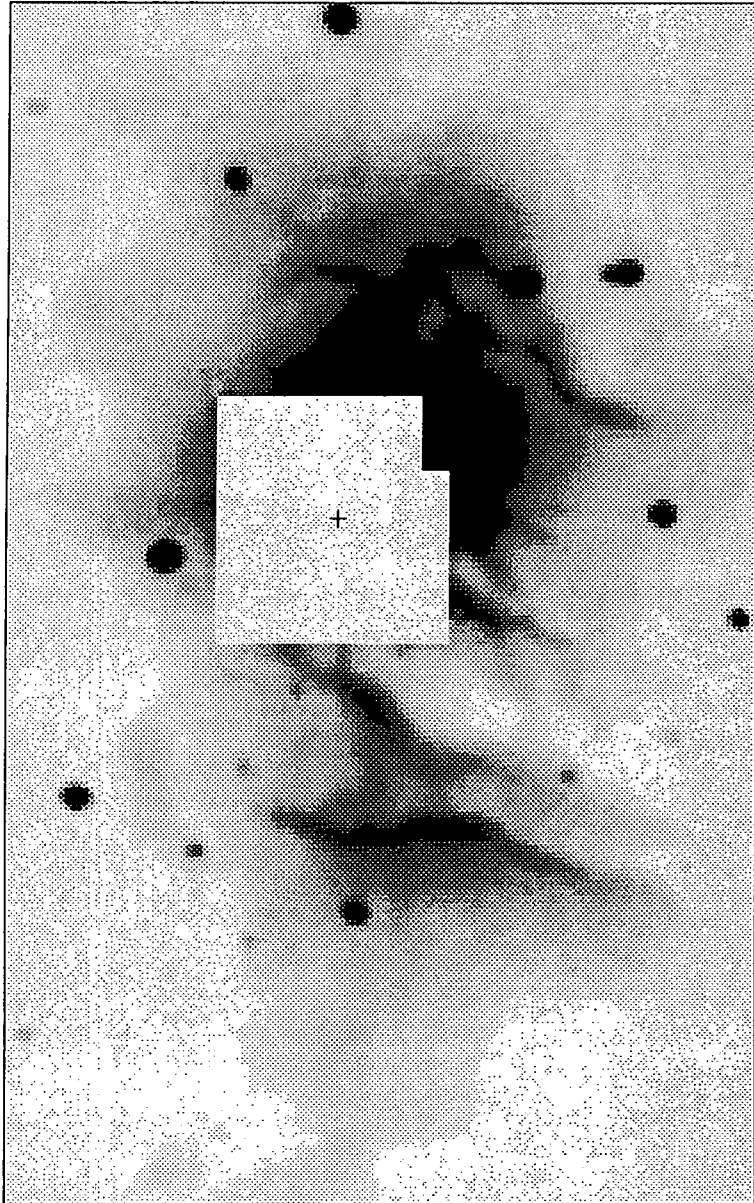


Figure 4.3: Intensity image of NGC 7023 in the *R* waveband. The field is  $2'.7 \times 4'.3$  in size.

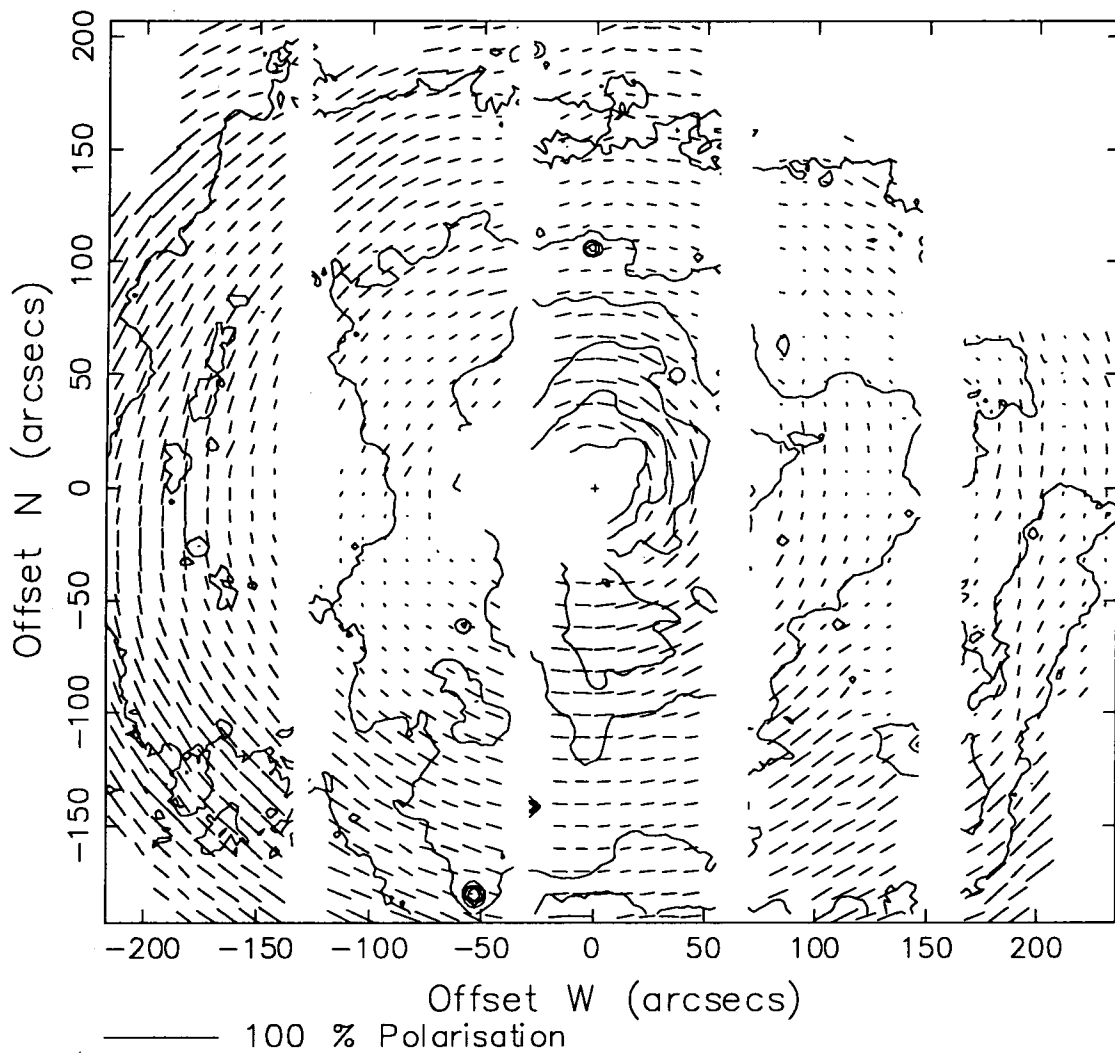


Figure 4.4: Polarization and intensity contour map of NGC 7023 in the *B* waveband.

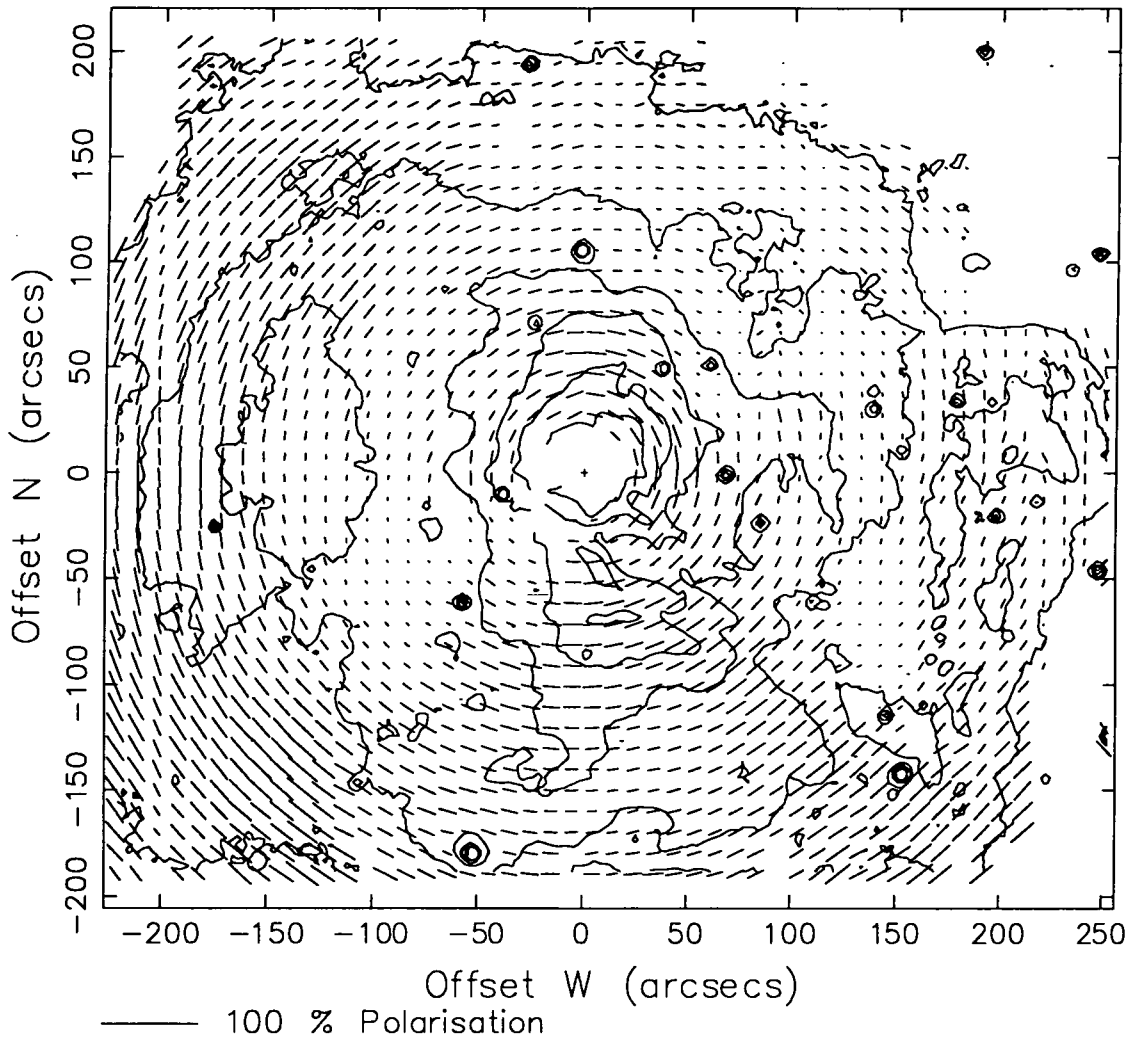


Figure 4.5: Polarization and intensity contour map of NGC 7023 in the V waveband.

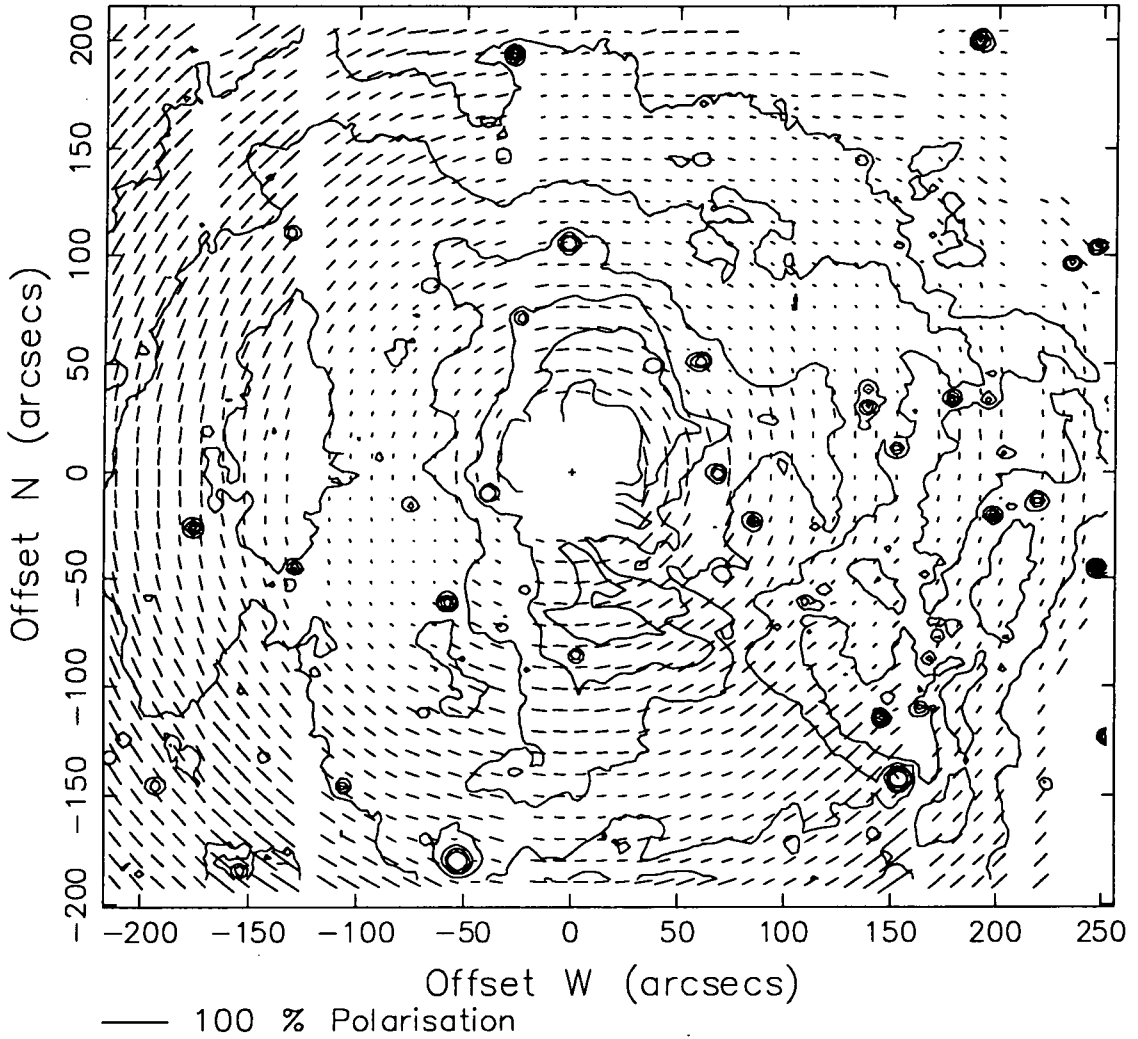


Figure 4.6: Polarization and intensity contour map of NGC 7023 in the *R* waveband.

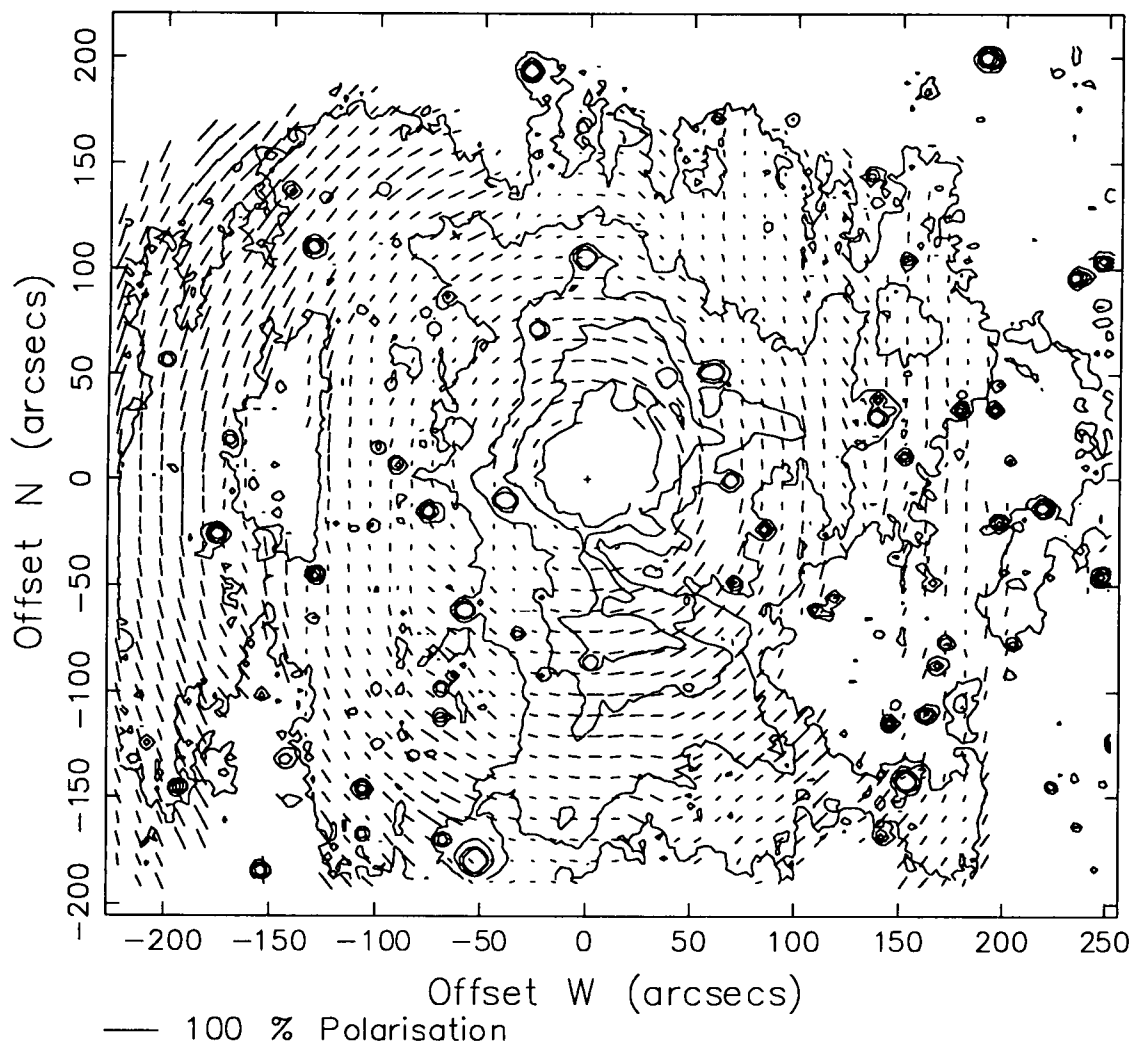


Figure 4.7: Polarization and intensity contour map of NGC 7023 in the *I* waveband.

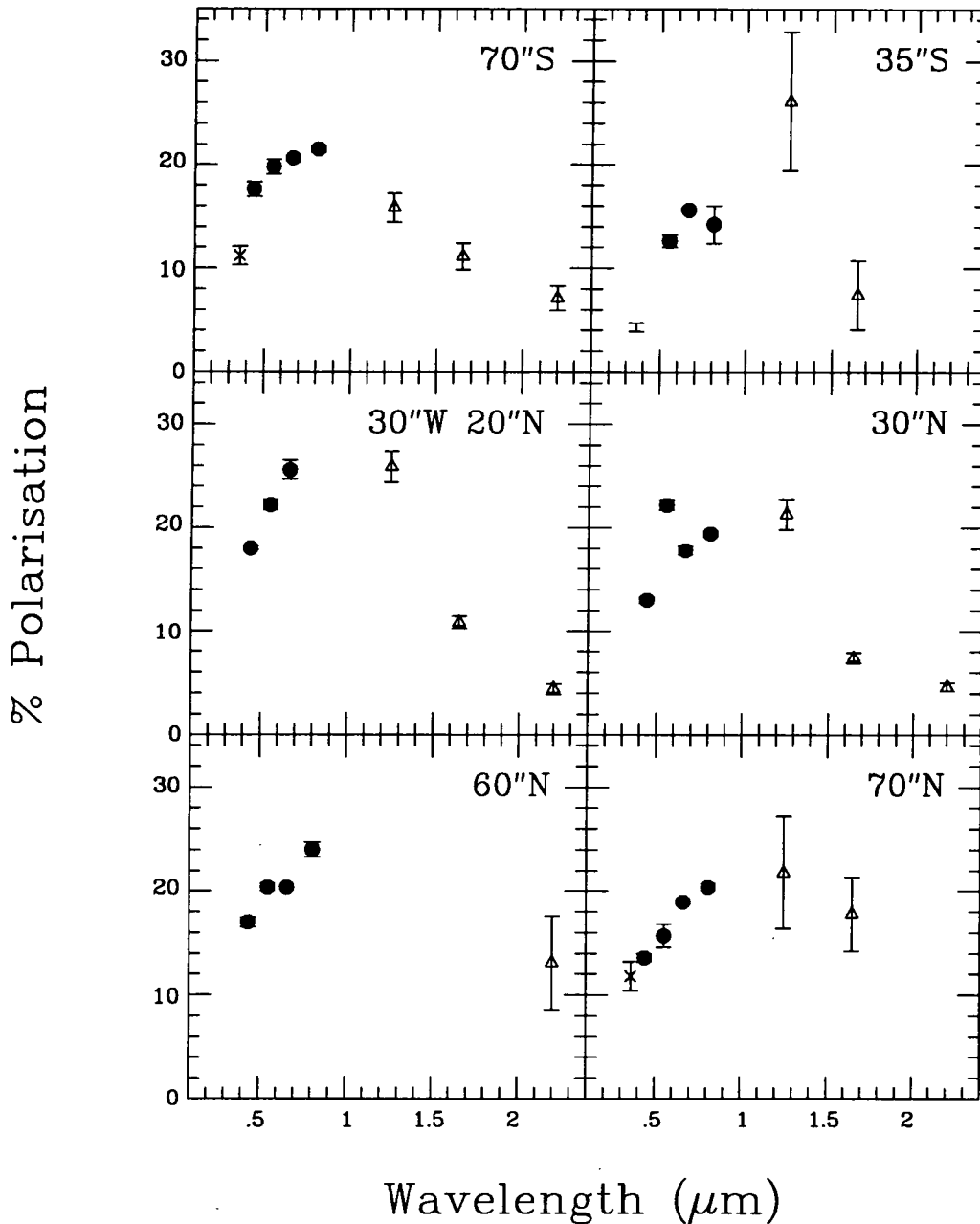


Figure 4.8: The wavelength dependence in five different regions of NGC 7023. The uncertainties are only plotted when larger than the size of the symbol. The ● are my data, the △ are from Sellgren, Werner and Dinerstein (1992) and the × are from Elvius and Hall (1967).

Position	<i>B</i>	<i>V</i>	<i>R</i>	<i>I</i>
Percentage Polarization				
70" S	17.7 ± 0.7	19.8 ± 0.7	20.6 ± 0.2	21.5 ± 0.3
35" S	...	12.6 ± 0.6	15.6 ± 0.1	14.2 ± 1.8
30" W, 20" N	18.0 ± 0.2	22.2 ± 0.5	25.6 ± 0.9	...
30" N	13.0 ± 0.3	22.2 ± 0.5	17.8 ± 0.4	19.4 ± 0.3
60" N	17.0 ± 0.5	20.4 ± 0.4	20.4 ± 0.1	24.0 ± 0.7
70" N	13.6 ± 0.4	15.7 ± 1.1	19.0 ± 0.2	20.4 ± 0.4
Polarization Position Angle				
70" S	90.1 ± 1.1	91.4 ± 1.1	90.5 ± 0.3	89.3 ± 0.4
35" S	...	91.9 ± 1.4	90.5 ± 0.2	89.4 ± 3.7
30" W, 20" N	30.7 ± 0.3	33.1 ± 0.6	30.8 ± 1.0	...
30" N	89.6 ± 0.6	...	91.2 ± 0.2	86.1 ± 0.4
60" N	90.1 ± 0.8	89.6 ± 0.6	91.1 ± 0.1	87.7 ± 0.9
70" N	90.5 ± 0.9	93.1 ± 2.0	91.1 ± 0.3	88.4 ± 0.5

Table 4.1: The variation in percentage polarization and position angle for five different positions in NGC 7023.

be illustrated through a colour difference diagram. The presence in a reflection nebula of excess emission in the *R* will reduce the colour differences (*V*−*R*) and (*B*−*R*) compared to the values expected from scattering alone, assuming that the *B* and *V* values are purely due to scattering. Likewise since there is also believed to be a small contribution to the *I* intensity from the ERE then this will also be expected to reduce the colour differences (*V*−*I*) and (*B*−*I*) compared to the values expected from scattering alone. Fig. 4.9 shows the colour difference diagram  $I_{V-R}$  where  $I_{V-R} = -2.5 \log[I_V/I_R]$ , *I* being the total intensity and *V* and *R* refer to the wavebands. Most of the nebulosity is relatively uniform in colour except for the regions which coincide with four of the prominent features described in the intensity image earlier, thus revealing more clearly the filamentary structure. However on the  $I_{B-R}$  diagram only two regions are seen where the nebula is definitely redder than elsewhere, one being the filament which lies 65" S of the central star and the other being the region approximately 53" N of the central star. Both these filaments

coincide with areas identified as sources of ERE by Witt and Schild on the basis of colour and spectroscopy. The filaments also appear to be narrower than those seen in the intensity image. The same results were found for the colour differences  $I_{V-I}$  and  $I_{B-I}$  the only difference being that the red filaments were not seen with as greater contrast.

Since the regions of suspected ERE showed no obvious features in the polarization maps further investigation is required. Polarization colour maps have been produced where the polarization colour  $P_{V-R} = -2.5 \log[(PI_V/I_V)/(PI_R/I_R)]$ ,  $PI$  and  $I$  being the polarized and total intensities respectively and  $V$  and  $R$  refer to the wavebands. In fig. 4.10 two regions are revealed in which the polarization colour is significantly reduced i.e. the ratio of the  $V$  and  $R$  polarization is lower than elsewhere in the nebula. Likewise the polarization colour  $P_{V-I}$  also shows the same regions to have a ratio of polarization in  $V$  to polarization in  $I$  lower than over the rest of the nebula. These regions correspond to the red filaments found in the intensity and colour images. North-south traces were thus made across both these filaments.

Fig 4.11 shows scans through the southern filament in all wavebands of the percentage polarization. In the  $B$  and  $V$  wavebands the polarization decreases slowly and monotonically with increasing radial distance across the filament. However in the  $R$  and  $I$  wavebands the polarization is markedly decreased in the narrow filament where the emission is suspected of being dominated by ERE rather than by scattered light. N-S traces have also been made in all wavebands of the polarized intensity i.e the product of the percentage polarization and the intensity, these are shown in fig 4.12. In all wavebands this shows an increase at the centre of the filament which means that there is an increase in the number of scatterers at this position but there is no obvious change in behaviour between the wavebands. Fig 4.13 shows N-S scans across the filament in colour  $I_{V-R}$  and  $I_{V-I}$ , at the top and polarization colour  $P_{V-R}$  and  $P_{V-I}$  at the bottom. The traces in colour show a rapid increase in reddening;  $\Delta I_{V-R} \approx 0.25$  mag,  $\Delta I_{V-I} \approx 0.2$  mag. The corresponding lower traces in polarization colour show a sudden fall due to the reduction in  $P_R$  and to a lesser

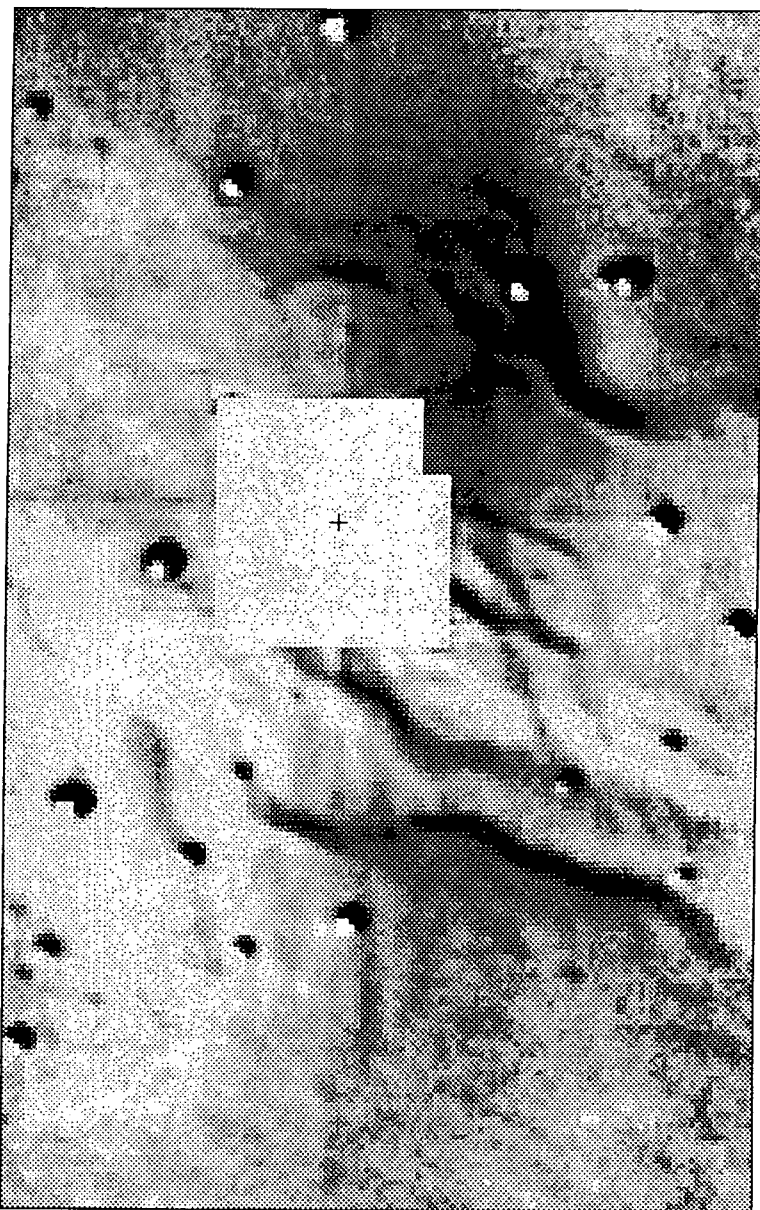


Figure 4.9: Colour difference image  $I_{V-R}$  of NGC 7023. The field is  $2'.7 \times 4'.3$  in size.

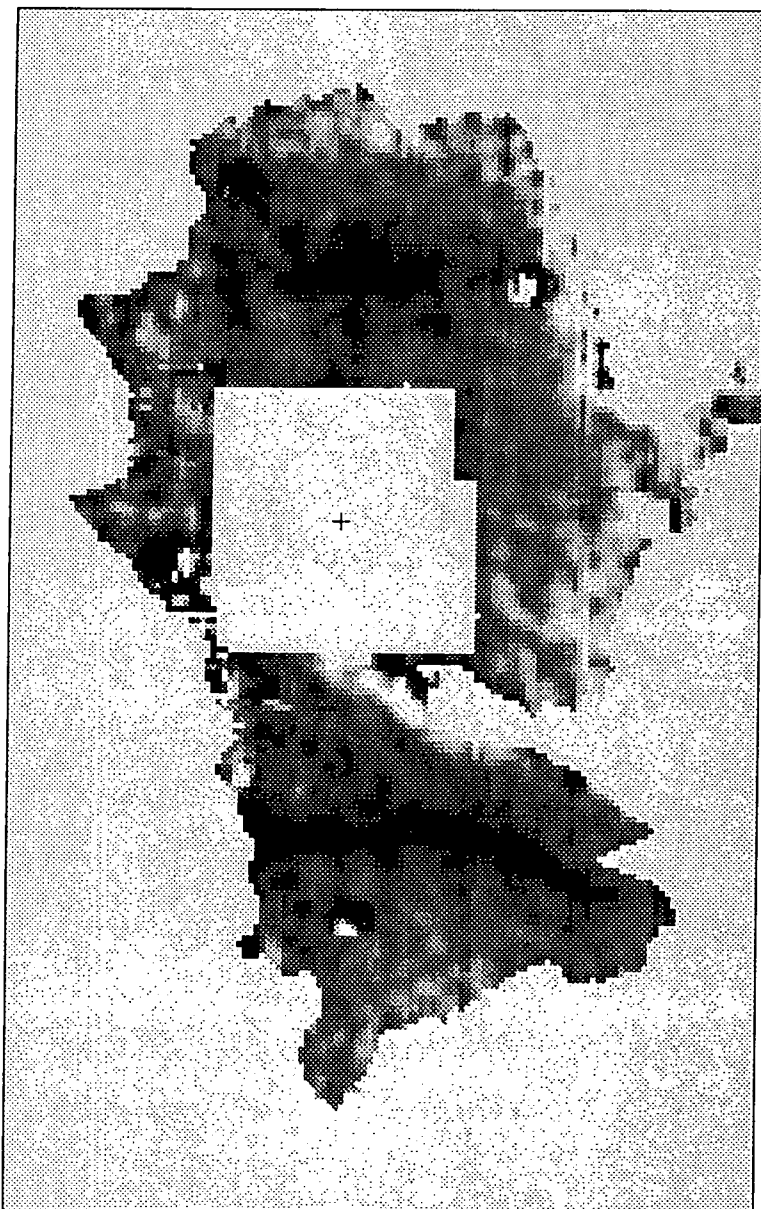


Figure 4.10: Polarization colour difference image  $P_{V-R}$  of NGC 7023. The field is  $2'.7 \times 4'.3$  in size.

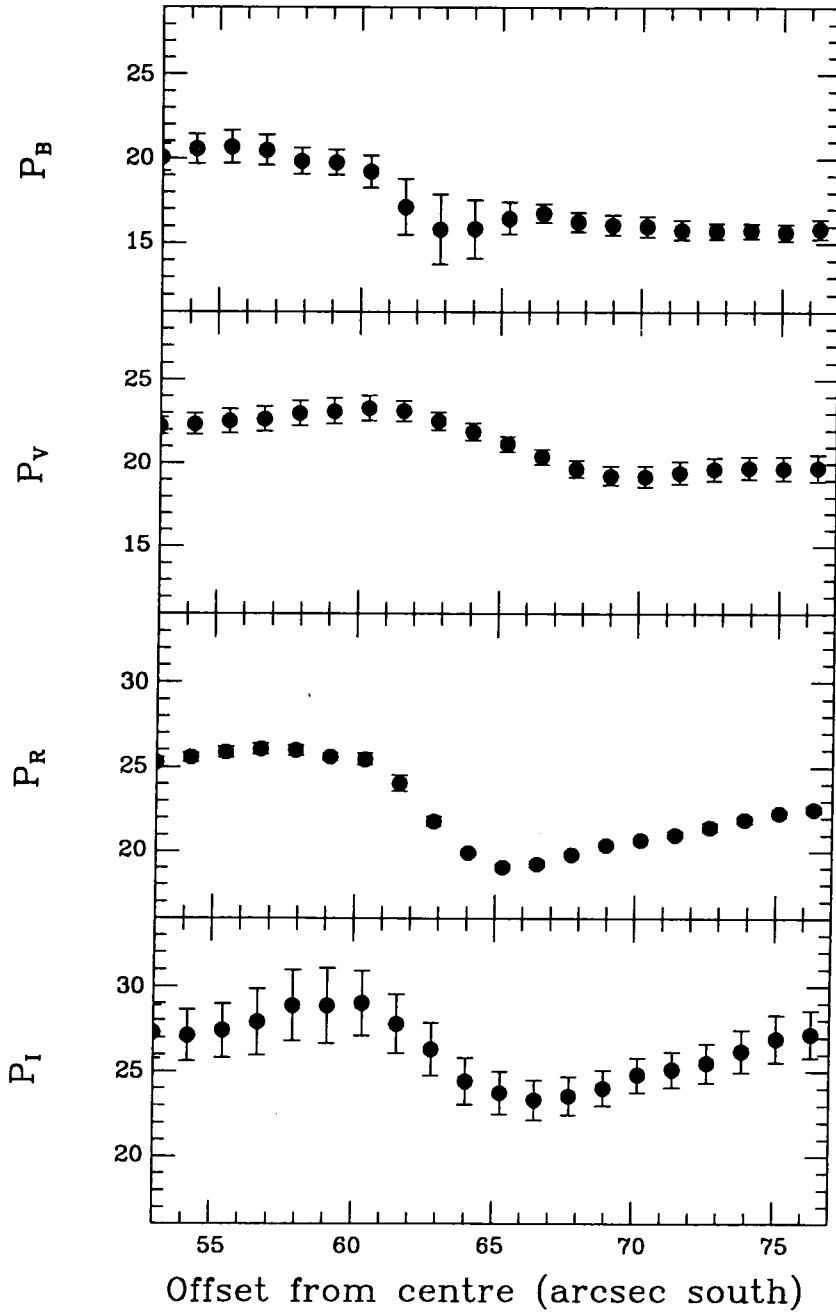


Figure 4.11: Traces of percentage polarization across the filament 65" S of HD 200775.

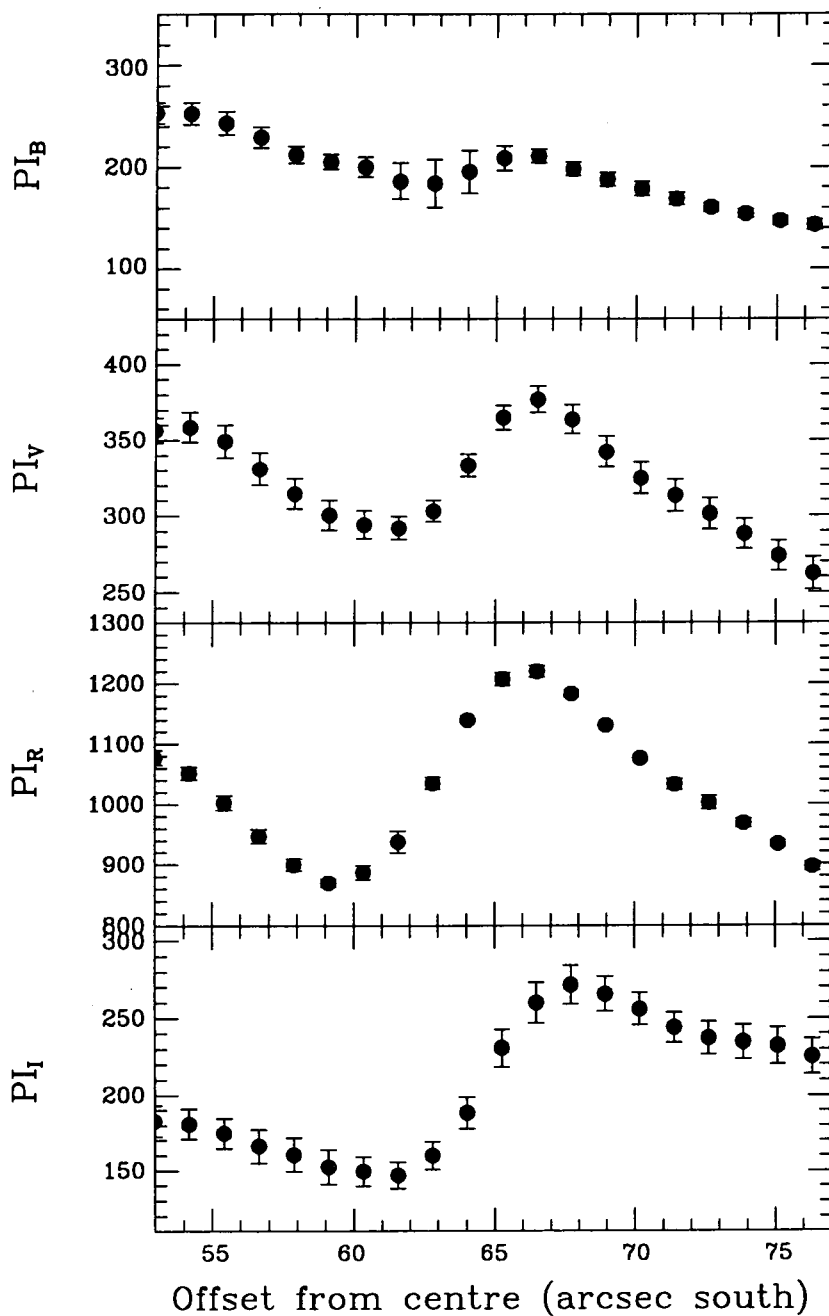


Figure 4.12: Traces of polarized intensity across the filament 65'' S of HD 200775.

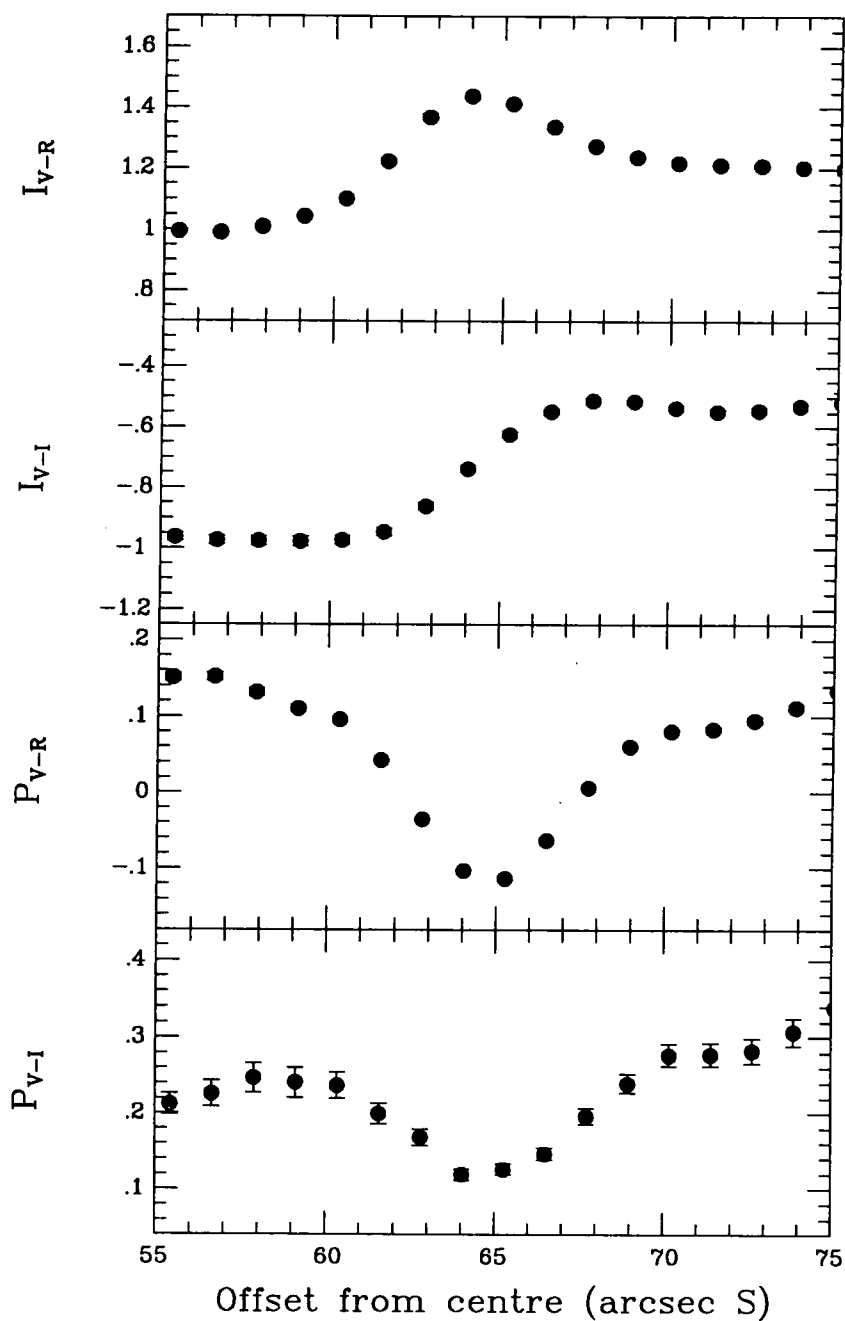


Figure 4.13: Traces of colour difference and polarization colour difference across the filament 65" S of HD 200775.

extent in  $P_I$ ;  $\Delta P_{V-R} \approx -0.22$  mag,  $\Delta P_{V-I} \approx -0.14$  mag. It should be noted that the minimum in the polarization colour occurs further south than the maximum in the intensity colour therefore suggesting that the ERE comes from the outer edge of the filament.

The same results were found for north-south scans made through the northern filament in all wavebands of the percentage polarization, fig 4.14. In the  $B$  and  $V$  wavebands the polarization increased slowly and monotonically with increasing radial distance across the filament before beginning to fall at  $\sim 59''$  north of HD 200775. However in the  $R$  and  $I$  wavebands the polarization is reduced at the position of the filament. The polarized intensity traces, fig 4.15, show the same trend in all wavebands, a steady decrease with radial distance across the filament. Again there is no obvious changes between the wavebands. Traces in colour  $I_{V-R}$  and  $I_{V-I}$  and polarization colour  $P_{V-R}$  and  $P_{V-I}$  can be seen in fig 4.16. A sudden increase in reddening is shown in the upper scans due to an increase in the red intensity;  $\Delta I_{V-R} \approx 0.18$  mag,  $\Delta I_{V-I} \approx 0.1$  mag. The corresponding lower scans in polarization colour, show a rapid reduction;  $\Delta P_{V-R} \approx -0.16$  mag,  $\Delta P_{V-I} \approx -0.13$  mag due to the fall in  $P_R$  and  $P_I$  seen on the individual polarization scans.

### 4.3 The Observation and Reduction Details of NGC 2023

The polarimetry data was obtained on three separate occasions using the Durham imaging polarimeter with a GEC coated CCD as detector. The first two runs were at the F/15 focus of the 1m JKT on La Palma with observations being made in 1988 on January 20 and in 1991 on four separate nights between November 5 and November 9. On each occasion the data was being recorded in three filters,  $V$ ,  $R$  and  $I$ . For the first run the nebula was centred to the left side of the image area with the central star carefully positioned behind a grid. Only one field position was recorded consisting of a set of four exposures each lasting 300s for the  $V$  and  $R$  wavebands and 400s for the  $I$  waveband. For the second run the image area was centred on

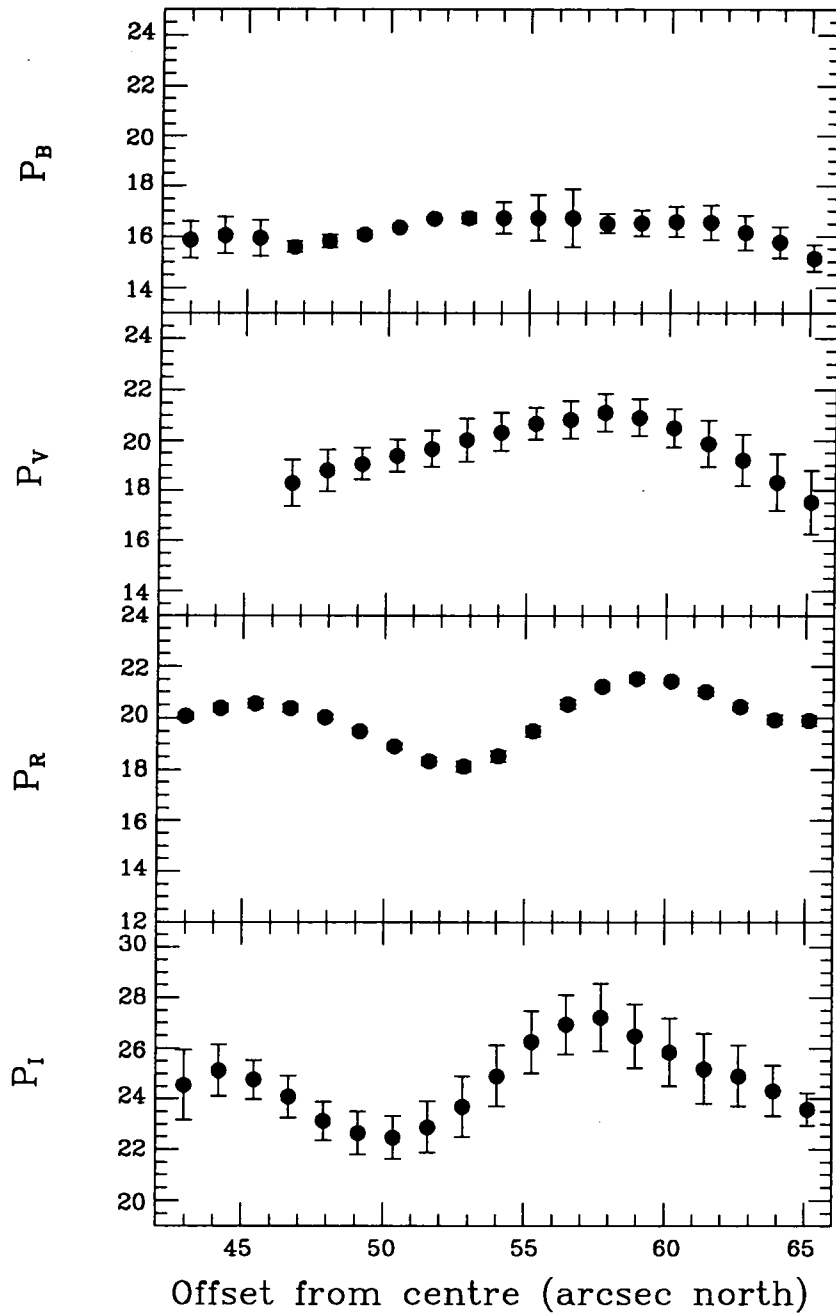


Figure 4.14: Traces of percentage polarization across the filament 53" N of HD 200775.

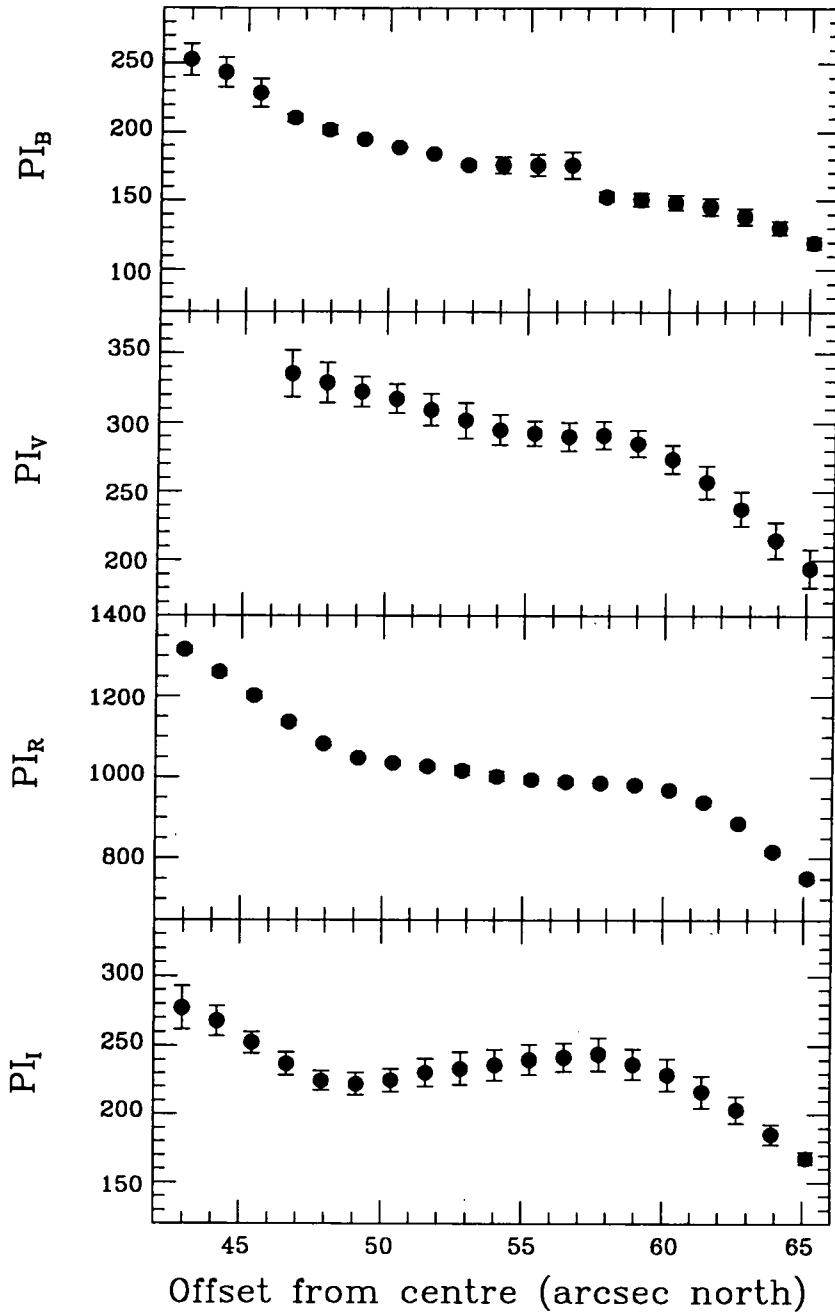


Figure 4.15: Traces of polarized intensity across the filament 53'' N of HD 200775.

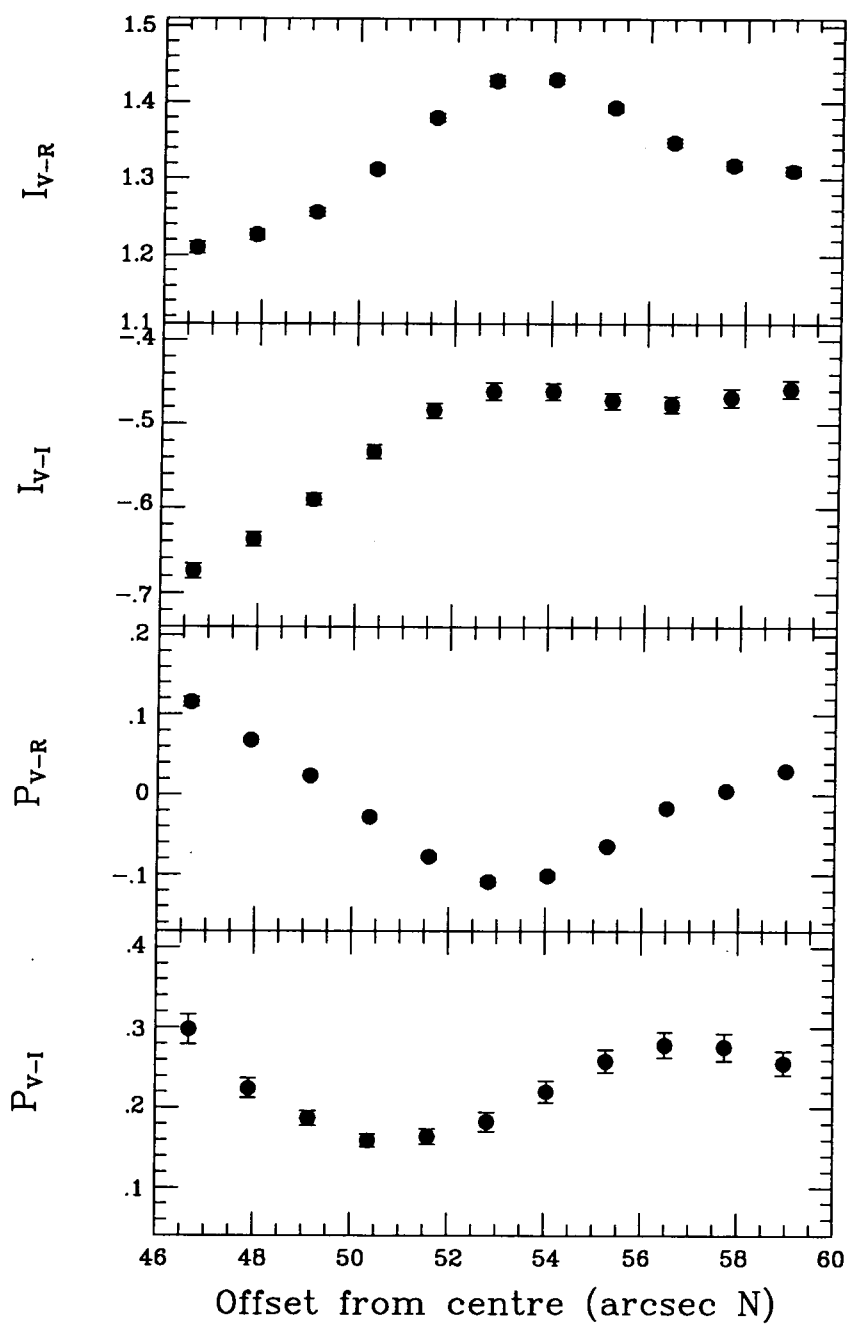


Figure 4.16: Traces of colour difference and polarization colour difference across the filament 53'' N of HD 200775.

HD 37903 and an opaque mask was used to block out the central star which like in the case of HD 200775 is bright enough to saturate the exposures. Four overlapping field positions in the region of NGC 2023 were obtained in each filter in order to form a complete field. Each field position consisted of a set of four exposures lasting 300 s each. The image scale of the telescope is  $1.23'' \text{ pixel}^{-1}$ . A third run was made at the F/15 focus of the 1 m SAAO in 1992 over a period of four nights from March 4 to March 8. Observations were made in two filters *V* and *I* with the image area centred on the illuminating star. Each field position consisted of a set of four exposures each lasting 300 s for the *V* waveband and 400 s for the *I* waveband. The image scale of the telescope is  $1.15'' \text{ pixel}^{-1}$ . The author was not one of the observers on the first or third run. The data was reduced as described in section 4.1. Common field stars were used to align the images and to correct for the difference in image scale. The main source of error was again the sky subtraction particularly on the data from the second run where the weather conditions were unfavourable.

Spectroscopic data was obtained at Cassegrain F/8 focus of the AAT in 1992 on January 11 using the RGO spectrograph and a Thompson CCD as detector. The slit was orientated E-W in order that part of the slit would sample sky as well as the regions of interest. A 1200 lines/mm grating was mounted in blaze to collimator. One spectrum was taken of HD 37903 with the exposure lasting 100 s and four spectra were taken of the nebula with the slit placed  $32''$  N of the central star, each exposure lasting 600 s. Flatfields were observed as was a Cu-Ar lamp for calibration purposes. The wavelength range spans from  $5700 \text{ \AA}$  to  $6300 \text{ \AA}$ . The data was reduced using the Figaro software package. First the data was flatfielded to correct for pixel to pixel variations. Then the sky subtraction was done two dimensionally by selecting one or more regions along the slit which were relatively free from the nebular light. The subtraction was made difficult since the nebula is quite extended. An average value was determined for each wavelength and then subtracted from each pixel in that column of the frame. The one dimensional spectra were extracted by selecting a particular region along a the slit and then summing

the counts along each column from the rows that make up the chosen region. The spectrum for the calibration lamp were constructed in the same way. The nebulae and star spectrum were then wavelength calibrated and rebinned to a common wavelength scale. The four individual nebulae spectra were then summed. It was then necessary to accurately subtract the scattered spectrum of the illuminating star since this constitutes the major portion of the nebulae spectrum in order to determine if there is any intrinsic emission in the nebula.

#### 4.4 Polarimetry Results of NGC 2023

In all the diagrams north is at the top and east is to the left, with the position of the central star being marked by a cross. Fig. 4.17 shows a greyscale intensity image of NGC 2023 in the *R* waveband, the field being  $6'.1 \times 6'.4$ . The nebula is clearly quite wispy but the only major filament is one which runs almost N-S,  $84''$  ENE of the illuminating star. The intensity shows many small scale variations. The polarization and intensity contour maps for all three filters *V*, *R* and *I* can be seen in figs. 4.18, 4.19 and 4.20. A low level intensity cut off was specified in order to eliminate the random vectors due to noise. Each waveband produces a circular pattern of vectors centred around HD 37903, confirming that this is a major source of illumination. The general behaviour is identical on all three maps, one common feature being a relatively low area of polarization in a sector immediately north-west of the central star. The percentage polarization varies according to position in the nebula but does in general appear to increase with offset distance. There is one area of anomalous behaviour common only to the *I* map,  $81''.3$  SSW of HD 37903 around star C. Here the polarization vectors are no longer perpendicular to the radius vector from the central star. This additional source of illumination is the bipolar nebula mentioned in section 3.2.2.

The percentage polarization and position angle has been measured at 12 different positions coincident with those recorded by Sellgren, Werner and Dinerstein (1992), using the same aperture size of  $10''.5$ . The results are given in table 4.2. Unlike

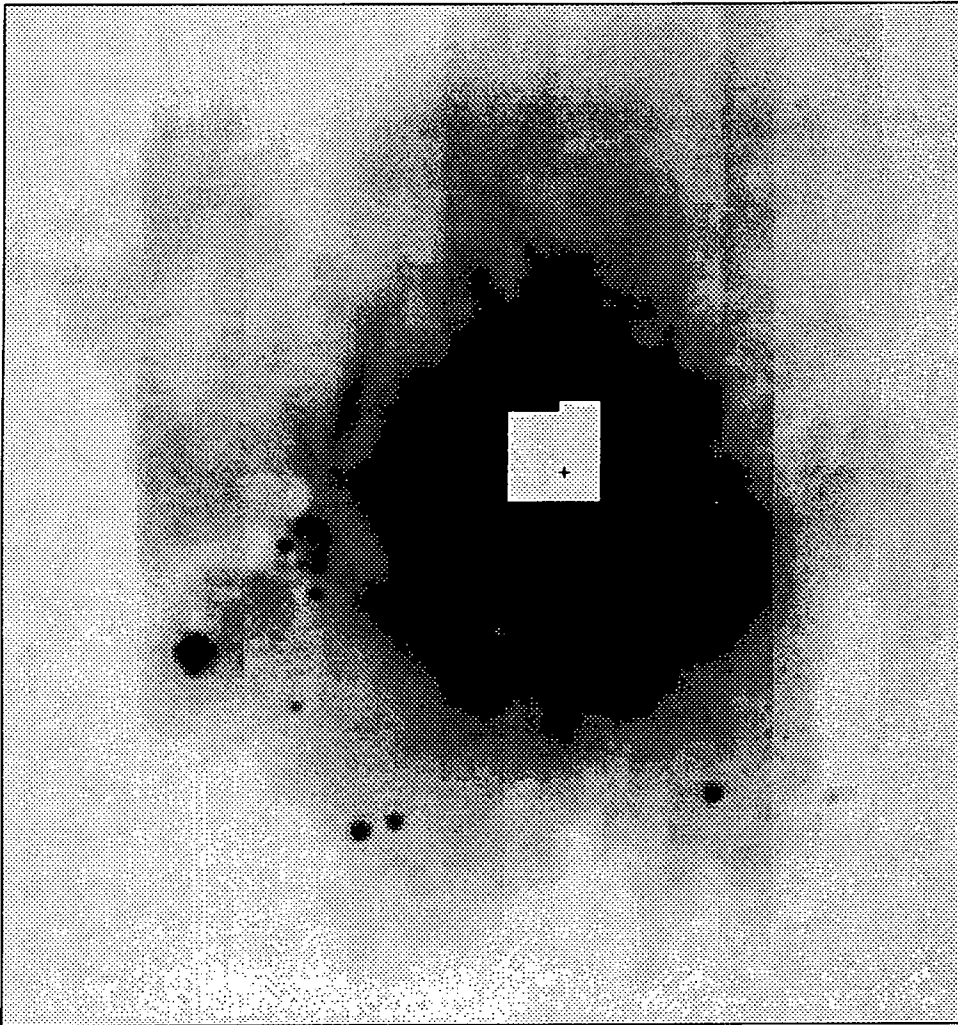


Figure 4.17: Intensity image of NGC 2023 in the *R* waveband. The field is  $6'.1 \times 6'.4$  in size.

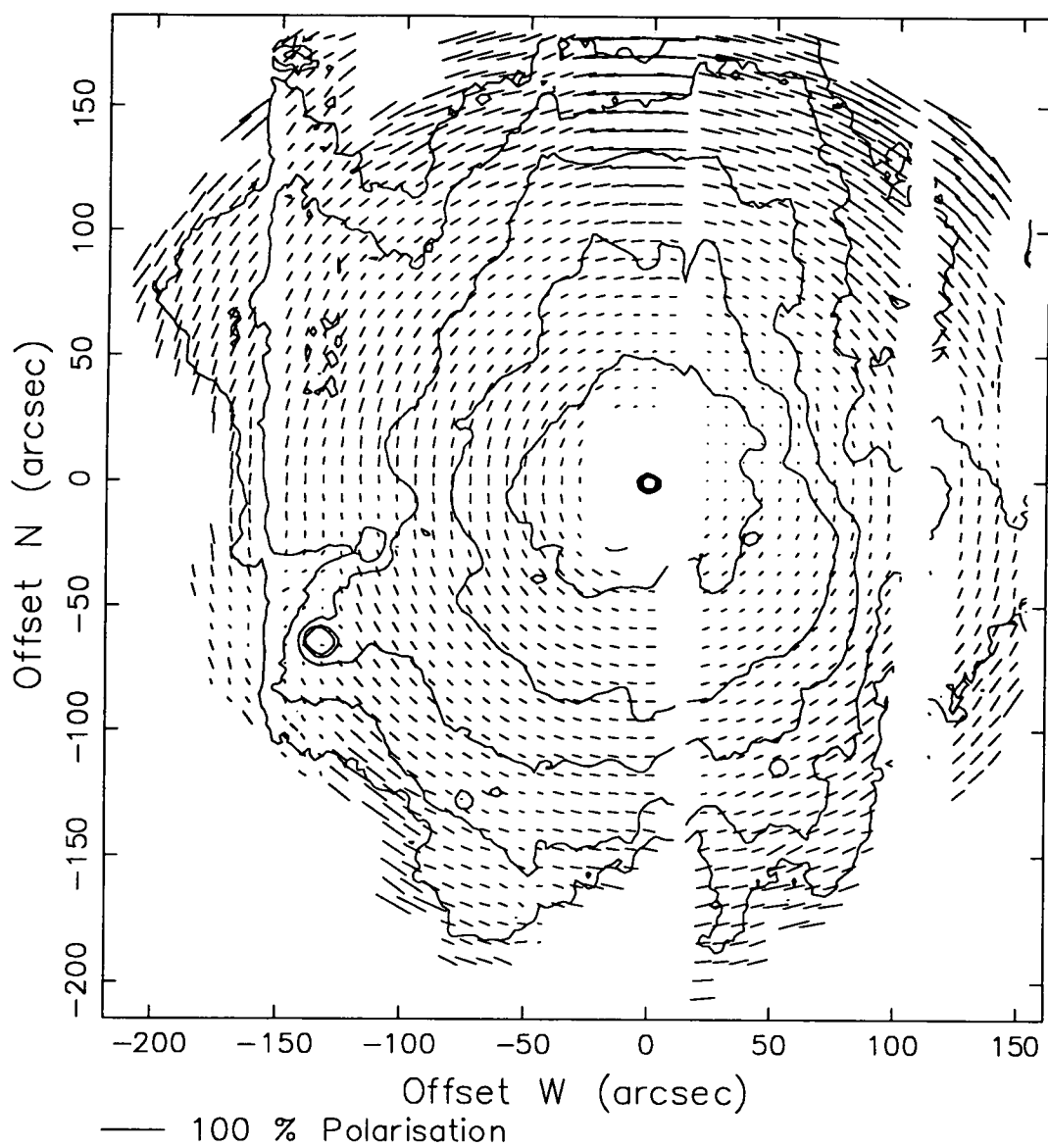


Figure 4.18: Polarization and contour image of NGC 2023 in the V waveband.

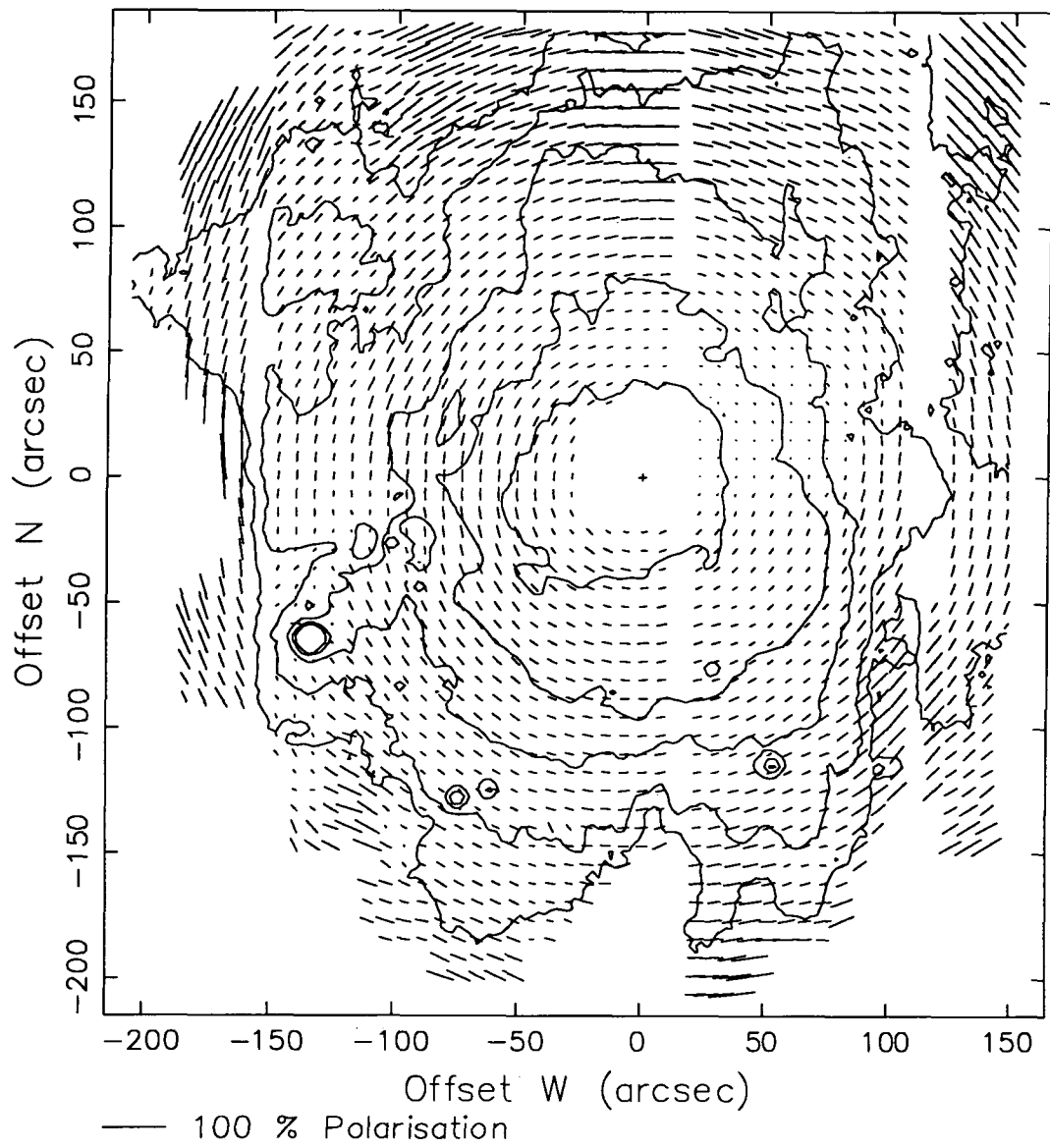


Figure 4.19: Polarization and contour image of NGC 2023 in the *R* waveband.

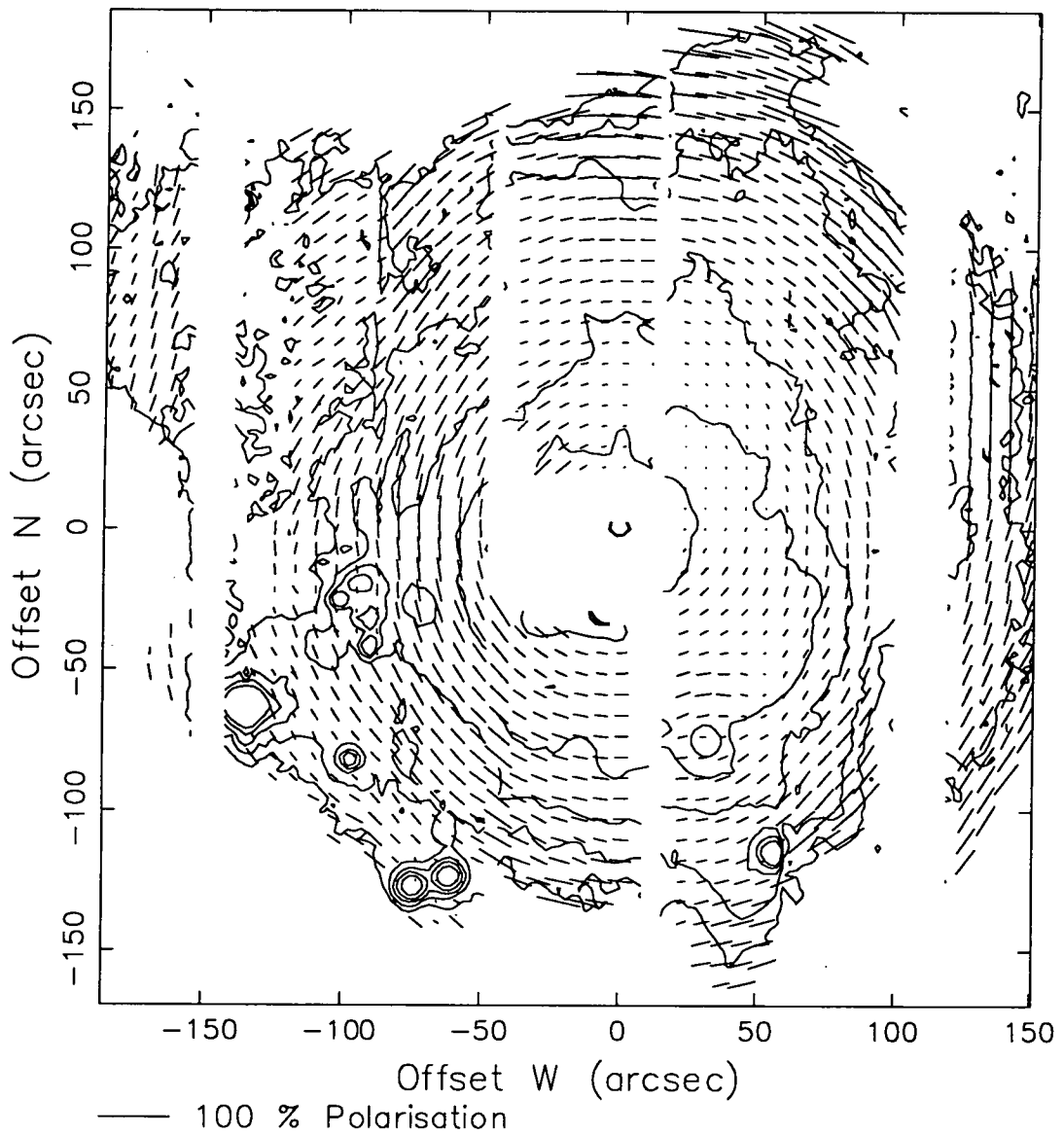


Figure 4.20: Polarization and contour image of NGC 2023 in the *I* waveband.

NGC 7023 the percentage polarization does not show a clear pattern of polarization with wavelength neither does the position angle remain constant in all cases. The position angle is however almost the same value for the *V* and *R* waveband. The change in angle in the *I* waveband is due to the increased importance of the bipolar nebulae around star C.

The same technique used to demonstrate the ERE in NGC 7023 is applied to NGC 2023 to show if this nebula too has a similar contribution due to intrinsic emission. A colour difference diagram  $I_{V-R}$  is shown in fig. 4.21, where  $I_{V-R} = -2.5 \log[I_V/I_R]$ , *I* being the total intensity and *V* and *R* refer to the wavebands. The image area is  $2'.8 \times 3'.8$ . Most of the nebula is uniform in colour except for several filaments, in particular one  $84''$  ENE and one  $62''$  ENE of HD 37903, where the nebula is considerably redder. Both these filaments have been suggested as possible sources of ERE by Witt and Schild. The filament furthest away from HD 37903 coincides with that seen on the intensity image earlier and as in NGC 7023 also appears to be narrower. However unlike NGC 7023 the colour difference diagram  $I_{V-I}$  shows no obvious increase in reddening at the position of the filaments.

Both the filaments suspected of being sources of ERE showed no obvious features in the polarization maps, neither do the polarization colour maps produced show any clear regions of a reduced polarization in either the *R* or the *I* wavebands. Traces were therefore made across the filaments in question in a direction perpendicular to that of the filament. Fig. 4.22 shows traces made in all wavebands of the polarized intensity. These simply show that the number of scatterers increases in the direction towards the center of the nebula, as expected. There is no change in behaviour across the wavebands. Traces in colour  $I_{V-R}$ , and  $I_{V-I}$  as well as scans in polarization colour  $P_{V-R}$  and  $P_{V-I}$  where  $P_{V-R} = -2.5 \log[(PI_V/I_V)/(PI_R/I_R)]$ , *PI* and *I* being the polarized and total intensities respectively and *V* and *R* refer to the waveband, are shown in fig. 4.23. The trace in  $I_{V-R}$  clearly shows a sudden increase in reddening at the position of the filament  $84''$  ENE and  $62''$  ENE of HD 37903. On the corresponding trace in polarization colour there is a rapid reduction at the

Position	V	R	I
Percentage Polarization			
60" S	13.5 ± 0.6	15.3 ± 0.9	19.3 ± 1.0
12" W, 57" S	...	14.2 ± 0.9	...
45" W, 46" S	8.8 ± 0.4	7.6 ± 0.5	8.5 ± 0.8
34" W, 46" S	8.6 ± 0.5	9.7 ± 0.5	14.4 ± 0.7
45" W, 42" S	8.9 ± 0.4	8.6 ± 0.5	6.2 ± 0.8
34" W, 42" S	9.4 ± 0.5	10.1 ± 0.5	12.1 ± 0.7
40" W, 40" S	9.0 ± 0.5	9.7 ± 0.5	9.2 ± 0.7
45" W, 35" S	9.0 ± 0.4	9.5 ± 0.5	8.0 ± 0.8
34" W, 35" S	9.3 ± 0.4	10.1 ± 0.5	10.7 ± 0.7
60" N	6.1 ± 0.5	7.3 ± 0.9	7.6 ± 1.1
12" W, 64" N	...	7.4 ± 1.0	...
60" W, 120" N	27.3 ± 1.4	20.4 ± 1.5	20.7 ± 3.6
Polarization Position Angle			
60" S	91.5 ± 1.2	91.6 ± 1.7	89.3 ± 1.5
12" W, 57" S	...	106.3 ± 1.7	...
45" W, 46" S	131.3 ± 1.4	126.2 ± 2.0	89.0 ± 2.6
34" W, 46" S	123.1 ± 1.6	119.9 ± 1.6	99.5 ± 1.4
45" W, 42" S	133.9 ± 1.3	131.1 ± 1.7	103.5 ± 3.6
34" W, 42" S	125.8 ± 1.4	124.5 ± 1.5	107.8 ± 1.7
40" W, 40" S	132.4 ± 1.5	129.8 ± 1.6	110.4 ± 2.3
45" W, 35" S	137.4 ± 1.3	136.9 ± 1.5	129.2 ± 2.7
34" W, 35" S	131.3 ± 1.4	130.5 ± 1.4	122.6 ± 1.8
60" N	95.0 ± 2.4	96.5 ± 3.5	88.7 ± 4.1
12" W, 64" N	...	88.3 ± 4.0	...
60" W, 120" N	66.8 ± 1.4	69.1 ± 2.0	61.0 ± 5.0

Table 4.2: The variation in percentage polarization and position angle for twelve different positions in NGC 2023.

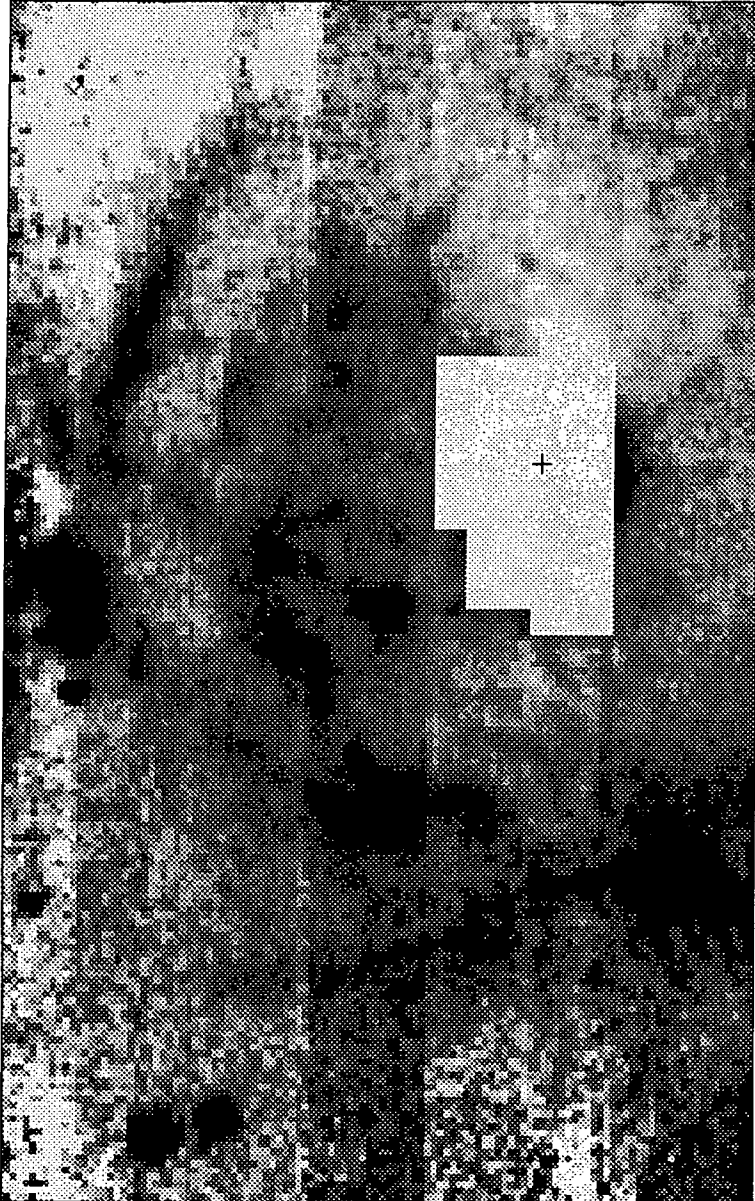


Figure 4.21: Colour difference image  $I_{V-R}$  of NGC 2023. The field is  $2'.8 \times 3'.8$  in size.

position of the filament furthest away from the central star which from examination of the individual polarization traces is due to a marked fall in  $P_R$ , however there is no apparent similar feature at the position of the filament nearest to HD 37903. Likewise the traces in  $I_{V-I}$  and  $P_{V-I}$  also show no obvious features expected if the ERE is present.

## 4.5 Spectroscopic Results of NGC 2023

An almost identical set up was used to observe the spectrum of NGC 2023 as for the Red Rectangle in order to search for the emission line features which were so prominent. Fig. 4.24 shows a total integrated one dimensional spectrum of the central star of NGC 2023. The spectrum clearly shows the diffuse interstellar band at  $5778/5780 \text{ \AA}$  as seen by Josafatsson and Snow (1987). The remaining DIB's are not seen since their equivalent widths are a factor of 10 smaller. In the case of the nebula a one dimensional spectrum was extracted by selecting the region along the slit where the filament  $84''$ ENE of the central star was and then summing the counts along each column from the rows that made up this region. An adjacent region was also extracted so that the continuum could be subtracted in order to identify the presence of any small scale emission features, the result is shown in Fig. 4.25. It can clearly be seen that there are no emission line features as seen in the Red Rectangle.

## 4.6 Discussion

Theoretical dust models (Mathis, Rumpl & Nordsieck 1977; Draine & Lee 1984), predict that both dust albedo and phase function asymmetry in the  $R$  band should be lower than the corresponding quantities in the  $V$  band which would produce an effect opposite to that observed by Witt and Schild. If the  $R$  excess in reflection nebulae is to be explained through a wavelength dependent albedo, for example, the albedo at  $R$  would need to be unity and even then some problems would remain. It is more likely that the  $R$  excess is related to the near infrared emission discovered

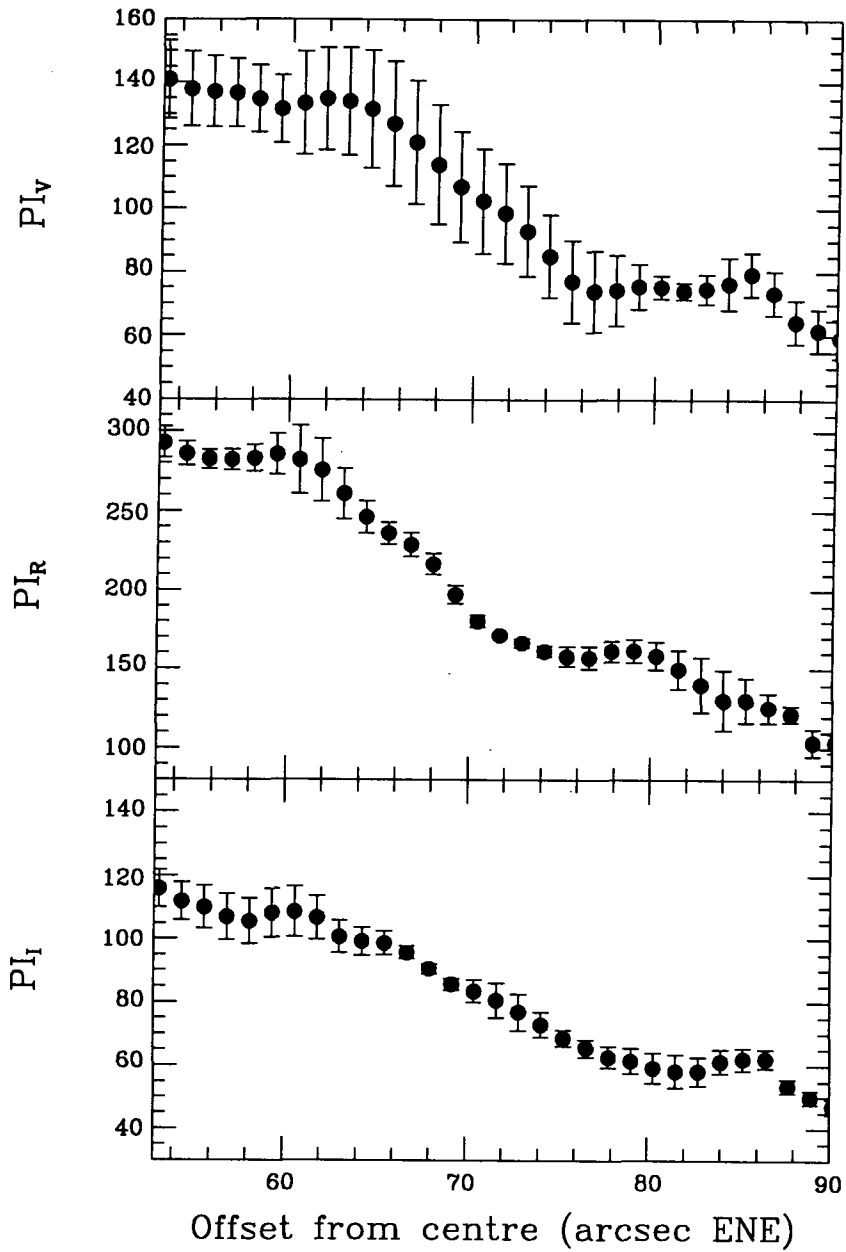


Figure 4.22: Traces of the polarized intensity across the filaments 84" ENE and 62" ENE of HD 37903.

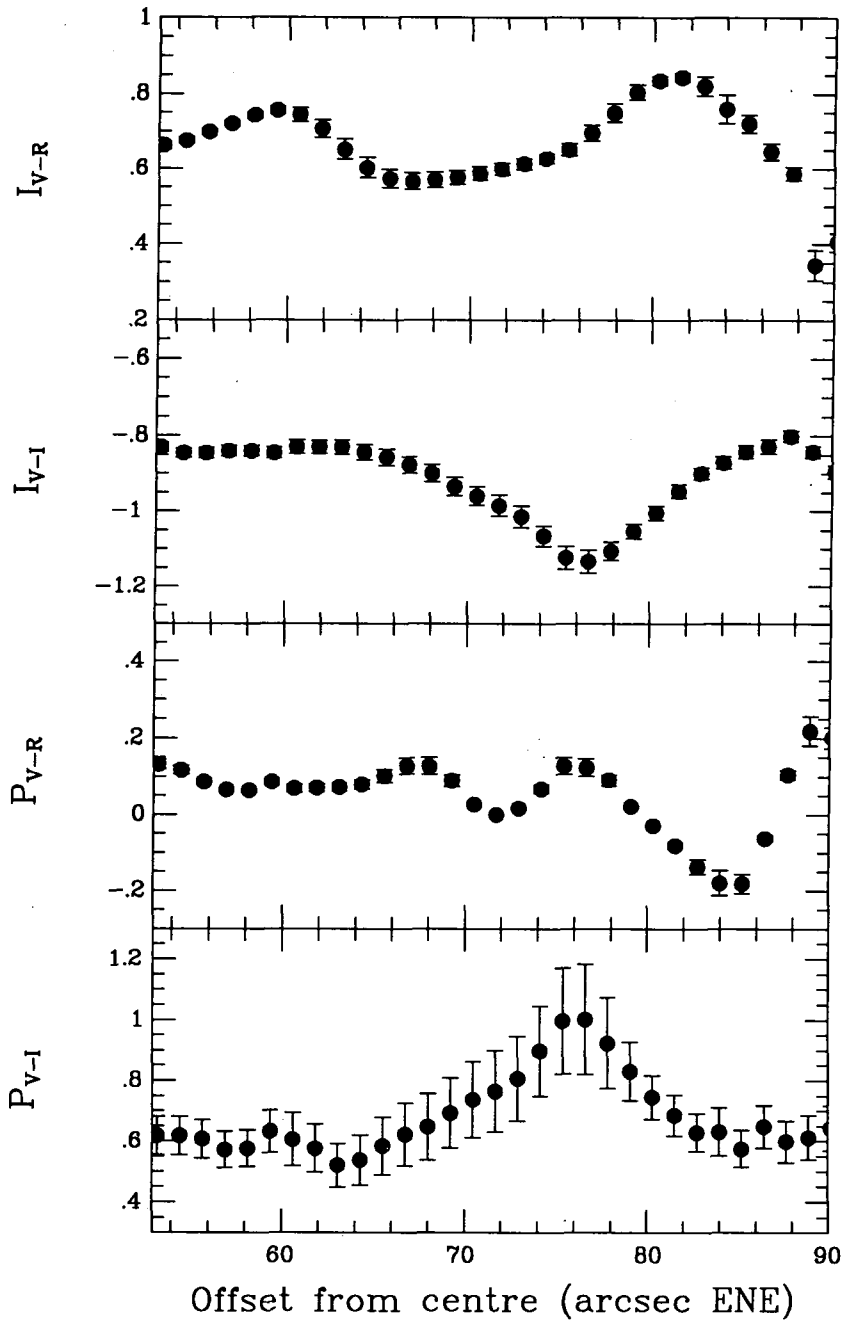


Figure 4.23: Traces of colour difference and polarization colour difference across the filaments 84" ENE and 62" ENE of HD 37903.

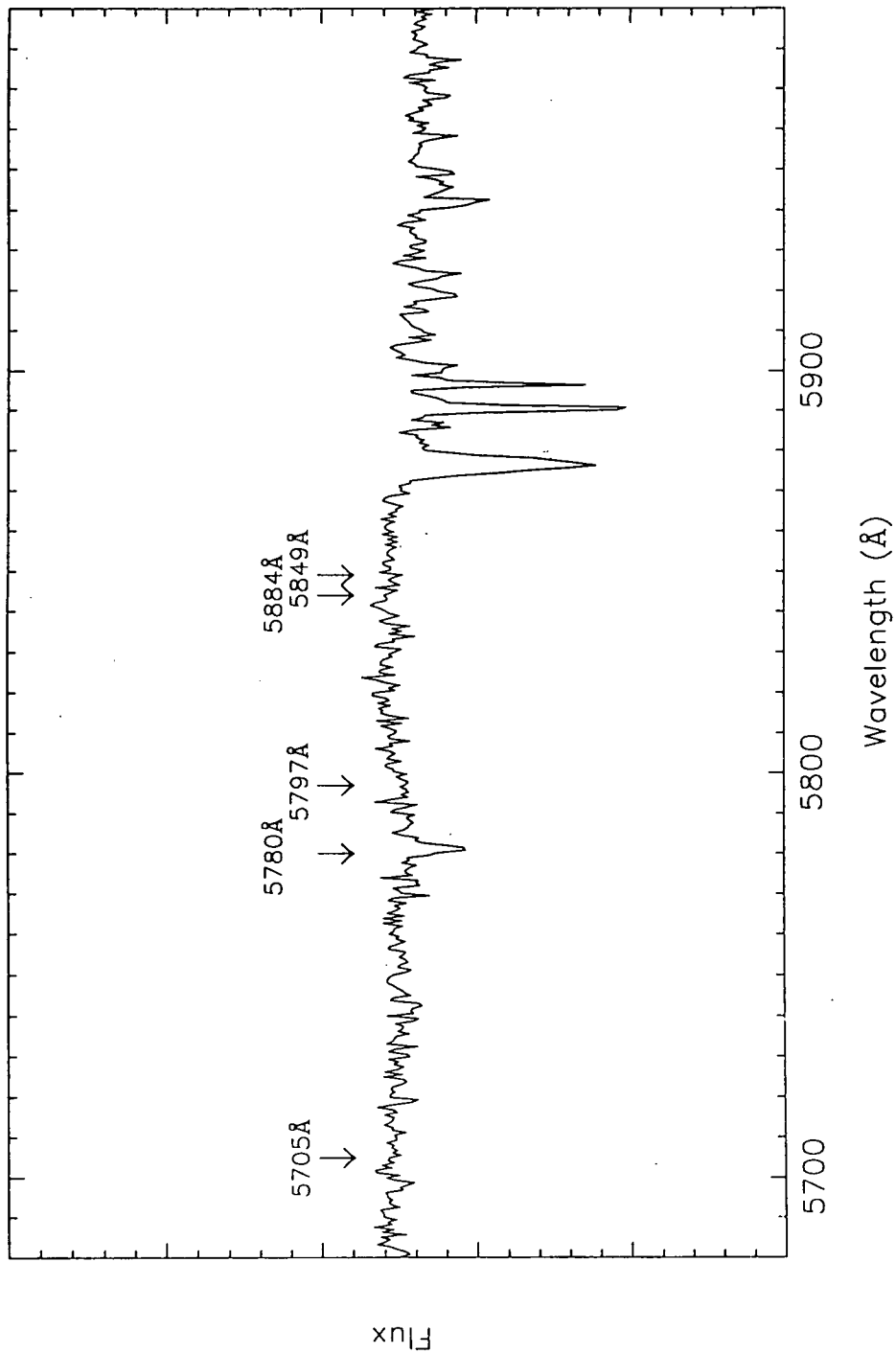


Figure 4.24: The spectrum of HD 37903 showing the diffuse interstellar absorption bands

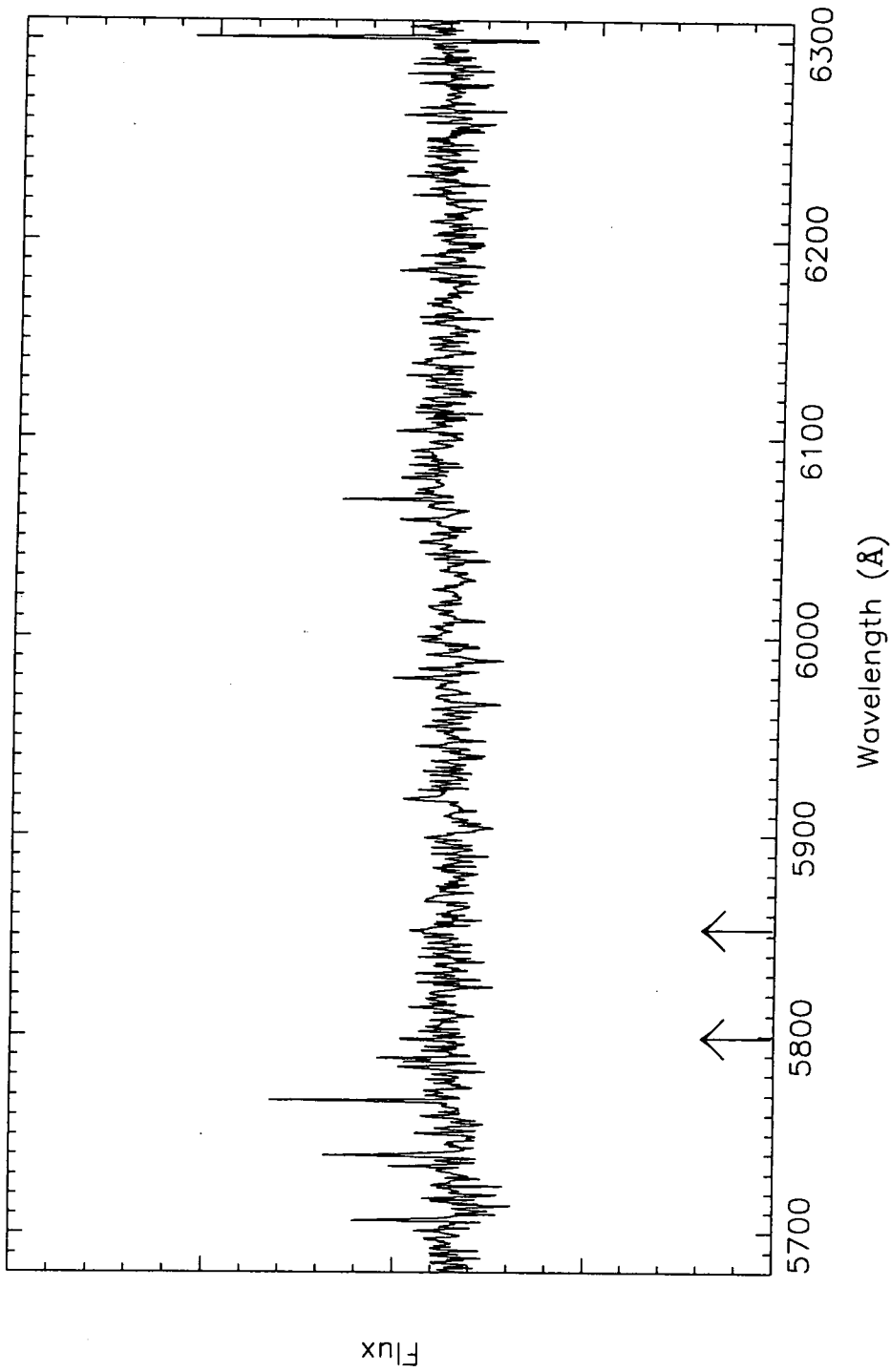


Figure 4.25: The nebula spectrum of NGC 2023 with the continuum subtracted. The slit was positioned across the filament 84"ENE of HD 37903. The ticks mark the positions of the emission line features in the Red Rectangle.

in reflection nebulae by Sellgren (1984).

The increase in red intensity that has been observed in the polarimetry data must have arisen either due to a decrease in the blue light or as a result of an additional intrinsic component to the red light such as ERE. For most positions studied in NGC 7023 the polarization was seen to increase monotonically with wavelength in the optical band which is as expected if the nebular emission is purely due to scattered light. However in regions of increased reddening this was not seen to be the case. The relative increase in the polarized intensity remained constant yet the corresponding changes in the polarization reveal a sudden reduction in the  $R$  and  $I$  wavebands compared to the  $V$  and  $B$  wavebands. This can only be the result of an excess of unpolarized light diluting the  $R$  and  $I$  polarized light thus producing the overall effect. This excess light must originate from the nebula itself since scattering produces polarized light. The reduction measured in the  $R$  and  $I$  polarizations implies that this intrinsic emission makes up  $\sim 22\%$  of the light in these wavebands for the filament south of HD 200775 and  $\sim 16\%$  for the filament north of the central star. These values are slightly higher than those measured by Witt and Boroson (1990). However their positions were  $20''$ W of those traced in fig. 4.12 and fig. 4.13. This is in agreement with the ERE varying with position in the nebula and the decreased polarization detected in the ERE filaments is consistent with the low infrared polarization found in NGC 7023 by Sellgren *et al.* (1992).

Since the excess emission is seen in the  $I$  waveband as well as in the  $R$  then this rules out the possibility that it could be due to line emission e.g.  $H_\alpha$  and must instead have a broad spectrum, at least several hundred Angstroms. This is in agreement with the spectrum found by Witt and Schild. Since the tail of the spectrum is in the  $I$  waveband this would then explain why the fall in polarization is not as great in the  $I$  as in the  $R$ . This excess is believed to be ERE which originates in the filaments as a result of some emission mechanism involving a component of the dust grains which constitute the nebula of which the precise nature is still unknown. Since the increase in the reddening at the position of the filaments is always slightly

greater than the corresponding decreases in polarization colour a slightly greater excess of red light would be required to explain the variation in intensity than in polarization if ERE is the only cause of change of colour. This implies that there may be a component due to obscuration in addition to ERE. Unfortunately it was not possible to make measurements at other regions of ERE detected by Witt and Boroson (1990) in NGC 7023 since these coincided with the central area originally blocked out due to the brightness of the central star.

In the case of NGC 2023 the picture is not as clear. For the filament nearest the central star since no corresponding decrease in polarization occurred at the position of reddening then there can be very little or no unpolarized light at all diluting the scattered light. Neither is there any increased reddening in the  $I$  or reduction in the  $I$  polarization suggesting that either there is no intrinsic emission at this position or that the level is too low to be detected by using imaging polarimetry. Which ever the case is it is most unlikely that the ERE can contribute as much as 29% to the light as claimed by Witt and Boroson (1990). The filament furthest away from the illuminating source must have a contribution due to some intrinsic emission since there is a decrease in the percentage polarization in the  $R$  waveband at the same point where the intensity is seen to become redder. Since no similar effect is obvious in the  $I$  waveband then it is not possible to rule out that the observed feature might simply be due to line emission, e.g.  $H_\alpha$  (6562.81 Å at rest) which would effect the  $R$  waveband and not the  $I$  waveband. Alternatively it could simply be that the  $I$  waveband was affected considerably by the adverse weather conditions during the observing run making detection of the ERE in this waveband extremely difficult. From the decrease in  $P_{V-R}$  if it is indeed due to ERE then calculations show that the ERE would make up  $\sim 32\%$  of the light, significantly lower than the 42% claimed by Witt and Boroson (1990).

The spectroscopy results show that none of the emission line features seen in the spectrum of the Red Rectangle, with the most prominent occurring at 5797Å and 5850Å, are present. Josafatsson and Snow (1987) clearly identify DIBs at these

particular wavelengths. However the DIBs were quite weak and therefore if the same carrier is responsible for the emission lines it could be that they are too weak to detect. However the lack of emission features agrees with the polarimetry results that ERE might not be present although it remains to be seen whether it is possible to detect the features without the presence of ERE.

The ERE would appear to be very localised. Since both the emission mechanism and the type of particles involved is still a matter of considerable debate it is not at this stage possible to explain why this might be the case. Since the technique used here is unable to show the ERE if it is of a very low level it could well be that it is more widespread. It is however very dependant on physical conditions e.g. temperature and density. Proposed organic components include hydrogenated amorphous carbon (HAC) or quenched carbonaceous composite (QCC) grains or polycyclic aromatic hydrocarbon (PAH) molecules (d'Hendecourt *et al.* 1986; Duley and Williams 1988; Sakata *et al.* 1992; etc). All of which have also been proposed as the possible source of the near-infrared continuum and emission features (see section 3.3.1). The ERE feature has also been linked to the diffuse interstellar bands and may arise from electronic transitions in gas phase molecules (see section 2.3.3).

# Chapter 5

## Summary and Conclusion

### 5.1 The Red Rectangle

The Red Rectangle is a small biconical reflection nebula whose optical spectrum exhibits a broad luminescence feature centered around 6900 Å. This feature has been attributed to intrinsic nebular emission, known as extended red emission (ERE). Various organic molecules have been proposed as the source of the ERE including PAHs, HACs and fullerenes as well as linear carbon chains. However the application of the results of the luminescence from organic molecules to the interpretation of the diffuse emission in the Red Rectangle is not straightforward since there are only a limited number of laboratory experiments available. It is possible though to obtain very broad and diffuse emission from an isolated electronically excited molecule so that it resembles the spectrum of the Red Rectangle. Superimposed on the broad feature are a set of emission lines which resemble molecular-like bands of which the most prominent emission features have been linked with one of the families of the diffuse interstellar bands (DIBs), (family 3 in Krelowski and Walker 1987).

A re-examination of the spectra reveals that the emission bands alter in shape in a symmetrical manner with distance from the central star. The bandwidth and peak wavelength converge with increasing offset towards the values of the associated DIBs. The bandwidth is  $\sim 4\text{Å}$  wider in the hotter regions near the central star than the outer cooler parts of the nebula and the peak wavelength changes by up to  $5\text{Å}$ .

The half maximum of the blue leading edge was found to remain fairly constant and within the measures of accuracy agreed with the value of the corresponding DIB. These results indicate that each emission/absorption pair has a common carrier.

The broad enhancement has now become quite a common feature amongst reflection nebulae, but the Red Rectangle is unique since it is the only nebula to also exhibit the emission lines. In connecting these bands to the DIBs which are seen throughout the Galaxy then one would also expect the bands to be more widespread. Perhaps the Red Rectangle provides the ideal conditions in terms of temperature, density and ultraviolet radiation from the central star. There could also be a high level of the molecular species responsible in this nebula which would agree with the theory that the nebular material is newly formed from an unresolved carbon star undergoing mass loss. If the abundance is considerably lower in other reflection nebulae then detection will be much harder.

So far ERE has mainly been detected in areas undergoing star formation. The Red Rectangle however is an isolated evolved object. It is possible that the molecular species is unable to survive in the dark dense clouds, which support star formation, as a single entity. A more extensive search is required, of other nebulae displaying ERE, for the narrow emission features.

## 5.2 NGC 7023 and NGC 2023

Imaging polarimetry has been used to explore the possibility of extended red emission in the reflection nebulae NGC 7023 and NGC 2023 by analysing colour and polarization colour diagrams.

The results of NGC 7023 show that there is a monotonic increase in polarization with wavelength while the position angle remains constant. However there are two regions, one 65''S and the other 53''N of the central star, in which there is a reduction in the polarization levels in the *R* and *I* wavebands relative to those in the *B* and *V*. These positions also coincide with an increase in reddening and are thus identified as being due to ERE. This broadband emission in the red and near-infrared dilutes the

scattered radiation hence reducing the polarization in these wavebands. We believe that the ERE arises from a component of the grains which scatters the central starlight to produce the reflection nebula. Calculations show the ERE contributes  $\sim 16 - 22\%$  of the total light in the *R* and *I* wavebands.

The results of NGC 2023 show no obvious trend in variation of polarization with wavelength neither does the position angle remain constant since it is affected by an embedded bipolar nebula only visible in the *I* waveband. Two regions, the first  $62''$  ENE and the second  $84''$  ENE of the central star, have been suggested by Witt and Boroson (1990) as areas containing ERE. The results show no clear evidence for this being the case for the position  $62''$  ENE. The second region shows a reduction in polarization in the *R* waveband coinciding with an increase in reddening but a similar case was not found in the *I* waveband, as expected. However it is possible that the level of ERE in the *I* waveband is too low to be detected using imaging polarimetry. The spectroscopic results show no evidence for the prominent emission line features seen in the Red Rectangle, for this second region.

We have managed to provide evidence for the existence of ERE in NGC 7023 using an independent technique which does not rely on data from the central star nor on information about the scatters. The existence of ERE in NGC 2023 however is inconclusive. There is tentative evidence to suggest that ERE is present in the filament  $84''$  ENE of HD 37903 but we can not be certain at this stage. However the lack of emission lines associated with the DIBs might suggest otherwise. Three cases might be possible; ERE and emission lines found together; ERE on its own; or emission lines on their own. Further studies are required to discover if these groups exist. This would involve obtaining polarimetry observations for a greater number of nebulae where the ERE has been suggested by others to exist. The location and contribution of ERE to the overall intensity can then be determined accurately and independantly. Spectroscopic studies are then required across the positions of ERE in order to look for the emission lines and search for a link with the DIBs. Spectroscopic observations are also required of nebulae where ERE is known not to

exist so that it is possible to conclude if the emission lines appear on there own.

## References

- Abell, G.O. & Margon, B., 1979. *Nature* **279** 701.
- Aitken, D.K. *et al.*, 1979. *Ap. J.* **233** 925.
- Aitken, D.K., 1981. *IAU Sympos.* **96** Infrared Astronomy.
- Allamandola, L.J., Greenberg, J.M. & Norman, C.A., 1979. *Astr. Ap.* **77** 66.
- Allamandola, L.J., Tielens, A.G.G.M. & Barker, J.R., 1985. *Ap. J.* **290** L25.
- Allamandola, L.J., Tielens, A.G.G.M. & Barker, J.R., 1986. *Physical Processes in Interstellar Clouds* ed. Morfill, G. & Scholer, M. Dordrecht:Reidel. L25
- Allamandola, L.J., Tielens, A.G.G.M. & Barker, J.R., 1989. *Ap. J. Suppl.* **71** 733.
- Altamore, A., Baratta, G.B., Cassatella, A., Grasdalen, G.L., Persi, P. & Viotti, R., 1980. *Astr. Ap.* **90** 290.
- Aveni, A.F. & Hunter, J.H., 1967. *Astr. J.* **72** 1019.
- Avouris, P., Gelbart, W.M. & El-Sayed, M.A., 1977. *Chem. Rev.* 794.
- Bachiller, R., Gómez-González, J., Bujarrabal, V. & Martin-Pintado, J., 1988. *Astr. Ap.* **196** L5.
- Bally, J. & Lada, C.J., 1983. *Ap. J.* **265** 824.
- Balma, S.P. & Jura, M., 1992. *Astr. Ap.* **261** L25.
- Barker, J.R., Allamandola, L.J. & Tielens, A.G.G.M., 1987. *Ap. J.* **315** L61.
- Barlow, M.J., 1983. *Planetary Nebulae* ed Flower, D.R..
- Beck, S.M., Powers, J.B. & Smalley, R.E., 1980. *J. Chem. Phys.* **73** 2019.
- Beck, S.M., Hopkins, J.B., Powers, D.E., Smalley, R.E., 1981. *J. Phys. Chem.* **74** 43.
- Bellamy, L.J., 1958. *The Infrared Spectra of Complex Organic Molecules* 2ed. New York:Wiley.

- Benvenuti, P. & Porceddu, I., 1989. *Astr. Ap.* **223** 329.
- Berlman, I.B., 1971. *Handbook of Fluorescence Spectra of Aromatic Molecules* 2nd ed. Academic:New York N.Y..
- Birks, J.B., 1970. *Photophysics of Aromatic Molecules* Wiley:London.
- Blanco, A., Borghesi, A., Fonti, S., Orofino, V., Bussoletti, E. & Colangeli, L., 1988. *Dust in the Universe* ed. Bailey, D.A. Williams. Cambridge:Univ. Press.
- Bodart, J.R. & Feldman, B.J., 1985. *Phys. Rev. B* **32** 1317.
- Bregman, J.D., & Rank, D.M., 1975. *Ap. J.* **195** L125.
- Brown, R.L., Knapp, G.R., Kuiper, T.B.H. & Rodriguez-Kuiper, E.N., 1975. *Ap. J.* **195** L23.
- Carrington, A. & Ramsay, D.A., 1982. *Phys. Scripta.* **25** 272.
- Caswell, J.L. & Goss, W.M., 1974. *Astr. Ap* **32** 209.
- Chlewicki, G., deGroot, M.S., van der Zwet, G.P., Greenberg, J.M., Alvarez, P.P. & Mampaso, A., 1987. *Astr. Ap.* **173** 131.
- Chlewicki, G., van der Zwet, G.P., van Ijzendoorn, L.J. & Greenberg, J.M., 1986. *Ap. J.* **305** 455.
- Chokshi, A., Tielens, A.G.G.M., Werner, M.W. & Castelaz, M.W., 1988. *Ap. J.* **334** 803.
- Clar, E., 1964. *Polycyclic Hydrocarbons* New York: Academic Press.
- Clar, E. & Stephen, J.F., 1965. *Tetrahedron* **21** 467.
- Clar, E. & Zander, M., 1956. *Chem. Ber.* **89** 740.
- Code, A.D., 1958. *Pub. A.S.P.* **70** 407.
- Cohen, M. *et al.*, 1975. *Ap. J.* **196** 179.
- Cohen, M. & Jones, B.F., 1987. *Ap. J.* **321** L151.
- Collins, O.C., 1937. *Ap. J.* **86** 529.
- Cossart-Magos, C. & Leach, S., 1990. *Astr. Ap.* **233** 559.
- Coveleskie, R.A., Dolson, D.A. & Parmenter, C.S., 1980. *J. Chem. Phys.* **72** 5774.
- Crawford, M.K., Tielens, A.G.G.M. & Allamandola, L.J., 1985. *Ap. J.* **293** L45.

- Dainty, J.C., Pipher, J.L., Lacasse, M.G. & Ridgway, S.T., 1985. *Ap. J.* **293** 530.
- Dalgarno, A. & Stephens, T.L., 1970. *Ap. J.* **160** L107.
- Danks, A.C. & Lambert, D.L., 1976. *M.N.R.A.S.* **174** 571.
- De Boer, K.S., 1983. *Astr. Ap.* **125** 258.
- DePoy, D.L., Lada, E.A., Gatley, I. & Probst, R., 1990. *Ap. J.* **356** L55.
- Deeming, T.J. & Walker, G.A.H., 1967. *Z. Ap.* **66** 175.
- Donn, B., 1968. *Ap. J.* **152** L129.
- Draine, B.T. & Lee, H.M., 1984. *Ap. J.* **285** 89.
- Duley, W.W., 1979a. *Ap. J.* **227** 824.
- Duley, W.W., 1979b. *Ap. Space Sci.* **61** 243.
- Duley, W.W., 1984. *Ap. J.* **287** 694.
- Duley, W.W., 1985. *M.N.R.A.S.* **215** 259.
- Duley, W.W., 1986. *Q. Jl R. astr. Soc.* **27** 403.
- Duley, W.W., 1987. *M.N.R.A.S.* **229** 203.
- Duley, W.W., 1988. *M.N.R.A.S.* **234** 61P.
- Duley, W.W., 1992. *M.N.R.A.S.* **258** 773.
- Duley, W.W. & Williams, D.A., 1984. *Interstellar Chemistry* Academic Press:London.
- Duley, W.W. & Williams, D.A., 1983. *M.N.R.A.S.* **205** 67P.
- Duley, W.W. & Williams, D.A., 1986. *M.N.R.A.S.* **219** 859.
- Duley, W.W. & Williams, D.A., 1988. *M.N.R.A.S.* **230** 1P.
- Duley, W.W. & Williams, D.A., 1990. *M.N.R.A.S.* **247** 647.
- Dwek, E., Sellgren, K., Soifer, B.T. & Werner, M.W., 1980. *Ap. J.* **238** 140.
- Edwards, S.A. & Leach, S., 1993. *Astr. Ap.* **272** 533.
- Elmegreen, D.M. & Elmegreen, B.G., 1978. *Ap. J.* **220** 510.
- Elvius, A. & Hall, J.S., 1966. *Lowell Obs. Bull.* **VI** 257.
- Elvius, A. & Hall, J.S., 1967. *Interstellar grains* ed. Greenberg, J.M. & Roark, T.P. NASA SP-140.
- Emerson, J.P., Furniss, I. & Jennings, R.E., 1975. *M.N.R.A.S.* **172** 411.

- Evans, N.J., 1981. *IAU Sympos.* **96** Infrared Astronomy.
- Federman, S.R., Kumar, C.K. & Vanden Bout, P.A., 1984. *Ap. J.* **282** 485.
- Frenklach, M. & Feigelson, E.D., 1989. *Ap. J.* **341** 372.
- Fossey, S.J., 1991. *Nature* **353** 393.
- Fuente, A., Martín-Pintado, J., Cernicharo, J. & Bachiller, R., 1990. *Astr. Ap.* **237** 471.
- Fuente, A., Martín-Pintado, J., Cernicharo, J. & Bachiller, R., 1993. *Astr. Ap.* **276** 473.
- Gatley, I., Hasegawa, T., Suzuki, H., Garden, R., Brand, P., Lightfoot, J., Glencross, W., Okuda, H. & Nagata, T., 1987. *Ap.J.* **318** L73.
- Geballe, T.R., Lacy, J.H., Persson, S.E., McGregor, P.J. & Soifer, B.T., 1985. *Ap. J.* **292** 500.
- Geballe, T.R., Tielens, A.G.G.M., Allamandola, L.J., Moorhouse, A. & Brand, P.W., 1989. *Ap. J.* **341** 278.
- Gehrels, T., 1967. *Astr. J.* **72** 631.
- Gelzahler, B.J. & Cohen, N.L., 1983. *Pub. A.S.P.* 489.
- Gezari, D.Y., Schmitz, M. & Mead, J.M., 1984. *Far Infrared Suppl. Catalog of Infrared Observations* **1119** .
- Gillet, F.C. & Stein, W.A., 1971. *Ap. J.* **164** 77.
- Gliese, N. & Walter, K., 1951. *Z. A.* **29** 94.
- Goldreich, P. & Kwan, J., 1974. *Ap. J.* **189** 441.
- Grasdalen, G.L. & Joyce, R.R., 1979. *Ap. J.* **205** L11.
- Grasdalen, G.L., Sloan, G.C. & LeVan, P.D., 1992. *Ap. J.* **384** L25.
- Greenberg, J.M., 1982. in *Comets* **p131** ed. Wilkening, L..
- Greenstein, J.L. & Oke, J.B., 1977. *Pub. A.S.P.* **89** 131.
- Guetter, H.H., 1968. *Pub. A.S.P.* **80** 197.
- Hall, D.I., Miles, J.R., Sarre, P.J. & Fossey, S.J., 1992. *Nature* **358** 629.
- Harvey, P.M., Thronson, Jr., H.A. & Gatley, I., 1980. *Ap. J.* **235** 894.
- Harwitt, M., 1975. *Ap. J.* **199** 398.

- Hasegawa, T., Gatley, I., Garden, R.P., Brand, P.W.J.L., Ohishi, M., Lightfoot, J.F., Hayashi, M. & Kaifu, N., 1987. *Ap. J.* **318** L77.
- Haslam, C.G.T., Hills, D.L., Matthews, H.E. & Salter, C.J., 1978. *Astr. Ap.* **70** 575.
- Hauffer, R.E., Chai, Y., Chibante, L.P.F., Fealich, M.R., Weisman, R.B., Curl, R.F. & Smalley, R.E., 1991. *J. Chem. Phys.* **95** 2197.
- Hecht, J., 1981. *Ap. J.* **246** 794.
- Heger, M.L., 1922. *Lick Obs. Bull.* **10** 146.
- Heintz, W.D., 1990. *M.N.R.A.S.* **245** 759.
- d'Hendecourt, L.B., Léger, A., Olofsson, G. & Schmidt, W., 1986. *Astr. Ap.* **170** 91.
- Henyey, I.G., 1936. *Ap. J.* **84** 609.
- Herbig, G.H., 1960. *Ap. J. Suppl.* **4** 337.
- Herbig, G.H., 1962. *Adv. in Astr. & Ap.* **1** 47.
- Herbig, G.H., 1975. *Ap. J.* **196** 129.
- Herbig, G.H., 1988. *Ap. J.* **331** 999.
- Herbig, G.H. & Kuhl, L.V., 1963. *Ap. J.* **137** 398.
- Herbig, G.H. & Leka, K.D., 1991. *Ap. J.* **382** 193.
- Herbig, G.H. & Rao, N.K., 1972. *Ap.J.* **174** 401.
- Herbig, G.H. & Soderblom, D.R., 1982. *Ap. J.* **252** 610.
- Herzberg, G., 1966. in *Electronic Spectra of Polyatomic Molecules* Van Nostrand & Reinhold.
- Howe, J.E., Jaffe, D.T., Genzel, R. & Stacey, G.J., 1987. *Ap. J.* **373** 158.
- Hubble, E., 1922. *Ap. J.* **56** 400.
- Huffman, D.R., 1977. *Adv. Phys.* **26** 129.
- Iida, S., Ohtaki, T. & Seki, T., 1984. *Am. Inst. Conf. Proc.* **120** 258.
- Jaffe, D.T., Genzel, R., Harris, A.I., Howe, J.E., Stacey, G.J. & Stutzi, J., 1990. *Ap. J.* **353** 193.
- Joblin, C., Maillard, J.P., d'Hendecourt, L. & Léger, A., 1990. *Nature* **346** 729.

- Jones, A.P., Duley, W.W. & Williams, D.A., 1987. *M.N.R.A.S.* **229** 213.
- Josafatsson, K. & Snow, T.P., 1987. *Ap. J.* **319** 436.
- Kaplan, S.A. & Pikelner, S.B., 1970. *Interstellar Medium* Cambridge Mass.:Harvard University Press.
- Keenan, P.C., 1936. *Ap. J.* **84** 600.
- Keller, R., 1987. *Polycyclic Aromatic Hydrocarbons and Astrophysics* p**387** Dordrecht:Reidel.
- Knapp, G.R., Brown, R.L. & Kuiper, T.B.H., 1975. *Ap J.* **196** 167.
- Knapp, G.R., Brown, R.L., Kuiper, T.B.H. & Kakar, R.K., 1976. *Ap J.* **204** 781.
- Knapp, G.R., 1986. *Ap. J.* **311** 731.
- Krelowski, J., 1989. *IAU Symp.* **135** Interstellar Dust.
- Krelowski, J. & Walker, G.A.H., 1987. *Ap. J.* **312** 860.
- Krelowski, J. & Westerlund, B.E., 1988. *Astr. Ap.* **190** 339.
- Kroto, H.W., 1987. *Nature* **329** 529.
- Kroto, H.W., Heath, J.R., O'Brian, S.C., Curl, R.F. & Smalley, R.E., 1985. *Nature* **318** 162.
- Kumar, C.K., Federman, S.R. & Vanden Bout, P.A., 1982. *Ap. J.* **261** L51.
- Kurchakov, A.V. & Matjagin, V.S., 1968. *Sov. Astron.* **12** 169.
- Leach, S., 1986. *Electron Spectrosc.* **41** 427.
- Leach, S. *et al.*, 1992. *Chem. Phys.* **160** 451.
- Lee, T.A., 1968. *Ap. J.* **152** 913.
- Léger, A. & d'Hendecourt, L., 1985. *Astr. Ap.* **146** 81.
- Léger, A. & d'Hendecourt, L., 1987. *Polycyclic Aromatic Hydrocarbons and Astrophysics* p**223** Dordrecht:Reidel.
- Léger, A., d'Hendecourt, L., Verstraete, L. & Schmidt, W., 1988. *Astr. Ap.* **203** 145.
- Léger, A. & Puget, J.L., 1984. *Astr, Ap.* **137** L5.
- Leinert, Ch. & Haas, M., 1989. *Astr. Ap.* **221** 110.
- Lépine, J.R.D. & Nguyen-Ouang-Rieu, 1975. *Astr. Ap.* **36** 469.

- Lin, S. & Feldman, B.J., 1982. *Phys. Rev. Letters* **48** 829.
- Liszt, H.S. & Linke, R.A., 1975. *Ap. J.* **196** 709.
- Loren, R.B., Vanden Bout, P.A. & Davis, J.H., 1973. *Ap. J.* **185** L67.
- Low, F.J., 1979. *High Resolution Stellar Interferometry* p154 eds. Davis, J. & Tango, W.J..
- Lynds, B.T., 1962. *Ap. J. Suppl. No. 64* 7 1.
- Maclean, S., Duley, W.W. & Millar, T.J., 1982. *Ap. J.* **252** L25.
- Madan, A. & Shaw, M.P., 1988. *The Physics and Applications of Amorphous Semiconductors* Academic Press:New York.
- Maier, J.P., 1980. *Chimia* **34** 219.
- Malin, D.F., Ogura, K. & Walsh, J.R., 1987. *M.N.R.A.S.* **227** 361.
- Mannion, M.D., 1987. *Ph.D. Thesis University of Durham* .
- Martel, M.T., 1958. *Ann. d'Ap. Suppl.* No. 7.
- Mathis, J.S., Rimpl, W. & Nordseieck, K.H., 1977. *Ap. J.* **217** 425.
- McGlynn, S.P., Azumi, T. & Kinoshita, M., 1969. *Molecular Spectroscopy of the Triplet State* Prentice-Hall International Series in Chemistry.
- McIntosh, A.D. & Webster, A., 1992. *M.N.R.A.S.* **255** 37P.
- McIntosh, A.D. & Webster, A., 1993. *M.N.R.A.S.* **261** L13.
- Meaburn, J., Walsh, J.R., Hebden, J.C., Morgan, B.L. & Vine, H., 1983. *M.N.R.A.S.* **205** 53P.
- Mendoza, E.E., 1958. *Ap. J.* **128** 207.
- Merrill, K.M., 1977. *in IAU Colloquium No. 42* ed. Kippenhahn, R., Rahne, J. & Strohmeier, W..
- Merrill, P.W., 1934. *Pub. A.S.P.* **46** 206.
- Meyer, D.M., 1983. *Ap. J.* **266** L51.
- Milkey, R.W. & Dyck, H.M., 1973. *Ap. J.* **181** 833.
- Milman, A.S., Knapp, G.R., Kerr, F.J., Knapp, S.L. & Wilson, W.J., 1975. *Astr. J.* **80** 93.
- Minin, I.N., 1965. *Sov. Astr.* **8** 528.

- Moore, P.J.R. McDonald, 1982. *Ph.D. Thesis, University of Durham* .
- Morris, M., Palmer, P., Turner, B.E. & Zuckerman, B., 1974. *Ap.J.* **191** 349.
- Münch, G., 1968. in *Nebulae & Interstellar Matter* ed. Middlehurst, B.M. & Aller, L.H..
- Ney, E.P., Hatfield, B.F. & Gehrz, R.D., 1980. *Proc. Nat. Acad. Sci. U.S.A.* **77** No.1 14.
- Omont, A., 1986. *Astr. Ap.* **164** 159.
- Pankonin, V. & Walmsley, C.M., 1976. *Astr. Ap.* **48** 341.
- Pankonin, V. & Walmsley, C.M., 1978. *Astr. Ap.* **67** 129.
- Parmenter, C.S., 1982. *J. Phys. Chem.* **86** 1735.
- Penzias, A.A, Solomon, P.M., Wilson, R.W. & Jefferts, K., 1971. *Ap. J.* **168** L53.
- Perkins, H.G., Scarrott, S.M., Murdin, P. & Bingham, R.G., 1981. *M.N.R.A.S.* **196** 635.
- Platt, J.R., 1956. *Ap. J.* **123** 486.
- Porceddu, I., Benvenuti, P. & Krelowski, J., 1991. *Astr. Ap.* **248** 188.
- Puget, J.L. & Léger, A., 1989. *Ann. Rev. Astr. Ap.* **27** 161.
- Puget, J.L. Léger, A. & Boulanger, F., 1985. *Astr. Ap.* **142** L19.
- Purcell, E.M., 1976. *Ap. J.* **206** 685.
- Racine, R., 1968. *Astr. J.* **73** 233.
- Robertson, J. & O'Reilly, E.P., 1987. *Phys. Rev. B.* **35** 2946.
- Romano, G., 1975. *Ap. & Sp. Sci.* **33** No.2 487.
- Rowan-Robinson, M. & Harris, S., 1983. *M.N.R.A.S.* **202** 767.
- Rush, W.F. & Witt, A.N., 1975. *Astr. J.* **80** 31.
- Russell, R.W., Soifer, B.T. & Willner, S.P., 1978. *Ap. J.* **220** 568.
- Rye, R.R., 1977. *Surface Sci.* **69** 653.
- Sakata, A., Wada, S., Narisawa, T., Asano, Y., Iijimar, Y., Onaka, T. & Tokunaga, A.T., 1992. *Ap. J.* **393** L83.
- Sakata, A., Wada, S., Okutsu, Y., Shintani, H. & Nakada, Y., 1983. *Nature* **301** 493.

- Sakata, A., Wada, S., Onaka, T. & Tokunaga, A.T., 1987. *Ap. J.* **320** L63.
- Sakata, A., Wada, S., Onaka, T. & Tokunaga, A.T., 1990. *Ap. J.* **353** 543.
- Sakata, A., Wada, S., Tanabe, T. & Onaka, T., 1984. *Ap. J.* **287** L51.
- Salama, F. & Allamandola, L.J., 1992. *Ap. J.* **395** 301.
- Sanner, F., Snell, R. & Vanden Bout, P., 1978. *Ap. J.* **226** 460.
- Sarre, P.J., 1991. *Nature* **351** 356.
- Scarrott, S.M., Rolph, C.D. & Mannion, M.D., 1989. *M.N.R.A.S.* **237** 1027.
- Scarrott, S.M., Warren-Smith, R.F., Pallister, W.S., Axon, D.J. & Bingham, R.G., 1983. *M.N.R.A.S.* **204** 1163.
- Scarrott, S.M., Watkin, S., Miles, J. & Sarre, P.J., 1992. *M.N.R.A.S.* **255** 11P.
- Schmidt, G.D., Cohen, M. & Margon, B., 1980. *Ap. J.* **239** L133.
- Schmidt, G.D. & Witt, A.N., 1991. *Ap. J.* **383** 698.
- Seab, C.G., 1987. *Interstellar Processes* p491 ed. Hollenbach, D.J. & Thronson, H.A. Dordrecht:Reidel.
- Seab, C.G. & Snow, T.P., 1984. *Ap. J.* **277** 200.
- Sellgren, K., 1983. *Astr. J.* **80** 985.
- Sellgren, K., 1984. *Ap. J.* **277** 623.
- Sellgren, K., 1986. *Ap. J.* **305** 399.
- Sellgren, K., 1990. in *Dust Objects in the Universe* ed. Bussoletti, E. & Vittone, A.A..
- Sellgren, K., Allamandola, L.J., Bregman, J.D., Werner, M.W. & Wooden, D.H., 1985. **299** 416.
- Sellgren, K., Luan, L. & Werner, M.W., 1990. *Ap. J.* **359** 384.
- Sellgren, K., Rouan, & Léger, 1988. *Astr. Ap.* **196** 252.
- Sellgren, K., Werner, M.W. & Dinerstein, H.L., 1983. *Ap. J.* **271** L13.
- Sellgren, K., Werner, M.W. & Dinerstein, H.L., 1992. *Ap. J.* **400** 238.
- Sharpless, S., 1952. *Ap. J.* **116** 251.
- Sitko, M.L., 1983. *Ap. J.* **265** 848.
- Sitko, M.L., Savage, B.D. & Merade, M.R., 1981. *Ap. J.* **246** 161.

- Slipher, V.M., 1918. *Pub. A.S.P.* **30** 63.
- Slipher, V.M., 1919. *Pub. A.S.P.* **31** 212.
- Smalley, R.E., 1983. *Ann. Rev. Phys. Chem.* **34** 129.
- Smith, F.W., 1984. *J. Appl. Phys.* **55** 764.
- Smith, W.H., Snow, T.P. & York, D.G., 1977. *Ap. J.* **218** 124.
- Snell, R.L. & Vanden Bout, P.A., 1981. *Ap. J.* **244** 844.
- Snow, T.P., 1973. *Pub. A.S.P.* **85** 590.
- Snow, T.P., 1992. *Ap. J.* **401** 775.
- Snow, T.P. & Seab, C.G., 1989. *Astr. Ap.* **213** 291.
- Stecher, T.P. & Williams, D.A., 1967. *Ap. J.* **149** L29.
- Street, R.A., 1980. *Phys. Rev. B.* **21** 5775.
- Stein, S.E., 1978. *J. Phys. Chem.* **82** 566.
- Strom, S.E., Strom, K.M., Yost, J., Carrasco, L. & Grasdalen, G., 1972. *Ap. J.* **173** 353.
- Strom, S.E., Strom, K.M. & Grasdalen, G.L., 1975. *Ann. Rev. Astr. Ap.* **13** 187.
- Takayanagi, K., Sakimoto, K. & Onda, K., 1987. *Ap. J.* **318** L81.
- Thronson, H.A.Jr., 1982. *Astr. J.* **87** 1207.
- Tielens, A.G.G.M. & Hollenbach, D.J., 1985. *Ap. J.* **291** 747.
- Tokunaga, A.T., Nagata, T., Sellgren, K., Smith, R.G., Onaka, T., Nakada, Y., Sakata, A. & Wada, S., 1988. *Ap. J.* **328** 709.
- Tokunaga, A.T. & Young, E.T., 1980. *Ap. J.* **237** L93.
- Tucker, K.D., Kutner, M.L. & Thaddeus, P., 1973. *Ap. J.* **186** L13.
- Van Breda, I.G. & Whittet, D.G.B., 1981. *M.N.R.A.S.* **195** 79.
- Van den Bergh, S., 1966. *Astr. J.* **71** 990.
- Van der Meer, B.J., Jonkman, H.T., Kommandeur, J., Meerts, W.L. & Majewski, W.A., 1982. *Chem. Phys. Letters* **92** 564.
- Van der Zwet, G.P. & Allamandola, L., 1985. *Astr. Ap.* **146** 76.
- Van Gorkom, J.H., Shaver, P.A. & Goss, W.M., 1979. *Astr. Ap.* **76** 1.
- Vanysek, V. & Svatos, J., 1964. *Acta. Univ. Carolinae - Maths & Phys. No.* **1** 1.

- Vietzke, E., Flashkamp, K., Philipps, V., Esser, G., Wienhold, P. & Winter, J., 1987. *Nucl. Mat.* **443** 145.
- Visvanathan, N., 1974. *Ap. J.* **192** 319.
- Waelkens, C., Van Winckel, H., Trams, N.R. & Waters, L.B.F.M., 1992. *Astr. Ap* **256** L15.
- Walker, G.A.H., Yang, S., Fahlman, G.G. & Witt, A.N., 1980. *Pub. A.S.P.* **92** 411.
- Walker, R. & Price, S.D., 1975. *AFCRL Infrared Sky Survey* Report AFCRL-TR-75-0373.
- Warren-Smith, R.F., 1979. *PhD. Thesis University of Durham* .
- Warren-Smith, R.F., 1983. *M.N.R.A.S.* **205** 337.
- Warren-Smith, R.F., Scarrott, S.M. & Murdin, P., 1981. *Nature* **292** 317.
- Watanabe, I., Hasegawa, S. & Kurata, Y., 1982. *Jap. J. Applied Phys.* **Vol.21** no.6 856.
- Watkin, S., Gledhill, T.M. & Scarrott, S.M., 1991. *M.N.R.A.S.* **252** 229.
- Watt, G.D., Burton, W.B., Choe, S.-U. & Liszt, H.S., 1986. *Astr. Ap.* **163** 194.
- Wdowiak, T.J., 1981. *Nature* **293** 724.
- Wdowiak, T.J., Donn, B., Nuth, J.A., Chappelle, E. & Moore, M., 1989. *Ap. J.* **336** 838.
- Webster, A., 1979. *M.N.R.A.S.* **189** 33P.
- Webster, A., 1980. *M.N.R.A.S.* **192** 7P.
- Webster, A., 1992. *M.N.R.A.S.* **255** 41P.
- Webster, A., 1993. *M.N.R.A.S.* **262** 831.
- Wehinger, P.A., Wycoff, S., Herbig, G.H., Herzberg, G., Lew, H., 1974. *Ap. J.* **190** L43.
- Weltner, W. & McLeod, D., 1964. *J. Chem. Phys.* **40** 1305.
- Westerlund, B.E. & Krelowski, J., 1988a. *Astr. Ap.* **189** 221.
- Westerlund, B.E. & Krelowski, J., 1988b. *Astr. Ap.* **203** 134.
- Weston, G.B., 1949. *Pub. A.S.P.* **61** 256.
- Weston, G.B., 1953. *Astr. J. No.* **1206** 48.

- Whitcomb, S.E., Gatley, I., Hilderbrand, R.H., Keene, J., Sellgren, K. & Werner, M.W., 1981. *Ap. J.* **246** 416.
- White, G.J., Phillips, J.P. & Watt, G.D., 1981. *M.N.R.A.S.* **197** 745.
- White, G.J., Sanderson, C., Monteiro, T.S., Richardson, K.J. & Hayashi, S.S., 1990. *Astr. Ap.* **227** 200.
- White, R.L., 1979. *Ap. J.* **229** 954.
- Whittaker, A.G., 1978. *Science* **200** 763.
- Willner, S.P., Soifer, B.T., Russell, R.W., Joyce, R.R. & Gillett, F.C., 1977. *Ap. J.* **217** L121.
- Witt, A.N., Bohlin, R.C. & Stecher, T.P., 1981. *Ap. J.* **244** 199.
- Witt, A.N., Bohlin, R.C. & Stecher, T.P., 1984. *Ap. J.* **279** 698.
- Witt, A.N. & Boroson, T.A., 1990. *Ap. J.* **355** 182.
- Witt, A.N. & Cottrell, M.J., 1980a. *Astr. J.* **85** 22.
- Witt, A.N. & Cottrell, M.J., 1980b. *Ap. J.* **235** 899.
- Witt, A.N. & Malin, D.F., 1989. *Ap. J.* **347** sc L25.
- Witt, A.N. & Schild, R.E., 1985. *Ap. J.* **294** 225.
- Witt, A.N. & Schild, R.E., 1986. *Ap. J. Suppl.* **62** 839.
- Witt, A.N. & Schild, R.E., 1988. *Ap. J.* **325** 837.
- Witt, A.N., Schild, R.E. & Kraiman, J.B., 1984. *Ap. J.* **281** 708.
- Witt, A.N., Walker, G.A.H., Bohlin, R.C. & Stecher, T.P., 1982. *Ap. J.* **261** 492.
- Wu, C-C., York, D.G. & Snow, T.P., 1981. *Ap. J.* **86** 755.
- Zellner, B., 1970. *Ph.D. Thesis University of Arizona* .
- Zuckerman, B., Gilra, D.P., Turner, B.E., Morris, M. & Palmer, P., 1976. *Ap. J.* **205** L15.

## Acknowledgements

I would like to start by acknowledging my supervisor, Dr S.M. Scarrott for providing me with the opportunity to pursue my interest in astronomy and for all the help he has given. It is my pleasure also to thank Dr J.V. Major for all the work he does for postgraduates.

I am greatly indebted to Chris Rolph, for his help and advice on all aspects of polarimetry and  $\text{\LaTeX}$  which has saved me endless hours with the manual when writing this thesis, to Rafael Guzman for all the countless tutorials on spectroscopy, to Peter Draper and Nick Eaton for all their help on computing matters, and to Rodney Warren-Smith and Tim Gledhill for writing the reduction software and making all this possible. I have appreciated the support and joviality of my colleagues and friends; David Stockdale, Neasa Foley, Roger Haynes, Gillian Wilson, Peter Doel, Kathy Romer, Isabelle Parkes, Andrew Ratcliffe, Omar Almaini, and Vicky Greener.

Data reduction was carried out on the Durham STARLINK node, and I am grateful to Alan Lotts for his hard work and expert management of the system as well as his advice on many occasions. I acknowledge Professor Martin and Professor Bloor, successive heads of department during my time as a research student, for all the facilities offered by the Physics department.

Finally I would like to thank my parents for all their love and support particularly during the difficult times, and to all the good friends I have made in Durham especially Helen Storey who has helped make these last few years enjoyable.

